University of Alberta

Changes in Late Neoglacial Perennial Snow and Ice Extent and Climate in the Queen Elizabeth Islands, Arctic Canada

by

Gabriel J. Wolken 

A thesis submitted to the Faculty of Graduate Studies and Research
in partial fulfillment of the requirements for the degree of

Doctor of Philosophy

Department of Earth and Atmospheric Sciences

Edmonton, Alberta
Fall 2006

Your file Votre référence
ISBN: 978-0-494-23128-9
Our file Notre référence
ISBN: 978-0-494-23128-9

ABSTRACT

The extent of snow and ice during the Little Ice Age (LIA, 1600-1900 AD) is used in this thesis to measure the impact of early twentieth century warming (~1900-1960) on perennial snow/ice cover in the Queen Elizabeth Islands (QEI), and to investigate the climatic conditions that might have favoured snow/ice reduction. Techniques are developed for the regional scale mapping of trimlines surrounding former LIA perennial snow/ice in the QEI using multispectral classification approaches, applied to high-resolution satellite imagery. Where mapped trimlines outlining the former margins of thin plateau ice caps are accordant with trimlines marking former perennial snowfields, their common elevation is interpreted to record the LIA equilibrium-line altitude (ELA) for that locality. The LIA ELA trend surface is modeled over the QEI and used to estimate the total area formerly covered by perennial snow/ice and to determine the area reduction between the LIA and 1960. Between the end of the LIA and 1960, the QEI experienced a 37% (62,387 km^2) reduction in perennial snow/ice cover, resulting from a <50 to >600 m increase in the ELA. The spatial distribution of ELA change reveals a high degree of local (<20 km) variability in the mountainous regions, but a strong regional-scale (~500 – 1,500 km) pattern of change over the QEI. Regional-scale spatial variation in ELA change is evaluated against Empirical Orthogonal Functions (EOFs) of meteorological variables computed from the NCEP-NCAR reanalysis (1949-2002). Warm and cold decadal episodes identified in the observational record are examined to determine their potential as modern analogs of early 20^{th} century and LIA climates. The spatial pattern of ELA change between the LIA and 1960 shows the greatest change occurring in the eastern QEI (from Devon to N Ellesmere islands), which corresponds to

EOF-1of mean summer surface air temperature (SAT; 1949-2002), the positive (negative) phase of which is strongly in place during the warm (cold) decade. Temperature anomalies during the warm (cold) decade are positively correlated with a weak (strong) polar vortex, higher (lower) than normal SSTs in the North Atlantic, and one of the lowest (highest) periods of sea-ice extent during the 20^{th} century.

ACKNOWLEDGEMENTS

In the beginning stages of this thesis, my estimated completion time was around 75 years. Although I substantially improved upon this estimate (completing in six years), at times it felt more like 75 years! Regardless of how you plan your route and monitor your pace, a PhD thesis is an endurance race.

I consider myself very fortunate to have had the opportunity to pursue a doctoral degree, and privileged to have been able to conduct this research on the magnificent and inspiring landscape of the Canadian High Arctic. This PhD research provided me with amazing experiences academically, professionally and personally, and I am grateful to the many people who contributed along the way.

First, I wish to thank my supervisor, John England, who introduced me to the Arctic. During this project, John provided helpful guidance and allowed me the freedom to make my own decisions and to develop my own ideas. John has also played a role in my life beyond supervision; he introduced me to hockey, and he provided friendship and personal support, these I will cherish always.

I would like to thank my committee members, Martin Sharp, Andy Bush, Dave Hik, and Ray Bradley (University of Massachusetts; who kindly served as external examiner), for their very helpful comments on the thesis. I am particularly grateful to Martin Sharp, who provided many hours of immeasurably valuable guidance and critical review. Thank you, Martin, for your support, advice, and friendship during the last few years. I would also like to extend my thanks to Art Dyke (GSC, Ottawa), who provided helpful direction, valuable advice, and helpful reviews during my work on this project.

Financial support for this research was provided by the Natural Sciences and Engineering Research Council of Canada (NSERC Discovery Grant A6680) and the NSERC Northern Chair Award, both to John England. Additional support was provided to me by the University of Alberta (FS Chai PhD Scholarship), the Harington Paleoenvironmental Scholarship, the Department of Earth and Atmospheric Sciences (University of Alberta), and the Canadian Circumpolar Institute (University of Alberta). The Polar Continental Shelf Project, Natural Resources Canada, provided logistical support during the summers of 2001 and 2003.

I would like thank my friends and family who played crucial roles in my life during my doctoral work (too many to list, you know who you are). Thank you to all in the "old/new" ice research groups, especially to Joel B. (we shared the struggle my friend), Nigel A., and Dave B.

Finally, I wish to express my gratitude to those who have sacrificed the most for my life pursuits. First, to my parents (Daryl and Shari Wolken), who have provided selfless love and support and have encouraged me to pursue my life goals, even if it meant I would be further away from them. And last, but not least, to my beloved wife Jane, who has gone the distance with me during my doctoral graduate work. She has provided unconditional love and unwavering support during the bitterest of days when I desperately need to be reminded of the important things in life. She has also shared (and is the reason for) many of my happiest moments. I look forward to returning the favour!

TABLE OF CONTENTS

LIST OF TABLES

LIST OF FIGURES

1 CHAPTER ONE

Introduction

1.1 Background

During the 20th century, global average surface temperature is reported to have increased by ~0.6 °C, and instrumental records indicate continued warming over an increasingly larger area of the globe (Osborn and Briffa, 2006). In polar regions, however, ubiquitous temperature increases have exceeded increases elsewhere on the planet and, by the mid-21st century, temperature increases in the Arctic are predicted to be >3 °C over present values (IPCC, 2001). Due to the inherent sensitivity of polar regions to climatic change, recent environmental modifications in these regions have been among the most severe globally (ACIA, 2004), and the need to produce accurate forecasts of future changes in these regions has become a critical societal issue.

In order to assess the significance of modern climatic change, it is imperative to place the observed change in a long-term perspective, and thus to, attempt to differentiate climate forcings resulting from natural climate variability from those ensuing from anthropogenic influence. This discrimination becomes arduous in high latitude regions because of the spatial and temporal paucity of instrumental data, which is especially true in the Canadian High Arctic, where there are only a few stations and the instrumental records extend back only ~56 yr. Hence, it is necessary to use paleoclimate proxy records to augment the observational record, so that natural climate variability may be considered over longer time scales, and used as a baseline against which modern variability can be assessed. In the Canadian High Arctic, paleoclimate proxy records

have been used to characterize the climatic variability throughout the Holocene (Bradley, 1990), and recent efforts have detailed the climatic variability of the last four centuries, illustrating the occurrence of high frequency variability superimposed on lower frequency trends (Overpeck *et al.*, 1997).

Among the many indicators of climatic variability in the Arctic is the large-scale fluctuation of glaciers, ice caps, and ice sheets. Recent studies have documented glacier responses to recent climate change in the Arctic (Dyurgerov and Meier, 1997; Church *et al.*, 2001; Arendt *et al.*, 2002; ACIA, 2004; Burgess and Sharp, 2004), and in the Canadian High Arctic, our knowledge of the behavior of terrestrial ice masses in response to late 20th century warming is being advanced by a growing body of research (Braun *et al.*, 2004; Burgess and Sharp, 2004; Burgess *et al.*, 2005; Mair *et al.*, 2005). However, little is known about the changes in terrestrial ice extent elicited by circum-arctic climate warming in the late 19th and early 20th centuries, and even less is known about the mechanisms that forced this abrupt multi-decadal warm event, which signalled the end of the Little Ice Age (LIA) in the Arctic (Overpeck *et al.*, 1997),

The end of the LIA in the Arctic occurred during the early 20th century (Bradley, 1990; Overpeck *et al.*, 1997; Johanesson, *et al.*, 2004). Paleoclimate proxy evidence indicates that 20th century temperatures in the Arctic were exceptionally high relative to the previous three centuries (Overpeck *et al.*, 1997), and temperatures in the Canadian High Arctic were the highest in more than a millennium (Bradley, 1990). The early 20th century warm period was hemispheric in scale, but had its maximum amplitude in the Arctic (Bengtsson *et al.*, 2004). Warming in the early part of the 20th century yielded to a circum-Arctic cooling event beginning in the mid-1960s, followed by a period of warmth,

which began around the late 1970s and continues through the present (Johannessen *et al.*, 2004). Mean summer temperatures in the Queen Elizabeth Islands (QEI), Canadian High Arctic, have only recently matched those of the latter part of the early 20th century warm period, as is true for the Arctic as a whole, which has led to some debate about the cause(s) of recent warming in the Arctic, that is; is it a consequence of anthropogenic effects or of natural variability in the climate system (Overpeck *et al.*, 1997; Polyakov and Johnson, 2000; Polyakov *et al.*, 2002; Bengtsson *et al.*, 2004; Johannessen *et al.*, 2004)? Although the early 20th century warm event seems to be a product of natural climate variability (Bengston *et al.*, 2004; Johanesson *et al.*, 2004), the internal feedbacks in the climate system leading to the event are still unclear. What is clear, however, is that the early 20th century warm event had a fundamental impact on the Arctic (Overpeck *et al.*, 1997) and that, in the QEI, it led to a substantial modification of the terrestrial crysophere.

1.2 Study Area

The QEI comprises the northernmost part of the Canadian Arctic Archipelago between 74.5° and 83.0° N (Fig. 1.1). Although classified as a polar desert, the QEI contain ~5% of the terrestrial ice found in the Northern Hemisphere, totalling ~110,000 km^2 (Williams and Ferrigno, 2002). The eastern QEI (Devon, Axel Heiberg, and Ellesmere Islands) consist of mountains reaching 2,500 m that support extensive ice caps and outlet glaciers. Additionally, numerous high plateaus are at or just below the local equilibrium-line altitude (ELA), and several support small ice caps (England *et al.*, 1981).

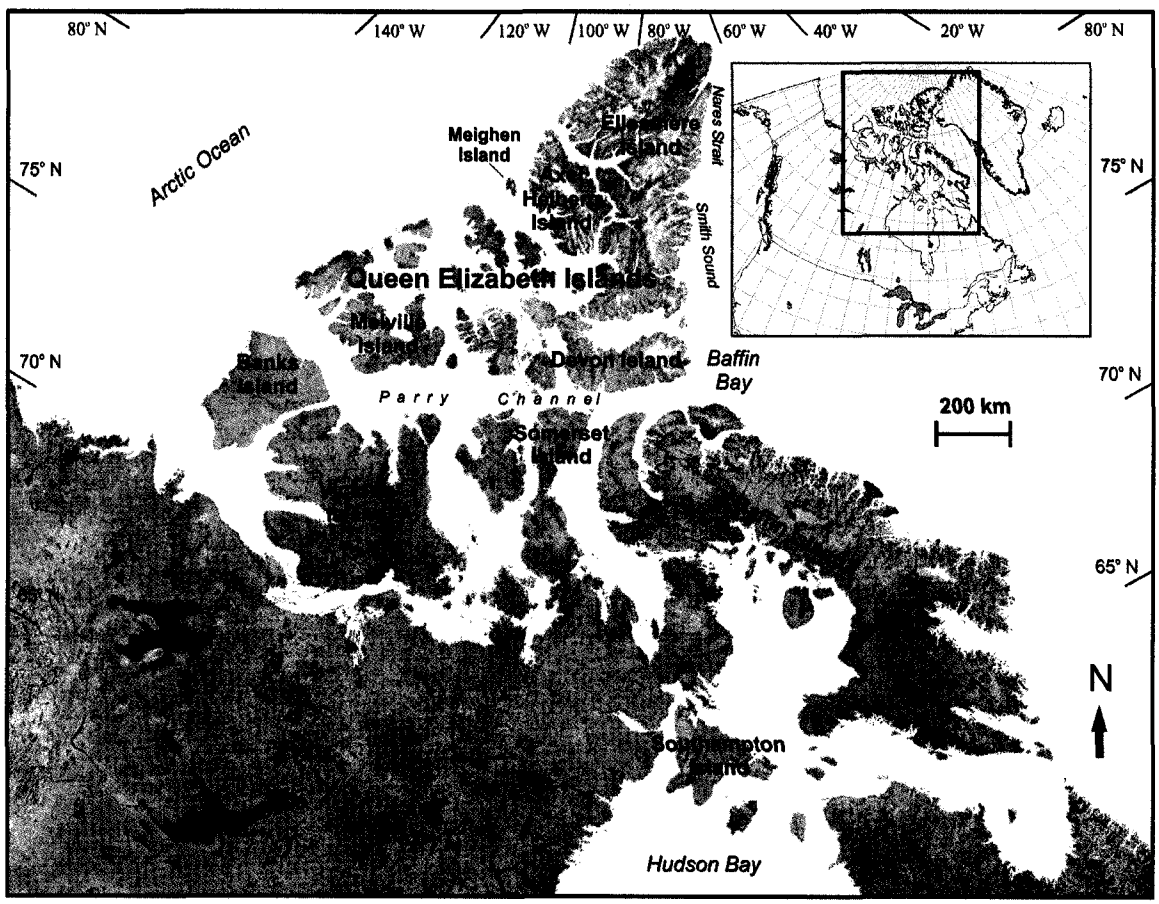

Figure 1. 1 Map of the Canadian Arctic Archipelago (Radarsat Orthomosaic of Canada courtesy of the Canadian Centre for Remote Sensing).

The modern ELAs throughout the eastern QEI range from less than 200 m along the north coast of Ellesmere Island to nearly 1,200 m in island interiors, where the climate is more continental. The western QEI are much lower, and hence, tend to be largely ice-free today, with the exception of Meighen Island, which supports a small ice cap below 300 m, and western Melville Island, where some plateaus above 600 m support small ice caps.

1.3 Objectives

Vegetation (lichens and plants) trimlines have been commonly interpreted as evidence of more extensive LIA terrestrial ice cover, and are most easily recognized on crystalline rocks that support well-developed plants and lichen communities in surrounding areas. Although trimlines also exist on carbonate terrain, they are more subtle, as a consequence of sparse vegetation, resulting from limited growth on calcareous substrates. One of the main reasons that LIA terrestrial ice extent has remained unknown in the QEI, is the large areal extent of carbonate terrain in this region, which makes the detection of trimlines, using conventional panchromatic images, difficult or impossible in many areas. This thesis is designed to extend the previous mapping of vegetation trimlines, conducted principally on the crystalline Precambrian terrain on islands in the southern Canadian Arctic Archipelago (Ives, 1962; Andrews *et al.*, 1975, 1976; Locke and Locke, 1977; Dyke, 1978; Hodgson, 1992; Hooper and Dyke, 2000; Dyke and Hooper, 2000; Dyke, 2000a-e; 2001a-e; 2003; 2004; Bednarski, 2002; Dredge, 2004 a-c), to the QEI, where the extent of LIA perennial snow/ice is poorly documented and the nature and magnitude of its reduction between the end of the LIA and 1959/60 (i.e., the first full aerial photography survey) remains unknown. This thesis

also investigates the variations in the equilibrium-line altitude (ELA) trend surface across the QEI and explores the complex feedbacks internal to the climate system which may have contributed to its changes during the early 20th century.

The objectives of this thesis are:

1. to re-evaluate hypotheses regarding the origin of trimlines in the Canadian High Arctic;
2. to map all discernable trimlines throughout the QEI relating to the former extent of LIA terrestrial perennial snow/ice;
3. to reconstruct the former LIA ELA trend surface across the QEI;
4. to estimate the total areal extent of LIA terrestrial ice cover in the QEI;
5. to estimate the total areal reduction of terrestrial ice cover between the LIA and 1960;
6. to determine the changes in the height of the equilibrium-line between the LIA and 1960 (Miller *et al.*, 1975) across the QEI;
7. to evaluate the spatial variations in ELA change against modern modes of climate variability, in order to identify possible modern analogs of early 20th century climate which may help explain the observed reduction in perennial snow/ice throughout the QEI (see objective 4).

1.4 Structure

This thesis is written in paper format, and is presented as a compilation of three independent papers forming the main chapters, which successively build upon each other.

Within each main chapter are the details specific to each paper relating to background, study area, data sources, methodology, results, and analysis and discussion.

Chapter 2, *Re-evaluating the relevance of vegetation trimlines in the Canadian Arctic as an indicator of Little Ice Age paleoenvironments* (a version of this paper has been published in Arctic, 58 (4): 341-353) addresses the origin of trimlines associated with so-called "lichen-free" areas in the Canadian Arctic, which has been attributed to both Little Ice Age (LIA) perennial snowfield expansion and seasonally persistent snow cover. Due to disparate hypotheses (ecological versus paleoclimatic) regarding the formation of these trimlines, their use as a paleoclimatic indicator has been abandoned for more than two decades. This debate is revisited and the validity of opposing hypotheses is readdressed in the light of new regional mapping of trimlines across the Queen Elizabeth Islands (QEI). The ecological hypothesis of insufficient duration of the growing season, resulting from seasonally persistent snow cover, fails to account for the poikilohydric nature of lichens, and their ability to endure short growing seasons. It also cannot adequately explain the existence of sharp trimlines, and does not account for those trimlines occurring on sparsely vegetated carbonate terrain. Furthermore, trimlines outlining the former extent of thin plateau ice caps are accordant with trimlines associated with former perennial snowfields, indicating that these trimlines record LIA snow and ice expansion rather than the seasonal persistence of modern snow cover. This paper revalidates the use of such trimlines as LIA climate indicators, and affirms the importance of their use in paleoclimatic reconstructions.

Chapter 3, *High-resolution multispectral techniques for mapping former Little Ice Age terrestrial ice cover in the Canadian High Arctic* (a version of this paper was

published in Remote Sensing of Environment, 101: 104-114) develops a methodology for mapping terrain formerly covered by LIA perennial snow/ice in the Canadian Arctic using multispectral classification approaches, applied to high-resolution ASTER and ETM+ satellite imagery. Four areas in the QEI with dissimilar surficial geology and diverse topographic complexity, believed to represent the surficial variability in the study area, were selected to test the efficacy of both sensors for mapping these subtle landscape features. Automated classification (band calculation) methods were found to be most effective on quartzitic sandstone and siliceous crystalline bedrock, whereas semi-automated (supervised classification) techniques were most successful on substrates comprised primarily of carbonate lithologies. ASTER's superior spatial resolution yielded higher accuracies in topographically complex areas; however, ETM+ was more effective over a wider variety of substrate lithologies and topographic settings.

Chapter 4, *Climatic conditions inferred from Little Ice Age trimlines across the Queen Elizabeth Islands, Arctic Canada* presents the reconstructed LIA terrestrial ice extent and the nature and magnitude of ice reduction in the QEI between the end of the LIA and 1960. This paper utilizes the techniques developed in Chapter 3, for mapping former LIA perennial snow/ice extent, by employing them on a broad-scale across the QEI. LIA ELA trend surfaces are reconstructed and used with the mapped ELAs for 1960 (Miller *et al.*, 1975) to calculate the spatial pattern of changes in the height of the equilibium-line throughout the QEI during the first 60 yrs of the 20th century. Regional-scale spatial variation in the change in ELA trend surfaces between the end of the LIA and 1960 corresponds qualitatively to specific patterns of climatic variability found in the modern record. These patterns are used to: (*i*) describe climatic conditions that, if

sustained, might produce patterns of perennial snow/ice similar to that documented in the physical record for the LIA; (*ii*) provide analogs to help explain climatic conditions that may have persisted during the early 20th century, which led to a significant reduction in the terrestrial perennial snow/ice cover in the QEI.

1.5 References

ACIA, 2004: *Arctic Climate Impacts Assessment.* Cambridge: Cambridge University Press, 1046 pp.

Andrews, J. T., Barry, R.G., Davis, P.T., Dyke, A.S., Mahaffy, M, Williams, L.D. and Wright, C., 1975: The Laurentide Ice Sheet: Problems of the mode and speed of inception. *World Meteorological Publication,* 421: 87-94.

Andrews, J. T., Davis, P. T., Wright, C., 1976: Little Ice Age permanent snowcover in the Eastern Canadian Arctic: Extent Mapped from Landsat-1 satellite imagery. *Geografiska Annaler,* 58A: 71-81.

Arendt, A. A., Echelmeyer, K. A., Harrison, W. D., Lingle, C. S., Valentine, V. B., 2002: Rapid wastage of Alaska glaciers and their contribution to rising sea level. *Science,* 297: 382-386.

Bednarski, J. H., 2002: Surficial geology, northeast Bathurst Island, Nunavut. *Geological Survey of Canada, Map 2011A, scale 1:100 000.*

Bengtsson, L., Semenov, V. A., and Johannessen, O. M., 2004: The early twentieth-century warming in the Arctic - A possible mechanism. *Journal of Climate,* 17: 4045-4057.

Bradley, R. S., 1990: Holocene paleoclimatology of the Queen Elizabeth Islands, Canadian High Arctic. *Quaternary Science Reviews,* 9: 365-384.

Braun, C., Hardy, D. R., and Bradley, R. S., 2004: Mass balance and area changes of four High Arctic plateau ice caps, 1959-2002. *Geografiska Annaler Series a-Physical Geography,* 86A: 43-52.

Burgess, D. O. and Sharp, M. J., 2004: Recent changes in areal extent of the Devon Ice Cap, Nunavut, Canada. *Arctic, Antarctic, and Alpine Research,* 36: 261-271.

Burgess, D. O., Sharp, M. J., Mair, D. W. F., Dowdeswell, J. A., and Benham, T. J., 2005: Flow dynamics and iceberg calving rates of Devon Ice Cap, Nunavut, Canada. *Journal of Glaciology,* 51: 219-230.

Church, J. A., Gregory, J.M., Huybrechts, P., Kuhn, M., Lambeck, K., Nhuan, M.T., Qin, D., and Woodworth, P. L., 2001: *Changes in sea level, in Climate Change 2001: The Scientific Basis*. Cambridge, New York: Cambridge University Press, 641-693 pp.

Dredge, L. A., 2004: Surficial geology, Ekalugad Fiord (West half), Baffin Island, Nunavut. Geological Survey of Canada, Map 2073A, scale 1:250 000.

Dredge, L. A., 2004: Surficial geology, McBeth Fiord (West half), Baffin Island, Nunavut. Geological Survey of Canada, Map 2074A, scale 1:250 000.

Dredge, L. A., 2004: Surficial geology, Lake Gillian, Baffin Island, Nunavut. Geological Survey of Canada, Map 2076A, scale 1:250 000.

Dyke, A. S., 1978: Indications of Neoglacierization on Somerset Island, District of Franklin. *Scientific and Technical Notes,,* Current Research, Part B; Geologica Survey of Canada: 215-217.

Dyke, A. S., 2000: Surficial geology, Phillips Creek, Baffin Island. Geological Survey of Canada, Map 1961A, scale 1:250 000.

Dyke, A. S., 2000: Surficial geology, Milne Inlet, Baffin Island. Geological Survey of Canada, Map 1962A, scale 1:250 000.

Dyke, A. S., 2000: Surficial geology, Moffet Inlet and Fitzgerald Bay, Baffin Island. Geological Survey of Canada, Map 1963A, scale 1:250 000.

Dyke, A. S., 2000: Surficial geology, Arctic Bay, Baffin Island. Geological Survey of Canada, Map 1964A, scale 1:250 000.

Dyke, A. S., 2000: Surficial geology, Navy Board Inlet, Baffin Island. Geological Survey of Canada, Map 1965A, scale 1:250 000.

Dyke, A. S. and Hooper, J., 2000: Surficial geology, Berlinguet Inlet and Bourassa Bay, Baffin Island. Geological Survey of Canada, Map 1960A, scale 1:250 000.

Dyke, A. S., 2001: Surficial geology, eastern Devon Island. Geological Survey of Canada, Map 1970A, scale 1:250 000.

Dyke, A. S., 2001: Surficial geology, central Devon Island. Geological Survey of Canada, Map 1971A, scale 1:250 000.

Dyke, A. S., 2001: Surficial geology, western Devon Island. Geological Survey of Canada, Map 1972A, scale 1:250 000.

Dyke, A. S., 2001: Surficial geology, Grinnell Peninsula, Devon Island. Geological Survey of Canada, Map 1973A, scale 1:250 000.

Dyke, A. S., 2001: Surficial geology, Cardigan Strait, Devon Island and Ellesmere Island. Geological Survey of Canada, Map 1974A; scale 1:250 000.

Dyke, A. S., 2003: Surficial geology, Erichsen Lake, Baffin Island, Nunavut., *Geological Survey of Canada, Open File 4484. CDROM with digital files (geology, topography, and hydrology) of Open Files 1598-1613 (previously released as paper maps at 1:50 000 scale).*

Dyke, A. S., 2004: Surficial geology, Erichsen Lake, Baffin Island, Nunavut., *Geological Survey of Canada, Map 2066A, scale 1:250 000.*

Dyurgerov, M. B. and Meier, M. F., 1997: Mass balance of mountain and subpolar glaciers: a new global assessment for 1961-1990. *Arctic and Alpine Research,* 29: 379-391.

Hodgson, D. A., 1992: Quaternary geology of western Melville Island, Northwest Territories. *Geological Survey of Canada,* Paper 89-21: 1-35.

Hooper, J. and Dyke, A. S., 2000: Surficial geology, Agu Bay and Easter Cape, Baffin Island. Geological Survey of Canada, Map 1959A, scale 1:250 000.

IPCC, 2001: *Climate Change 2001: The Scientific Basis.* Cambridge, New York: Cambridge University Press, 408 pp.

Ives, J. D., 1962: Indication of recent extensive glacierization in north central Baffin Island, N.W.T. *Journal of Glaciology,* 4: 197-205.

Johannessen, O. M., Bengtsson, L., Miles, M. W., Kuzmina, S. I., Semenov, V. A., Alekseev, G. V., Nagurnyi, A. P., Zakharov, V. F., Bobylev, L. P., Pettersson, L. H., Hasselmann, K., and Cattle, A. P., 2004: Arctic climate change: observed and modelled temperature and sea-ice variability. *Tellus Series a-Dynamic Meteorology and Oceanography,* 56: 328-341.

Locke, C. W. and Locke, W. W., 1977: Little Ice Age snow-cover extent and paleoglaciation thresholds: North-central Baffin Island, N.W.T., Canada. *Arctic and Alpine Research,* 9: 291-300.

Mair, D., Burgess, D., and Sharp, M., 2005: Thirty-seven year mass balance of Devon Ice Cap, Nunavut, Canada, determined by shallow ice coring and melt modeling.

Journal of Geophysical Research-Earth Surface, 110, F01011, doi:10.1029/2003JF000099.

Osborn, T. J. and Briffa, K. R., 2006: The spatial extent of 20th-Century warmth in the context of the past 1200 years. *Science,* 311: 841-844.

Overpeck, J., K., Hughen, K., Hardy, D., Bradley, R., Case, R., Douglas, M., Finney, B., Gajewski, K., Jacoby, G., Jennings, A., Lamoureux, S., Lasca, A., MacDonald, G., Moore, J., Retelle, M., Smith, S., Wolfe, A., and Zielinski, G., 1997: Arctic environmental change of the last four centruries. *Science,* 278: 1251-1256.

Polyakov, I. V. and Johnson, M. A., 2000: Arctic decadal and inter-decadal variability. *Geophysical Research Letters,* 27: 4097-4100.

Polyakov, I. V., Alekseev, G. V., Bekryaev, R. V., Bhatt, U., Colony, R. L., Johnson, M. A., Karklin, V. P., Makshtas, A. P., Walsh, D. and Yulin, A. V., 2002: Observationally based assessment of polar amplification of global warming. *Geophysical Research Letters,* 29: 1878.

Wolken, G. J., England, J.H. and Dyke, A. S., 2005: Re-evaluating the Relevance of Vegetation Trimlines in the Canadian Arctic as an Indicator of Little Ice Age Paleoenvironments. *Arctic,* 58: 341-353.

Wolken, G. J., 2006: High-resolution multispectral techniques for mapping former Little Ice Age terrestrial ice cover in the Canadian High Arctic. *Remote Sensing of Environment,* 101: 104-114.

2 CHAPTER TWO

Re-evaluating the relevance of vegetation trimlines in the Canadian Arctic as an indicator of Little Ice Age paleoenvironments

2.1 Introduction

During the Neoglacial, (i.e., the last 3000 years), the Canadian High Arctic was markedly colder than it was during the early to middle Holocene (~9000 to 3000 BP) (Bradley, 1990; Kaufman *et al.*, 2004). This period of climatic deterioration led to widespread expansion of the terrestrial snow and ice cover, as well as sea ice and ice shelves, which reached their maximum Neoglacial extent during the Little Ice Age (LIA) (~1600-1900 AD) (Grove, 1988; Koerner and Fisher, 1990). Subsequently, there has been an equally dramatic reduction of this snow and ice cover, occasioned by climate amelioration, following the LIA. The temporal chronology and the cause of the LIA in Arctic Canada are not well understood, nor is it clear which factors led to its termination (Overpeck *et al.*, 1997). Because the instrumental record in the Canadian High Arctic extends back only ~56 years, a better understanding of the LIA will help to document the nature of climatic variability over longer time scales. This information can then be used to test the ability of climatic models to reproduce past environmental change, thereby, improving our ability to forecast future conditions.

Vegetation trimlines surrounding poorly vegetated terrain have commonly been interpreted as evidence of the retreat of LIA snowfields, glaciers, and ice caps (Ives, 1962; Andrews *et al.*, 1975, 1976; Locke and Locke, 1977; Dyke, 1978; Edlund, 1985; Levesque and Svoboda, 1999; Hooper and Dyke, 2000; Dyke and Hooper, 2000; Dyke, 2000a-e; 2001a-e; 2003; 2004; Dredge, 2004 a-c). Consequently, a large reduction in

snow and ice cover has been mapped on northern Baffin and Devon Islands, where lighter-toned areas with minimal vegetation are evident on airphotos and satellite images. These areas have been interpreted as areas of incipient plant recolonization following melting of perennial névés. Similar areas occur on more northerly Arctic Islands, but they have not been mapped (Fig. 2.1). Ives (1962) was the first to recognize expansive but sharply delineated areas with little or no vegetation across the north-central plateau of Baffin Island (Fig. 2.1). He attributed these to recent melting of former "ice patches and snow-beds" and referred to them as "lichen-free" zones (synonymous with the term 'lichen-kill,' and includes the destruction of plants as well as lichens). Field observations revealed that the lighter-toned areas on aerial photographs are areas nearly devoid of plants and lichens, whereas the darker-toned areas support mature plant and lichen communities, which in this region typically cover 50-100% of the ground where the soil is acidic. Building on Ives' observations, Falconer (1966:200) investigated a "sharply defined" trimline encircling a hilltop near the Tiger Ice Cap, Baffin Island, which has now completely melted. The trimline separates "...a near continuous growth of large crustose lichens" at the summit from a lichen-free zone below (Falconer, 1996:200). Based on estimated lichen growth rates for this area (Andrews and Webber, 1964), Falconer proposed that the hilltop must have remained a nunatak for several hundred years. Falconer also noted a band of preserved but dead lichen and plant cover around the retreating margin of the Tiger Ice Cap. Inside the trimline, and next to the retreating margin of the ice cap, Falconer collected a clump of preserved, dead moss that was ^{14}C dated to 330 ± 75 yr BP (I-1204). This sample provided a maximum age estimate for the

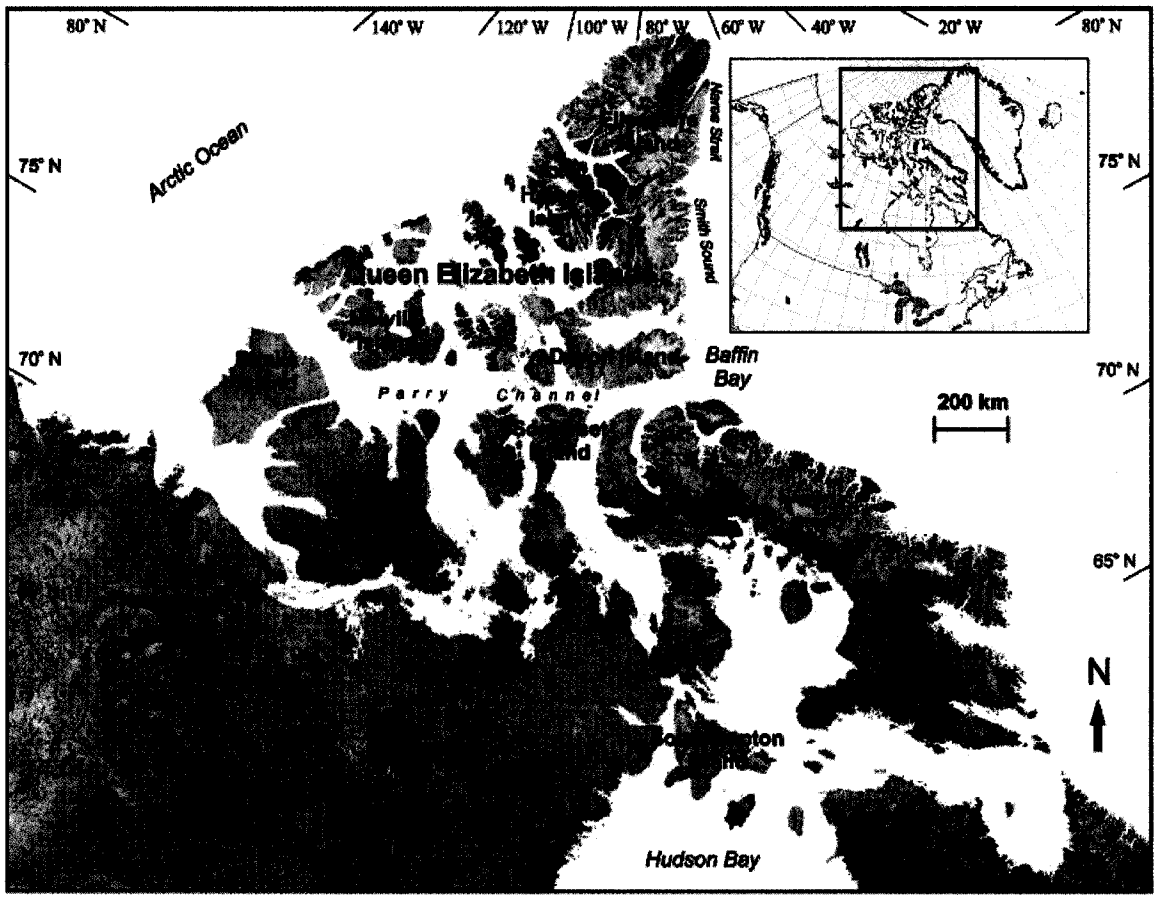

Figure 2. 1 Map of the Canadian Arctic Archipelago (Radarsat Orthomosaic of Canada courtesy of the Canadian Centre for Remote Sensing).

last snow and ice expansion, and thus strengthened the interpretation that the "lichen-kill" event occurred during the LIA.

In contrast, Koerner (1980) argued that growing seasons of insufficient duration were responsible for the barren sites described by Ives and subsequent workers. This hypothesis departs not only from the traditional interpretation of trimlines on the plateaus of Baffin Island, but also the generally accepted interpretation of similar trimlines around glaciers in alpine areas around the globe. This debate is central to the interpretation of lichen-free zones, that is: do prominent trimlines record the limit of former LIA perennial snowfields and ice caps (Ives, 1962), or as Koerner (1980) suggests, do they simply record the limit of consistently occurring late lying snowfields that result in an insufficient growing season for lichens? Although surficial geologists have continued to portray these trimlines in accordance with Ives' hypothesis (references above; Hodgson, 1992), one result of Koerner's rejection of Ives' hypothesis is that these features have not been used for explicit paleoclimatic reconstructions since the early 1980's. Thus, their usage as a measure of climatic change has been abandoned. In a recent review of the postglacial climate history of Arctic Canada, for example, Gajewski and Atkinson (2003:73) stated, "...dating of a more extensive snow cover is not well established, nor is its extent or impacts on arctic ecosystems." The purpose of this paper, therefore, is to revisit the views of both Ives and Koerner in the light of new regional mapping of trimlines across the Queen Elizabeth Islands (QEI) and to use these observations to address their origin and applicability to past climatic change.

2.2 Overview of Trimlines in Arctic Canada

2.1.1 Trimline Concept

Throughout Arctic Canada, and elsewhere in glaciated regions, light-toned, barely vegetated terrains displaying abrupt outer margins, extend back to modern glaciers and ice caps (Fig. 2.2). These margins, referred to as "trimlines," have been universally ascribed to the removal of vegetation, to the freshening of rock surfaces, or to the deposition of new drift, all caused by former glacial cover. Where the former ice cover was neither erosive nor depositional, the result is strictly a vegetation trimline. Such vegetation trimlines will inevitably become indistinct as vegetation slowly becomes re-established in these areas (Benn and Evans, 1998: 606). In the Canadian High Arctic, vegetation trimlines around glaciers and ice caps are widespread, but identical features also occur on plateaus that are currently ice-free or nearly so. Vegetation trimlines are best developed on crystalline Precambrian terrain that supports well-developed vegetation and lichen communities immediately distal to them (Figs. 2.3 and 2.4). Although trimlines also exist on carbonate terrain, they are more subtle due to the depauperate nature of vegetation and lichen communities on calcareous soils, which typically support a vegetation cover of 5% or less (Fig. 2.5). Nevertheless, trimlines on carbonate substrates are subtly apparent on airphotos and high-resolution satellite imagery, where they outline areas of greater albedo. As seen on the ground, these lighter-toned areas are surfaces having slightly less surface clast weathering, more frequent flat-lying clasts, and less patterned ground microrelief (Fig. 2.5). In several places, finely nested arrays of lateral meltwater channels are inset within these light-toned terrains.

Figure 2. 2 Former limit of ice extent indicated by a lighter-toned zone of reduced vegetation and lichens, delineated distally by an abrupt trimline (white arrows) and proximally by the modern terminus. The distance from the terminus to the trimline is ~140 m. Twin Glacier, Alexandra Fiord, Ellesmere Island, Canada.

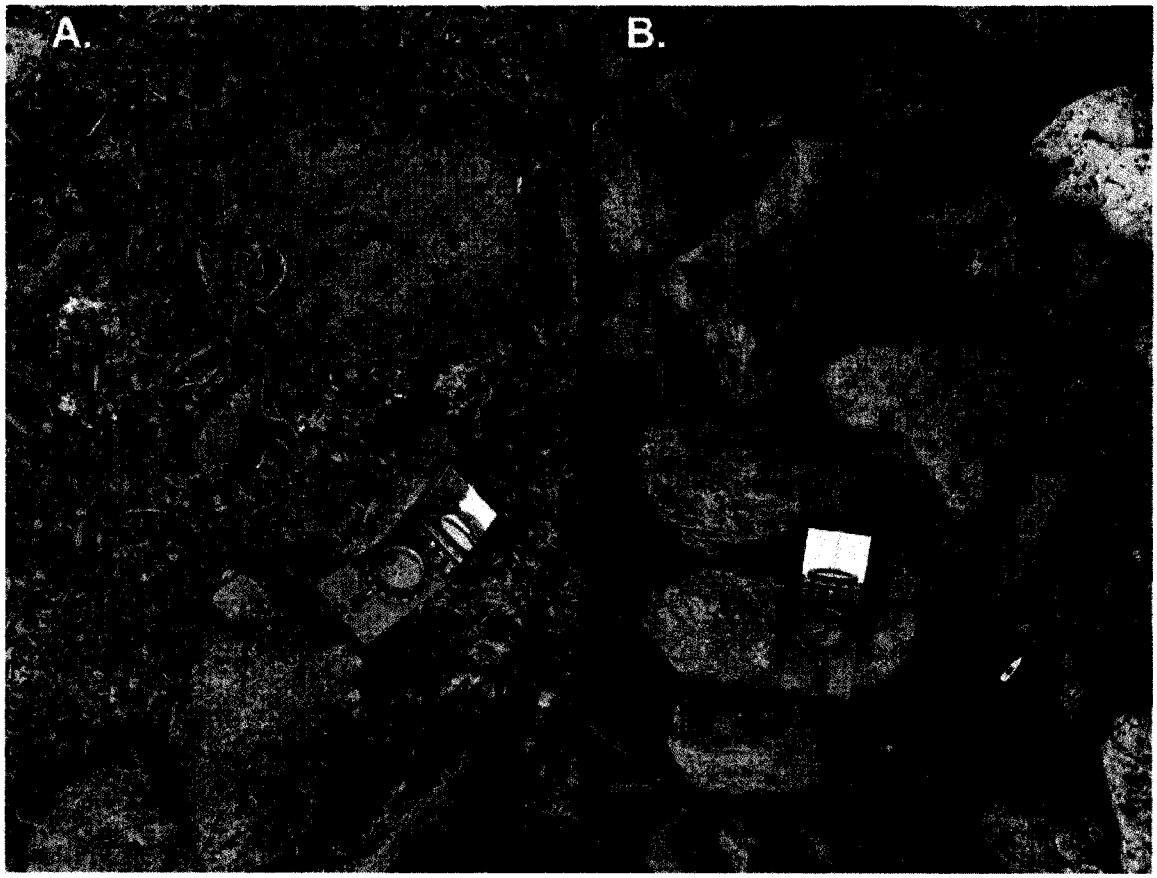

Figure 2. 3 Siliceous Precambrian substrate with (A) mature plant and lichen communities distal to LIA trimline, and (B) plant and "lichen-free" area within the expansion area, Johan Peninsula, Ellesmere Island. Bedrock in A and B is Precambrian Shield.

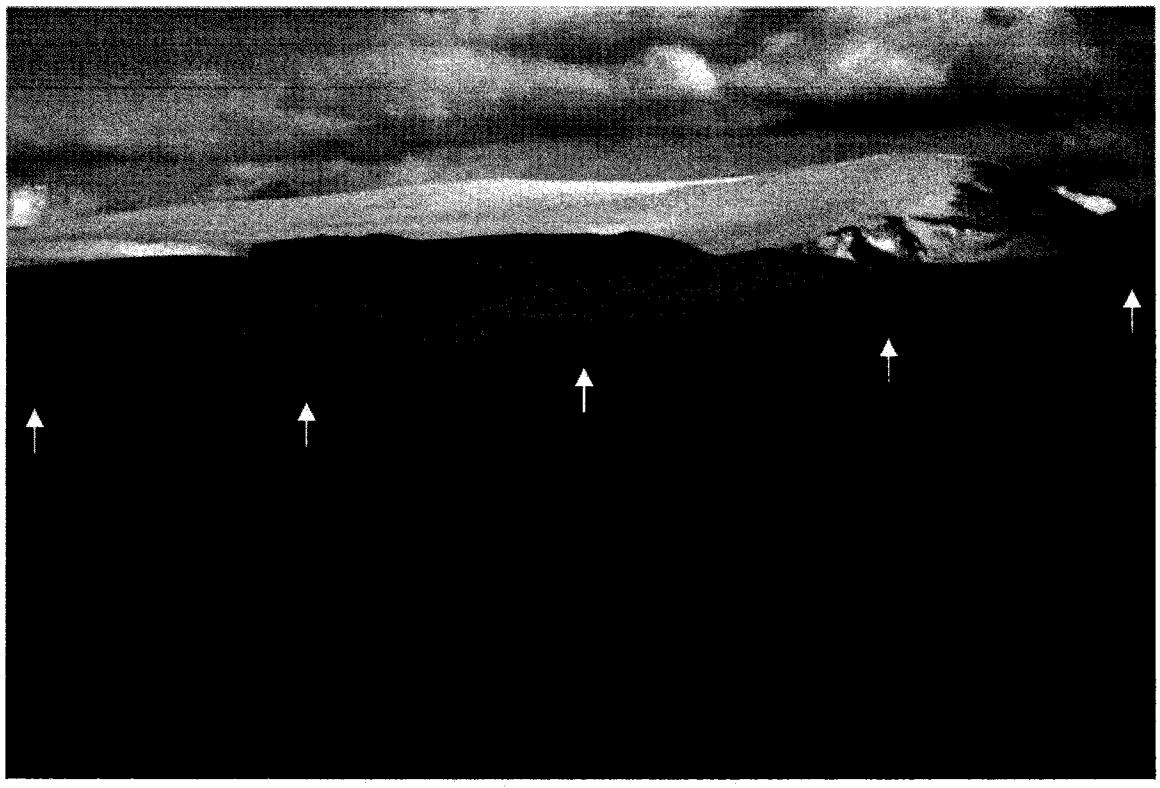

Figure 2. 4 Recently exposed terrain with a diffuse boundary (white arrows) separating "lichen-free" areas from areas with mature lichen, bryophyte, and vascular plant communities that remained free of LIA perennial snow and ice. Thorvald Peninsula, E Ellesmere Island.

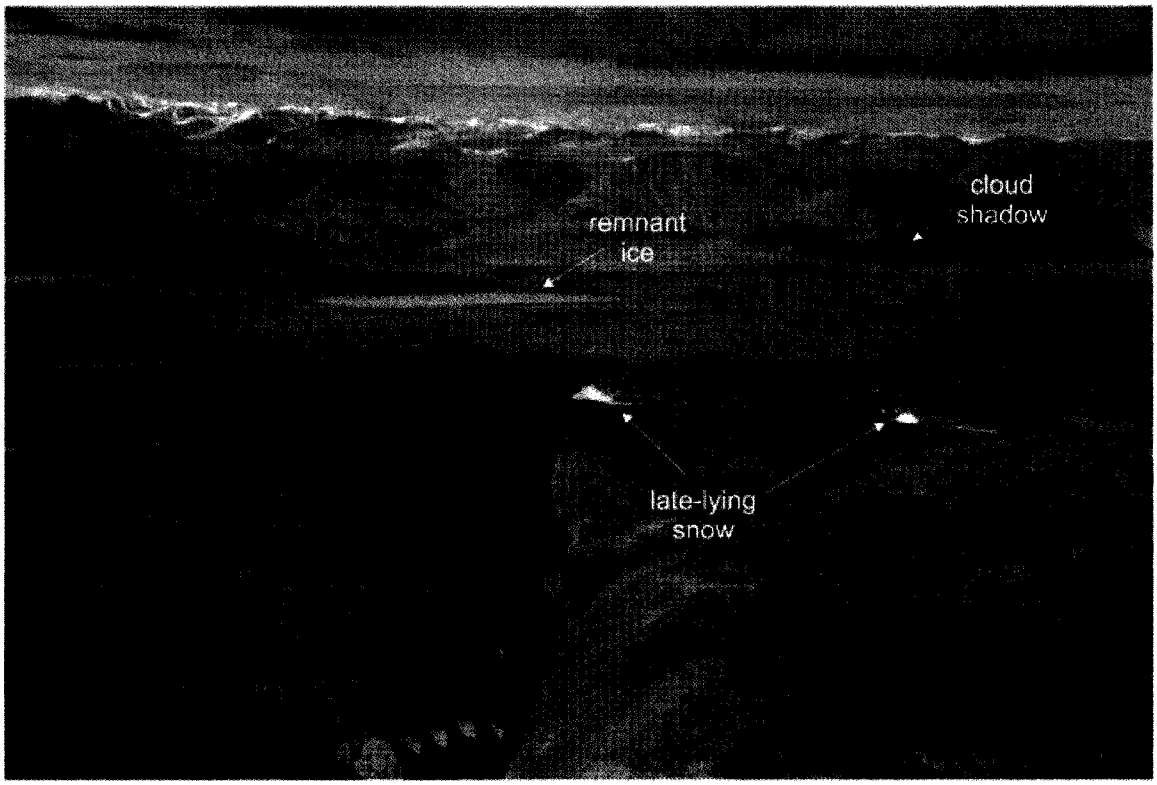

Figure 2. 5 Trimlines and recently exposed terrain on a carbonate substrate surrounding a small plateau ice cap. Solid lines show abrupt trimlines and dashed lines indicate areas of transition (diffuse trimlines) from more weathered to less weathered terrain. Distal to the abrupt trimline, a conspicuous break in slope is visible, whereas the diffuse trimline is found on gently sloping terrain. Bache Peninsula, E Ellesmere Island.

2.2.1 Previous Trimline Research in the Canadian Arctic

The perspectives offered by Ives (1962) and Falconer (1966), proposing a substantial increase in snow and ice in the recent past, regenerated interest in Ives' (1957) earlier hypothesis of instantaneous glacierization. This term implied that the onset of glaciation was occasioned by the lowering of the snowline onto expansive plateaus of northern Canada (Keewatin, Labrador and Baffin Island), which through increased albedo resulted in a positive feedback, promoting snowfield expansion. In this view, the expansion of snow and ice during the LIA, as recorded by the distribution of recently exposed trimlines, offered insights regarding processes of ice-sheet inception and growth (Flohn, 1974; Andrews *et al.*, 1975, 1976; Barry, 1975; Ives *et al.*, 1975; Williams, 1975).

Based on this trimline model, Andrews *et al.* (1975, 1976) compiled the first reconstruction of LIA perennial snow cover for north-central Baffin Island. This reconstruction was based on the mapping of light-toned areas from aerial photo and Landsat-1 satellite imagery, combined with fieldwork. Chronological control for trimline age was based on ^{14}C and lichenometric dates, the latter based on the diameter of the widespread crustose species *Rhizocarpon geographicum*. From these observations, Andrews *et al.* (1976) concluded that the lowering of the regional snowline during the LIA ranged from 100 to 400 m below its modern elevation (~900 m asl, Miller *et al.*, 1975). Locke and Locke (1977) also used aerial photos and Landsat-1 satellite imagery of north-central Baffin Island to map lichen-free areas. They reported that during the LIA, ice cover was ~35% greater than the modern ice cover within the study area, and

was accompanied by a lowering of the glaciation level (GL) and ELA by as much as 400 m.

Subsequent research has reported similar lichen-free zones from other islands of the Canadian Arctic Archipelago (Fig. 2.1). To the west of Baffin Island, Dyke (1978:215) described lichen-free areas close to 400 m asl on parts of NW Somerset Island, which "does not support late-lasting snowbanks today." Dyke suggested that the presence of greater snow and ice in the recent past (unspecified) precluded recolonization of this area. He also reported that other parts of the island that are underlain by calcareous rocks have ice retreat landforms of Neoglacial age, such as lateral meltwater channels and small esker-like ridges. In the western Arctic, Edlund (1985) identified several areas of possible Neoglacial snow and ice expansion on Melville Island based on vegetation trimlines in areas that she reported to have been then snow-free for several weeks during the summer. Hodgson (1992) portrayed these areas with the same interpretation on his surficial geology map of western Melville Island, and Bednarski (2002) mapped similar features on Bathurst Island.

Following Koerner's (1980) paper, nearly fifteen years elapsed before an interest in lichen-free areas in Arctic Canada was renewed. Levesque and Svoboda's (1999) interpretations of barely vegetated upland terrain on Ellesmere Island are fully compatible with Ives' (1962) hypothesis, but were now being advanced by botanists.

2.3 Discussion

Koerner's (1980) paper: "The problem of lichen-free zones in Arctic Canada," challenged the interpretation of so-called 'lichen-free' areas, claiming that there were

inconsistencies in Ives' (1962) original hypothesis to the point that it is fundamentally incorrect. Koerner proposed that lichen-free areas resulted from insufficient growing seasons due to the persistence of late-lying snow banks. In this context, Koerner (1980) posed five basic objections with regard to: (1) lichen survival under perennial snow/ice; (2) the method of lichen removal to develop trimlines; (3) the form of the trimlines; (4) the time interval, based on ^{14}C dates, assigned to the snow and ice cover expansion; and (5) the apparent "degree" of lichen-kill reported in the literature.

2.3.1 Vegetation Trimlines and Lichen Physiology

Vegetation trimline formation is largely a function of the physiological requirements of lichen growth and survival. Lichen survival in extreme environments is credited to their poikilohydric lifestyle (Green *et al.*, 1999); that is, to their ability to become dormant for long periods and reactivate rapidly. Dormancy is a result of a lichen's ability to undergo desiccation, whereby a thickening of the upper cortex prohibits photosynthesis and protects the lichen from temperature extremes and intense light (Raven *et al.*, 1992). Reactivation is a result of rapid imbibition, allowing the upper cortex to thin and become translucent, thereby, permitting photosynthesis to resume.

Lichen survival under snow or ice is largely a function of their exposure to subnival moisture. In both the Arctic and Antarctic, lichen communities are often found alive under seasonally persistent snow banks, which occupy the same location year after year (Schroeter *et al.*, 1994; Kappen *et al.*, 1998; Green *et al.*, 1999; Pannewitz *et al.*, 2003). Pannewitz *et al.* (2003:37), describe lichen activity under snow in continental Antarctica, stating that "Lichens exposed for the first time late in the season will have almost the

same productivity as those exposed earlier and there is little disadvantage to extended burial in snow as long as melting does eventually, and consistently, occur each season." They maintain that this productivity is primarily due to similar photosynthetic activity periods, which are dictated by initial hydration from the melting snow edge, and terminated, by means of desiccation, upon snow removal. However, lichen mortality occurs when a multi-year snow cover, greater than ~30 cm thick, prohibits photosynthetic activity of lichens that are hydrated (Körner, 1999; Pomeroy and Brun, 2001). This results in diminished carbon availability as a consequence of continued respiration when lichen thalli are hydrated (Gannutz, 1970; Benedict, 1990; Kappen *et al.*, 1995). If carbon reserves are not replenished, the fungal member of the lichen will parasitize the algal partner, ultimately causing the lichen to expire (Gannutz, 1970).

2.3.2 Responding to Koerner's Objections

2.3.2.1 Objection 1. The survival of lichen under perennial snow/ice

Koerner's first objection (above) concerns the manner of lichen kill. He cited observations by Beschel (1961) who claimed that lichens could survive in a state of dormancy under the protective cover of perennial snow or ice if basal meltwater was absent. Koerner (1980:88) expanded on this concept, stating, "...if the formation of permanent snowfields in the LIA was rapid, no melt may have penetrated to the basal layers of the permanent snowfields and there would be lichen survival rather than lichen-kill." Consequently, in Koerner's view lichens should have been able to reactivate and resume photosynthesis without delay following re-exposure after the termination of the LIA (Lang, 1972, cited by Koerner, 1980). Although the duration for which lichens can

endure this dormancy is not stated and may be unknown, it seems unlikely that it is without limits (e.g., Twin Glacier below).

Perennial snow and ice cover is inimical to the continuance of lichen and plant growth once the organism is buried, and their death can likely result from the duration of that burial or the subnival environment (e.g., basal wetting). Recession of cold-based ice margins occasionally exhumes intact but dead lichen and plant communities. For example, Bergsma *et al.* (1984) reported well-preserved but dead plants being exposed by the retreat of Twin Glacier in Alexandra Fiord, E. Ellesmere Island. Twin Glacier, like many High Arctic glaciers, is cold-based at its terminus; therefore, the preservation of ice-entombed dead vegetation and lichen communities occurs due to the overall absence of subglacial meltwater and limited subglacial erosion. The preserved dead lichen and plant communities can be seen with high-resolution multi-spectral satellite imagery as a dark band bordering the terminus of Twin Glacier (Fig. 2.6). In southwest Yukon, Farnell *et al.* (2004), reported dark lichen covered rock exposed at the retreating edge of alpine ice patches. These dark bands are surrounded by a "halo" of lichen-free terrain, the outer limit of which was thought to represent the LIA maximum ice patch extent (Farnell *et al.*, 2004:251). As these ice masses retreat, renewed exposure to weathering and erosion expedites the disintegration and removal of dead vascular plants, mosses, and fruiticose lichens first, followed by the more persistent epipetric crustose lichen species, which remain exposed for about 5-10 years prior to their removal (G. Henry, pers. comm. 2003). This duration is consistent with Benedict's (1990) observations in alpine regions of the Colorado Rocky Mountains, where he reported the complete removal of *Rhizocarpon*

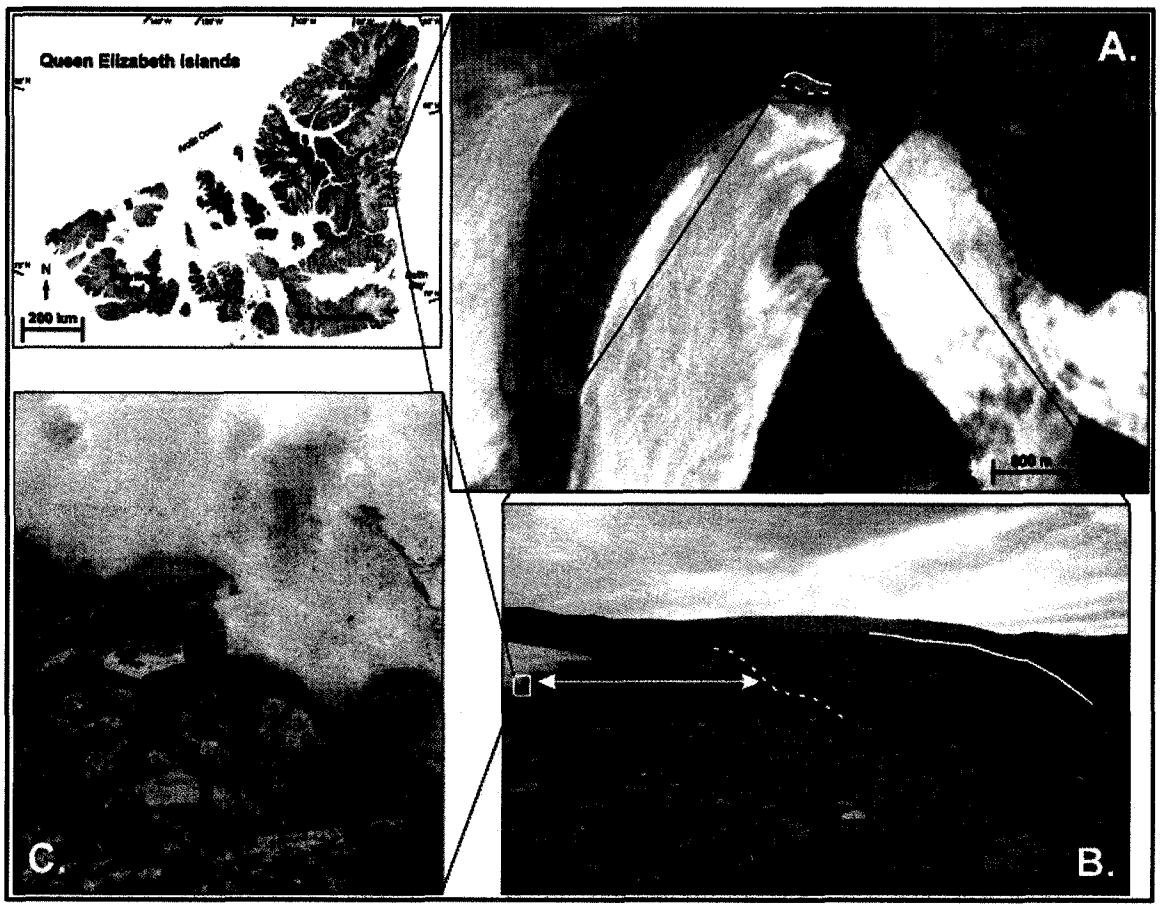

Figure 2. 6 Twin Glacier, Alexandra Fiord, Ellesmere Island. (A) ASTER (SC:AST_L1A.003:2007830294) image showing preserved dead lichen, bryophytes, and vascular plant communities as a dark band bordering the terminus of West Twin Glacier (between white dashed line and ice margin). Beyond the dashed line, the solid line indicates the abrupt trimline marking the former LIA margin. (B) Ground view showing the abrupt trimline (solid line, as in A) and outer margin of gradational dark zone (dashed line in A, and arrow) marking exhumed dead lichens, bryophytes, and vascular plants that have just been exposed by ongoing ice retreat (C).

thalli by erosive agents 1-3 years following their death, although some dead lichen persisted for up to 6 years. Similar sequences of ice burial and subsequent exposure and removal of lichen and plant communities could also have applied to the former LIA snowfields and icecaps postulated by Ives and followers.

Regardless of the duration of dormancy, however, lichen populations could have been destroyed during the initiation phase of the LIA event alone. If the onset of this cool interval was not constant, but rather was characterized by greater variability of temperature and precipitation (Lamoureux, 2000; 2001; 2002), there would have been ample opportunity for basal wetting to occur beneath newly established LIA névés, causing lichen thalli to become hydrated. As cooler intervals yielded to intervening warmer ones, the perennial snowfields would have been subjected to melt, providing more than enough opportunity for meltwater to percolate to their bases. Therefore, during these intra–Neoglacial warm periods, lichen populations within the trimline boundary would be damaged (if not killed) by subnival meltwater, especially since underlying permafrost would have extended close to the surface, ensuring a perched water table (i.e., super-saturation).

2.3.2.2 Objection 2. The method of lichen removal

Koerner's second objection was primarily based on the absence of bands of dead lichens, such as those seen at Twin Glacier (Bergsma *et al.*, 1984) and in southwest Yukon (Farnell *et al.*, 2004), and his scepticism with regard to a mechanism for their removal. He states that "...on none of the aerial photographs that I have examined of the plateau northwest of the Devon Ice Cap is there any sign of a band of dead lichens (dark

tone) flanking the retreating ice caps," and that, "...expansion of the permanent snow and ice cover during the Little Ice Age must have been over ground with an already sparse lichen cover..." (Koerner, 1980:89). There are several evident retorts to these comments. First, apart from some Precambrian outcrops of Canadian Shield (where lichen communities characteristically thrive), the area northwest of the Devon Ice Cap is principally comprised of carbonate rocks; hence, the lichen and plant cover on this terrain is already sparse, as a result of this inhospitable substrate. Consequently, there would not be conspicuous bands of dead lichens surrounding retreating ice masses on this terrain. Second, as stated above, there would have been numerous opportunities to kill (basal wetting) and remove (erosion after exposure) lichen and plant communities during intra-Neoglacial warm periods prior to or during the LIA, regardless of lichen and plant cover or substrate type. Therefore, the terrain that was covered during the LIA expansion would have been sparsely populated with lichens due to previous kill and removal events. Third, if most dead lichens were removed during intra-Neoglacial warm periods, the only locations where one might have seen a dark band of dead lichens flanking a retreating ice cap would have been at the former limit of the largest expansion (advance), assuming that the greatest expansion occurred during the LIA. Moreover, the dark band of dead lichens would have been visible for only about 3-10 years (see above) following the peak of the LIA in the Canadian Arctic, roughly 160 years ago (Overpeck *et al*, 1997). Fourth, the localities where most perennial snow and ice expansions occurred are classified as polar deserts; recolonization would have been thwarted by the brevity of intra-Neoglacial warm periods, as this process today makes little progress within a century (Levesque and Svoboda, 1999). Finally, Koerner's objections regarding the manner of lichen kill, the

mechanism of lichen removal, and the subsequent formation of trimlines are simply not applicable to the non-vegetative trimlines that occur on carbonate terrain.

2.3.2.3 Objection 3. The form of the trimlines

Koerner's third objection was in reference to the abruptness of the trimline. He argued, "... a diffuse boundary between lichen-free and lichen-covered areas should have developed rather than a trimline. This is because permanent snow and ice fields expand and contract areally in response to the varying intensity of melting from summer to summer. A permanent snowfield 1 to 2 m thick would disappear every few years after a particularly warm summer to reform a year or so later" (Koerner, 1980:90) First, the use of the descriptive terms "abrupt" and "diffuse" are entirely dependent on the scale at which the mapping is being conducted. A gradational transition of several meters on the ground may appear abrupt to analysts using remote sensing imagery (satellite or aerial images), an effect that would have been especially true for early investigators (Andrews *et al.*, 1976; Locke and Locke, 1977) using Landsat 1 imagery, which has a ground resolution of 80 m. Second, according to Ives' (1962) hypothesis, the trimlines represent the outer margins of perennial snow and ice expansions that were of sufficient duration to kill the affected plant and lichen cover. The hypothesis does not exclude intervals of greater snow cover that were too brief to kill the plant cover, nor does it specify an unvarying snowfield configuration throughout the LIA. Compositionally, the margin of this expansion must have been firn or superimposed ice. The abruptness of most trimlines indicates that the firn (or ice) was sufficiently thick to withstand variations in the annual melt rate for a duration sufficient to kill the plant cover to that limit. The

annual snowline, however, could have occupied positions below or above the elevation of the firn/ice margin in any particular year, just as it does today on glaciers and icecaps (Fig. 2.7). Therefore, the firn (or ice) margin that produced the well-defined trimline was the integrated (multi-year) ELA, developed in response to snowline oscillations that occurred over several, perhaps many, years.

Although most trimlines are abrupt, Ives' hypothesis does not exclude the possibility of "diffuse trimlines." In fact, there are many areas where diffuse boundaries did form rather than abrupt trimlines (Figs. 2.4, 2.7 and 2.8). Diffuse trimlines simply reflect perennial snowfields whose margins were more vulnerable to movement caused by variations in melt intensity. These diffuse trimlines are typically found on low angle slopes of fiord uplands or plateaus, where a small change in the altitude of the annual snowline would cause a larger area to be incorporated into either the accumulation or ablation areas. Abrupt trimlines are generally found in broad meltwater channels, on hilly terrain, and on uneven terrain (Fig. 2.8). Modern accumulation in broad meltwater channels and on hilly terrain generally reflects the prevailing wind direction (i.e., accumulation on the lee side of hills or former channel banks); therefore, trimlines associated with these features should reflect the prevailing wind direction during the time of trimline formation. On uneven or undulating terrain the processes of wind drifting favour accumulation in depressions and deflation from ridges capable of sustaining lichen cover (Figs.2.7 and 2.9). Koerner correctly identified this, but he insisted that it was linked to seasonally persistent snowfields, and that, "An exclusively climatic control would surely produce the reverse effect of permanent snowfields (i.e., lichen-free zones) on higher ground." (Koerner, 1980:92). In the simplest sense, this point is not argued; an

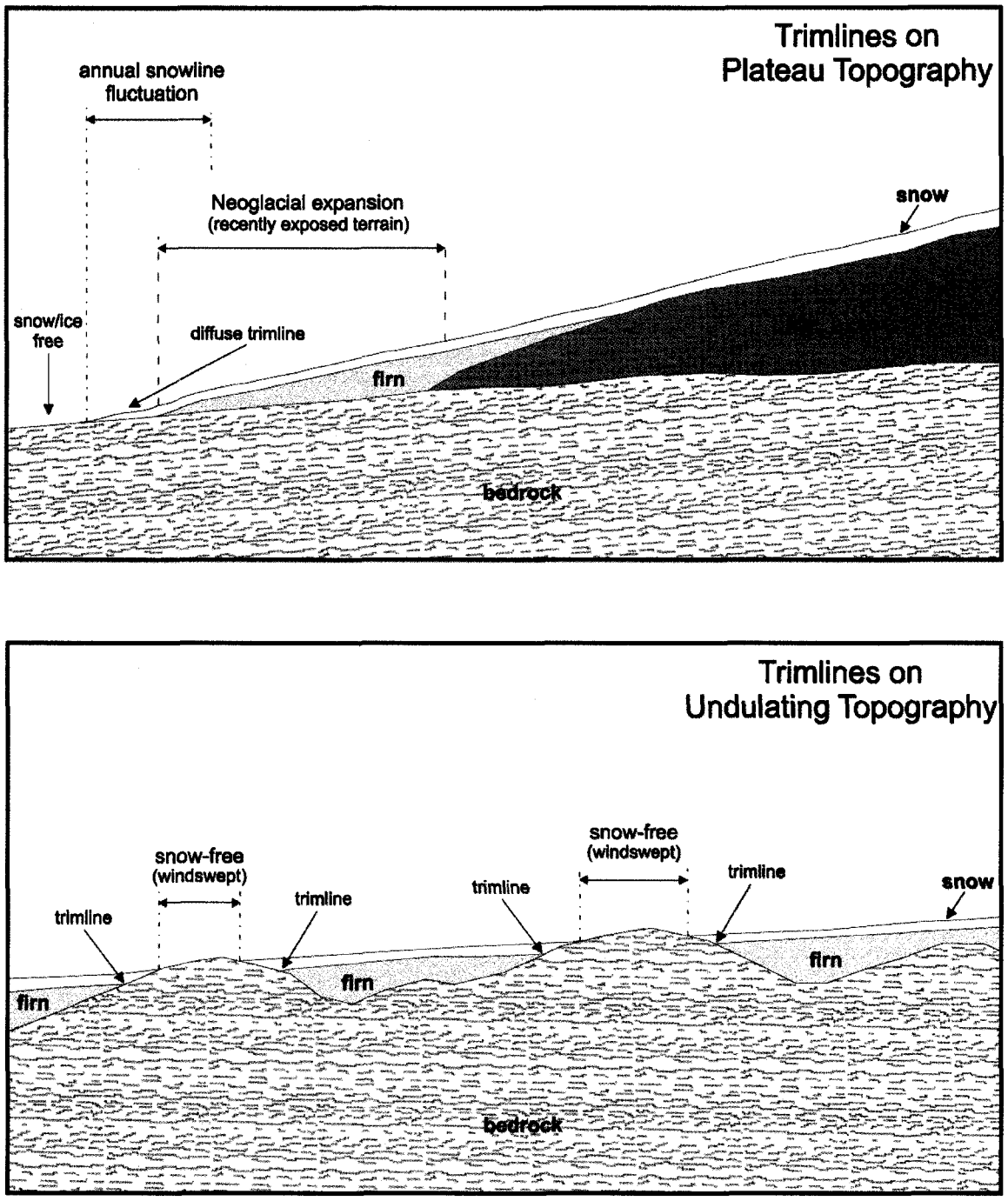

Figure 2. 7 Cross-section model of trimline formation. (A) diffuse trimline forming as a result of long-term snowline lowering on gently sloping terrain typical of plateau topography. After the snow has survived one melt season it is transformed into firn. The annual snowline fluctuates, intermittently exposing the firn/ice layer to melt, which results in the formation of a diffuse trimline. (B) trimlines formed on undulating terrain where the tops of the hillocks are deflated and the depressions are filled with drifted snow, eventually transformed into firn/ice. This creates a discontinuous trimline configuration and gives a mottled appearance to the landscape.

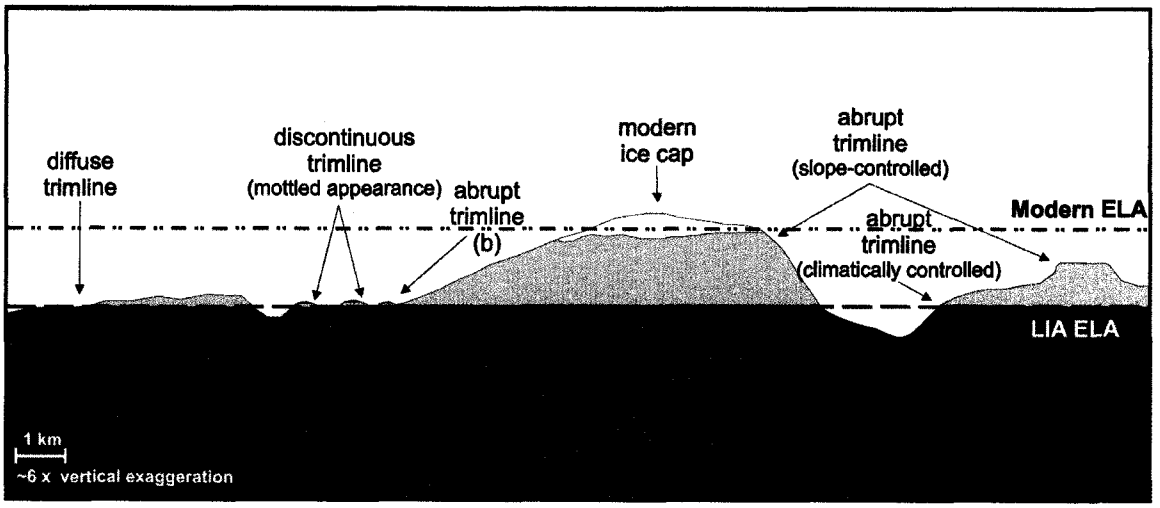

Figure 2. 8 Cross-section model of a High Arctic landscape showing modern ELA vs. LIA ELA. Lighter toned land above the LIA ELA indicates those areas which were largely covered by perennial snow and ice (i.e., within the accumulation area). Trimline forms are discontinuous, diffuse, abrupt climatically-controlled, and abrupt slope-controlled. Abrupt slope-controlled trimlines form where the terrain becomes too steep for snow to accumulate. Since these occur above the ELA, they are not considered climatically significant.

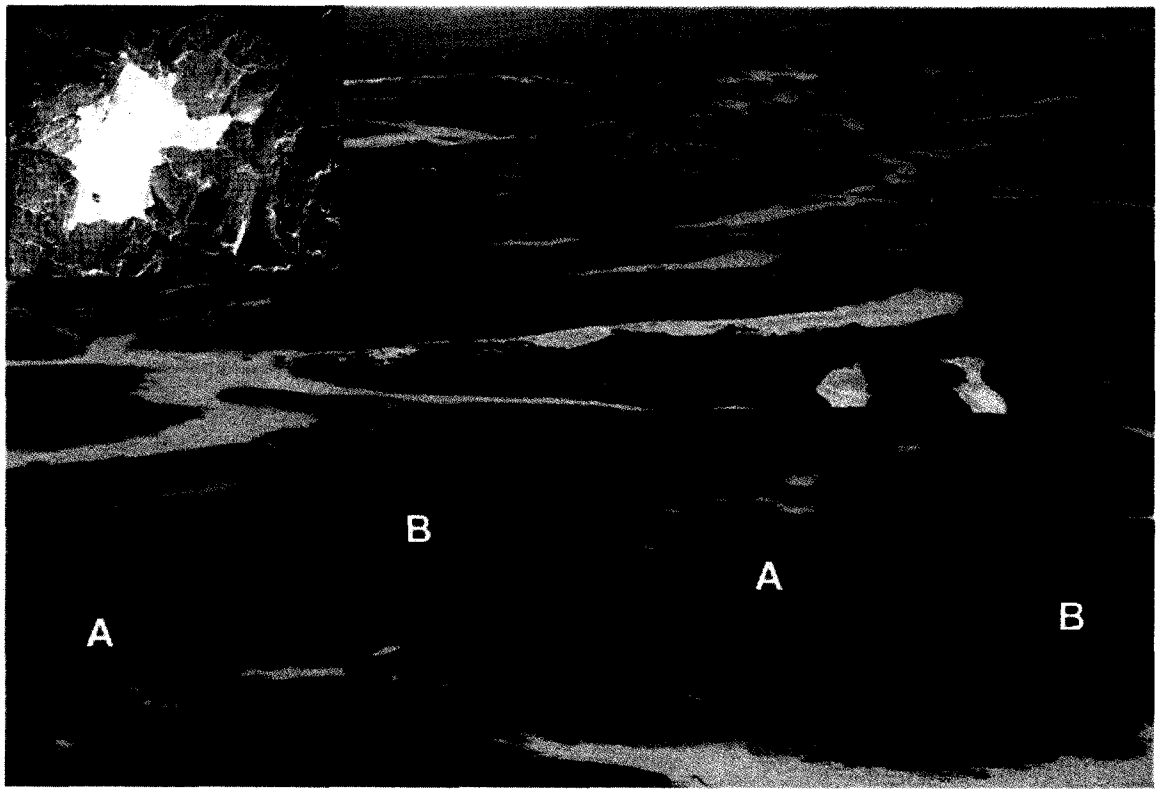

Figure 2. 9 Distal (lowest) region of a former plateau ice cap expansion area showing (A) lichen-free areas that resulted from accumulation and preservation of snow and ice in depressions, and (B) lichen covered higher areas where snow was removed by deflation (see Fig. 2.7b for related schematic diagram). Inset is a Landsat 7 ETM+ (2001) subset of the Blue Hills region and the south ice cap of W Melville Island. The dark rectangle on the inset image shows the approximate area captured by the photograph.

example of this "exclusively climatic control," causing lichen-free zones on higher ground, can be seen on numerous plateaus throughout the Canadian High Arctic (Fig. 2.9). However, on more topographically complex terrain, the climatic effect is complicated, but it is still a "climatic control," much the same as those controls that affect levels of glaciation in a region. Furthermore, if these topographically low areas are prone to frequent accumulation today, surely during the LIA, or other cold intervals throughout the Neoglacial, this condition would have been common because snow melt would have been limited.

2.3.2.4 Objection 4. The time of lichen-kill

Koerner's fourth objection was in regard to the time of lichen-kill, (i.e., the age of the perennial snow and ice expansion). He argued that, based on a few ^{14}C dates "... the evidence for a Little Ice Age permanent snowfield expansion and lichen-kill is not very compelling... only two dates are attributable to the Little Ice Age and these are on material collected close to present day ice masses..." (Koerner, 1980:90). This argument is correct: there were then and are now too few suitable ^{14}C dates on the event. The relevance of the existing age determinations is that they place the lichen and plant-kill event in the latest Holocene, which is all that can be expected of the method, given the non-constant atmospheric carbon production for this time interval (Stuiver, 1978). Refining the temporal constraints on this event is fundamental, and new methods for obtaining these must be explored.

2.3.2.5 Objection 5. The "degree" of lichen-kill

Koerner's final objection was based on the use of the terms "heavy" and "moderate" as applied by Andrews *et al.* (1976:76) in their descriptions of the extent of lichen-kill for large areas. Koerner stated, "Compounding the problem is the fact that there is a degree of lichen-kill... It is difficult to see how some permanent snowfields are more lethal than others'." (Koerner, 1980:89). This is an argument of semantics. Although the terms were not explicitly defined, Andrews *et al.* used "heavy" lichen-kill to describe vast areas devoid of mature lichen and plant covers, and "moderate" to portray those areas that have discontinuous (mottled) or diffuse patterns of lichen-kill. The word "heavy" is also used by Andrews *et al.* to portray a densely populated or mature lichen cover; hence, in both cases, "heavy" becomes synonymous with 'clearly defined.'

2.3.3 Revisiting Koerner's Hypothesis for the Origin of Trimlines

Koerner's objections to Ives' (1962) hypothesis do not lead us to reject the use of trimlines as a tool for paleoclimatic reconstruction. Furthermore, there appears to be a fundamental gap in Koerner's alternative ecological hypothesis for the formation of lichen-free zones, particularly in instances where sharp trimlines are observed. In Koerner's hypothesis, he states, "...lichen-free zones are coincident with snow covers that persist through a large part of, but not all, the melt season. These snow covers inhibit lichen growth by drastically reducing their growing season." (Koerner, 1980:91). According to this hypothesis, there are two possible mechanisms to explain sharp trimlines. The first possibility is that a sharp trimline must be formed by a pause (for

some critical length of time), of the annually retreating snow edge, followed by continued retreat. The location where the snow edge consistently pauses every year would then divide the terrain into biologically viable and biologically non-viable. The second possibility is that the annual retreat of the snow edge must progress at the same rate every year, whereby, the critical threshold in the growing season length is reached at the same location on the landscape year after year. These mechanisms are not feasible, given the inter-annual variability in snowline position in the Canadian Arctic. We found no consistently late-lasting snow cover in areas where trimlines have been documented. Moreover, even if consistent late-lasting snow cover had been observed, there seems to be no disadvantage to lichens that are uncovered later in the season compared to those that are uncovered earlier in polar desert environments (see Lichen Physiology above, Pannewitz *et al.*, 2003).

2.3.4 Using LIA Trimlines for Equilibrium-line Altitude Reconstruction

How can trimlines be used to reconstruct past climatic conditions? In order to answer this question, it is necessary to consider the type of perennial ice mass that was responsible for the creation of the trimlines, and whether the trimlines record a synchronous ice advance and retreat across a given region, such as the QEI.

In the High Arctic, numerous plateaus are at or just below the modern ELA (England *et al.*, 1981). Today, trimlines are widespread on these plateaus, and can be found around thin, stagnant cold-based ice caps (Figs. 2.4 and 2.5), as well as on fiord uplands and plateaus where ice has entirely disappeared (Fig. 2.8). These trimlines are analogous to those originally identified by Ives (1962) on Baffin Island, and are attributed

here to long-term snowline lowering below a former ice margin, forming snow aprons rather than expansion by active internal flow. If snow apron expansion produced these trimlines, then they record the former ELA, which provides an important proxy for climatic reconstruction. This interpretation is strengthened when ice cap trimlines are accordant with nearby trimlines linked to former perennial snowfields. In these cases, the trimlines must be the product of snowline lowering (rather than ice flow) beyond the former margin, and can be used as a record of the LIA ELA. Where ice cap trimlines extend to lower elevations than neighbouring trimlines produced by perennial snowfields, this disparity must be due to flow carrying ice into the ablation zone, precluding the use of these flow-produced trimlines as a record of the former ELA. Trimlines associated with former perennial snowbanks that were influenced by topography can also record exceptionally low ELAs that are less precise indicators of regional climate. While these features do provide some information about former environmental conditions, their survival is often the product of other factors, such as wind drifting and aspect.

2.4 Conclusions

Trimlines associated with former snow and ice expansions in the Canadian Arctic can be used for paleoenvironmental reconstruction. Their interpretation involves both glaciological and biological considerations, especially concerning lichenological research relevant to their origin. One of the key arguments that trimlines do record former ELAs comes from widespread areas where the lower limit of former perennial snowfields or ice patches, as defined by trimlines, are accordant with trimlines left by small plateau ice caps. However, there is still a lack of certainty with regard to the timing of the event that

produced the trimlines; the application of new dating techniques on this facet of the Arctic landscape is essential to refining the temporal resolution of its formation.

Revalidating the use of LIA trimlines is important for several reasons. First, mapping LIA trimlines may offer further insight into past glaciations by using the Neoglacial ice cover as an example of Arctic ice nucleation, serving as a possible precursor to the build-up of the Innuitian Ice Sheet that occupied the QEI during the last glaciation (i.e., late Wisconsinan, Blake, 1970; 1972; 1992; Bednarski, 1998; Dyke, 1999; England, 1999; Dyke *et al.*, 2002). Second, they can be used to provide a measure of the amount of snow and ice present near the onset of the 20th century and hence, as a measure of the subsequent reduction that has occurred. Third, relative to modern climatic conditions, the reconstructed ELAs can be used to help estimate temperature and precipitation changes between the LIA and present. Finally, mapping LIA trimlines can provide a valuable dataset of snow and ice extent and attendant climatic conditions to test coupled ice-climate model simulations of the LIA and post-LIA warming; successfully modeling these changes will help improve our ability to assess the impacts of predicted future climate change on Arctic glaciers and sea level.

2.5 References

Alexopoulos, C. J., Mims, C. W., Blackwell, M., 1996: *Introductory Mycology*. Toronto: John Wiley and Sons, Inc., 868 pp.

Andrews, J. T. and Webber, P., 1964: A lichenometrical study of the northwestern margin of the Barnes Ice Cap; a geomorphological technique. *Canada Department of Mines and Technical Surveys, Geography Bulletin (Ottawa),* 22: 80-104.

Andrews, J. T., Barry, R.G., Davis, P.T., Dyke, A.S., Mahaffy, M, Williams, L.D. and Wright, C., 1975: The Laurentide Ice Sheet: Problems of the mode and speed of inception. *World Meteorological Publication,* 421: 87-94.

Andrews, J. T., Davis, P. T., Wright, C., 1976: Little Ice Age permanent snowcover in the Eastern Canadian Arctic: Extent Mapped from Landsat-1 satellite imagery. *Geografiska Annaler,* 58A: 71-81.

Bahr, D. B., Pfeffer, W. T., Sassolas, C., Meier, M. F., 1998: Response time of glaciers as a function of size and mass balance: 1. Theory. *Journal of Geophysical Research,* 103: 9777-9782.

Barry, R. G., Andrews, J.T., Mahaffy, M.A., 1975: Continental ice sheets: conditions for growth. *Science,* 190: 979-981.

Bednarski, J. H., 1998: Quaternary history of Axel Heiberg Island bordering Nansen Sound, Northwest Territories, emphasising the last glacial maximum. *Canadian Journal of Earth Sciences,* 35: 520-533.

Bednarski, J. H., 2002: Surficial geology, northeast Bathurst Island, Nunavut. *Geological Survey of Canada, Map 2011A, scale 1:100 000.*

Benedict, J. B., 1990: Lichen Mortality Due to Late-Lying Snow - Results of a Transplant Study. *Arctic and Alpine Research,* 22: 81-89.

Benedict, J. B., 1991: Experiments on Lichen Growth .2. Effects of a Seasonal Snow Cover. *Arctic and Alpine Research,* 23: 189-199.

Benn, D. I., Evans, D. J. A., 1998: *Glaciers and Glaciation.* . London: Oxford University Press, 734 pp.

Bergsma, B. M., Svoboda, J., Fredman, B., 1984: Entombed plant communities released by a retreating glacier at Central Ellesmere Island, Canada. *Arctic,* 37: 49-52.

Beschel, R., 1961: "Dating Rock Surfaces by Lichen Growth and its Application to Glaciation and Physiography (Lichenometry),". *Geology of the Arctic*: 1044-1062.

Blake, W., Jr., 1970: Studies of the glacial history in Arctic Canada I: Pumice, radiocarbon dates and differential postglacial uplift in the eastern Queen Elizabeth Islands. *Canadian Journal of Earth Sciences,* 7: 634-664.

Blake, W., Jr., 1972: Climatic implications of radiocarbon-dated driftwood in the Queen Elizabeth Islands, Arctic Canada. *In* Vasari, Y., Hyvarinen, H., and and Hicks, S. (eds.), *Climatic change in the arctic areas during the last ten thousand years.* Oulu, Finland, 77-104.

Blake, W., 1992: Holocene Emergence at Cape-Herschel, East-Central Ellesmere-Island, Arctic Canada - Implications for Ice-Sheet Configuration. *Canadian Journal of Earth Sciences,* 29: 1958-1980.

Bradley, R. S., 1990: Holocene paleoclimatology of the Queen Elizabeth Islands, Canadian High Arctic. *Quaternary Science Reviews,* 9: 365-384.

Bradley, R. S., 1999: *Paleoclimatology: Reconstructing climates of the Quaternary*. 2nd ed. San Diego: Academic Press.

Dredge, L. A., 2004: Surficial geology, Ekalugad Fiord (West half), Baffin Island, Nunavut. Geological Survey of Canada, Map 2073A, scale 1:250 000.

Dredge, L. A., 2004: Surficial geology, McBeth Fiord (West half), Baffin Island, Nunavut. Geological Survey of Canada, Map 2074A, scale 1:250 000.

Dredge, L. A., 2004: Surficial geology, Lake Gillian, Baffin Island, Nunavut. Geological Survey of Canada, Map 2076A, scale 1:250 000.

Dyke, A. S., 1978: Indications of Neoglacierization on Somerset Island, District of Franklin. *Scientific and Technical Notes,,* Current Research, Part B; Geologica Survey of Canada: 215-217.

Dyke, A. S., 1999: Last Glacial Maximum and deglaciation of devon island, Arctic Canada: support for an Innuitian Ice Sheet. *Quaternary Science Reviews,* 18: 393-420.

Dyke, A. S., 2000: Surficial geology, Phillips Creek, Baffin Island. Geological Survey of Canada, Map 1961A, scale 1:250 000.

Dyke, A. S., 2000: Surficial geology, Milne Inlet, Baffin Island. Geological Survey of Canada, Map 1962A, scale 1:250 000.

Dyke, A. S., 2000: Surficial geology, Moffet Inlet and Fitzgerald Bay, Baffin Island. Geological Survey of Canada, Map 1963A, scale 1:250 000.

Dyke, A. S., 2000: Surficial geology, Arctic Bay, Baffin Island. Geological Survey of Canada, Map 1964A, scale 1:250 000.

Dyke, A. S., 2000: Surficial geology, Navy Board Inlet, Baffin Island. Geological Survey of Canada, Map 1965A, scale 1:250 000.

Dyke, A. S. and Hooper, J., 2000: Surficial geology, Berlinguet Inlet and Bourassa Bay, Baffin Island. Geological Survey of Canada, Map 1960A, scale 1:250 000.

Dyke, A. S., 2001: Surficial geology, eastern Devon Island. Geological Survey of Canada, Map 1970A, scale 1:250 000.

Dyke, A. S., 2001: Surficial geology, central Devon Island. Geological Survey of Canada, Map 1971A, scale 1:250 000.

Dyke, A. S., 2001: Surficial geology, western Devon Island. Geological Survey of Canada, Map 1972A, scale 1:250 000.

Dyke, A. S., 2001: Surficial geology, Grinnell Peninsula, Devon Island. Geological Survey of Canada, Map 1973A, scale 1:250 000.

Dyke, A. S., 2001: Surficial geology, Cardigan Strait, Devon Island and Ellesmere Island. Geological Survey of Canada, Map 1974A; scale 1:250 000.

Dyke, A. S., Andrews, J.T., Clark, P.U., England, J.H., Miller, G.H., Shaw, J., Veillette, J.J., 2002: The Laurentide and Innuitian ice sheets during the Last Glacial Maximum. *Quaternary Science Reviews,* 21: 9-31.

Dyke, A. S., 2003: Surficial geology, Erichsen Lake, Baffin Island, Nunavut., *Geological Survey of Canada, Open File 4484. CDROM with digital files (geology, topography, and hydrology) of Open Files 1598-1613 (previously released as paper maps at 1:50 000 scale).*

Dyke, A. S., 2004: Surficial geology, Erichsen Lake, Baffin Island, Nunavut., *Geological Survey of Canada, Map 2066A, scale 1:250 000.*

Edlund, S. A., 1985: Lichen-free zones as neoglacial indicators on western Melville Island, District of Franklin. *Current Research, Part A, Geological Survey of Canada,* Paper 85-1A: 709-712.

England, J., Kershaw, L., LaFarge-England, C., Bednarski, J., 1981: *Northern Ellesmere Island: A natural resources inventory.* Edmonton: University of Alberta, Department of Geography, 237 pp.

England, J., 1999: Coalescent Greenland and Innuitian ice during the Last Glacial Maximum: revising the Quaternary of the Canadian High Arctic. *Quaternary Science Reviews,* 18: 421-456.

England, J., Atkinson, N., Dyke, A., Evans, D., and Zreda, M., 2004: Late Wisconsinan buildup and wastage of the innuitian Ice Sheet across southern Ellesmere Island, Nunavut. *Canadian Journal of Earth Sciences,* 41: 39-61.

Falconer, G., 1966: Preservation of vegetation and patterned ground under a thin ice body in north Baffin Island, N.W.T., Canada. *Geographical Bulletin,* 8: 194-200.

Farnell, R., Hare, P. G., Blake, E., Bowyer, V., Schweger, C., Greer, S., and Gotthardt, R., 2004: Multidisciplinary investigations of Alpine ice patches in southwest Yukon, Canada: Paleoenvironmental and paleobiological investigations. *Arctic,* 57: 247-259.

Flohn, H., 1974: Background to a geophysical model of the initiation of the next glaciation. *Quaternary Research,* 4: 385-404.

Gajewski, K. and Atkinson, D. A., 2003: Climatic change in northern Canada. *Environmental Reviews,* 11: 69-102.

Gannutz, T. P., 1970: Photosynthesis and Respiration of Plants in the Antarctic Peninsula Area. *Antarctic Journal of the United States,* 5: 49-51.

Green, T. G. A., Schroeter, B., and Sancho, L. G., 1999: *Plant life in Antarctica.* New York: Dekker, 495-543 pp.

Grove, J. M., 1988: *The Little Ice Age.* London: Methuen, 500 pp.

Hodgson, D. A., 1992: Quaternary geology of western Melville Island, Northwest Territories. *Geological Survey of Canada,* Paper 89-21: 1-35.

Hooper, J. and Dyke, A. S., 2000: Surficial geology, Agu Bay and Easter Cape, Baffin Island. Geological Survey of Canada, Map 1959A, scale 1:250 000.

IPCC, 2001: *Climate Change 2001: Impacts, Adaptation andVulnerability.* Cambridge, New York: Cambridge University Press, 1042 pp.

Ives, J. D., 1957: Glaciation of the Torngat Mountains, Northern Labrador. *Arctic,* 10: 67-87.

Ives, J. D., 1962: Indication of recent extensive glacierization in north central Baffin Island, N.W.T. *Journal of Glaciology,* 4: 197-205.

Ives, J. D., Andrews, J. T., Barry, R.G., 1975: Growth and decay of the Laurentide Ice Sheet and comparisons with Fenno-Scandinavia. *Naturwissenschaften,* 62: 118-125.

Johannesson, T., Raymond, C. F., Waddington, E. D., 1989: Time-scale adjustments of glaciers to changes in mass balance. *Journal of Glaciology,* 35: 355-369.

Kappen, L., Sommerkorn, M., and Schroeter, B., 1995: Carbon acquisition and water relations of lichens in polar regions - Potentials and limitations. *Lichenologist,* 27: 531-545.

Kappen, L., Schroeter, B., Green, T. G. A., and Seppelt, R. D., 1998: Microclimatic conditions, meltwater moistening, and the distributional pattern of Buellia frigida on rock in a southern continental Antarctic habitat. *Polar Biology,* 19: 101-106.

Kaufman, D. S., Ager, T.A., Anderson, N.J., Anderson, P.M., Andrews, J.T., Bartlein, P.J., Brubaker, L.B., Coats, L.L., Cwynar, L.C., Duvall, M.L., Dyke, A.S., Edwards, M.E., Eisner, W.R., Gajewski, K., Geirsdottir, A., Hu, F.S., Jennings, A.E., Kaplan, M.R., Kerwin, M.W., Lozhkin, A.V., MacDonald, G.M., Miller, G.H., Mock, C.J., Oswald, W.W., Otto-Bliesner, B.L., Porinchu, D.F., Ruhland, K., Smol, J.P., Steig, E.J. and Wolfe, B. B., 2004: Holocene thermal maximum in the western Arctic (0-180°W). *Quaternary Science Reviews,* 23: 529-560.

Koerner, R. M., 1980: The problem of lichen-free zones in Arctic Canada. *Arctic and Alpine Research,* 12: 87-94.

Koerner, R. M., 1989: *Queen Elizabeth Islands Glaciers. In Chapter 6, Quaternary Geology of the Queen Elizabeth Islands, In Quaternary Geology of Canada and Greenland*: Geological Survey of Canada, 464-473 pp.

Koerner, R. M. and Fisher, D. A., 1990: A record of Holocene summer climate from a Canadian high-Arctic ice core. *Nature,* 343: 630-631.

Körner, C., 1999: *Alpine plant life.* New York: Springer.

Lamoureux, S., 2000: Five centuries of interannual sediment yield and rainfall-induced erosion in the Canadian High Arctic recorded in lacustrine varves. *Water Resources Research,* 36: 309-318.

Lamoureux, S. F., England, J. H., Sharp, M. J. and Bush, A. B. G., 2001: A varve record of increased 'Little Ice Age' rainfall associated with volcanic activity, Arctic Archipelago, Canada. *The Holocene,* 11: 243-249.

Lamoureux, S. F., Gilbert, R., and Lewis, T., 2002: Lacustrine sedimentary environments in high arctic proglacial Bear Lake, Devon Island, Nunavut, Canada. *Arctic Antarctic and Alpine Research,* 34: 130-141.

Levesque, E. and Svoboda, J., 1999: Vegetation re-establishment in polar "lichen-kill" landscapes: a case study of the Little Ice Age impact. *Polar Research,* 18: 221-228.

Lewkowicz, A. G. and Harry, D. G., 1991: Internal structure and environmental significance of a perennial snowbank, Melville Island, NWT. *Arctic,* 44: 74-82.

Locke, C. W. and Locke, W. W., 1977: Little Ice Age snow-cover extent and paleoglaciation thresholds: North-central Baffin Island, N.W.T., Canada. *Arctic and Alpine Research,* 9: 291-300.

Miller, G. H., Bradley, R. S. and Andrews, J. T., 1975: The glaciation level and lowest equilibrium line altitude in the High Canadian Arctic: maps and climatic interpretation. *Arctic and Alpine Research,* 7: 155-168.

Nye, J. F., 1963: On the Theory of the Advance and Retreat of Glaciers. *Geophysical Journal of the Royal Astronomical Society,* 7: 431-456.

O' Cofaigh, C. O., England, J., and Zreda, M., 2000: Late Wisconsinan glaciation of southern Eureka Sound: evidence for extensive Innuitian Ice in the Canadian High Arctic during the Last Glacial Maximum. *Quaternary Science Reviews,* 19: 1319-1341.

Oerlemans, J., 2002: On glacial inception and orography. *Quaternary International,* 95-6: 5-10.

Overpeck, J., K., Hughen, K., Hardy, D., Bradley, R., Case, R., Douglas, M., Finney, B., Gajewski, K., Jacoby, G., Jennings, A., Lamoureux, S., Lasca, A., MacDonald, G., Moore, J., Retelle, M., Smith, S., Wolfe, A., and Zielinski, G., 1997: Arctic environmental change of the last four centruries. *Science,* 278: 1251-1256.

Pannewitz, S., Schlensog, M., Green, T. G. A., Sancho, L. G., and Schroeter, B., 2003: Are lichens active under snow in continental Antarctica? *Oecologia,* 135: 30-38.

Pfeffer, W. T., Sassolas, C., Bahr, D. B., Meier, M. F., 1998: Response time of glaciers as a function of size and mass balance: 2. Numerical experiments. *Journal of Geophysical Research,* 103: 9783-9789.

Pomeroy, J. and Brun, E., 2001: Physical properties of snow. *In* Jones, H. G., Pomeroy, J., Walker, D.A., and Hoham, R. (eds.), *Snow ecology: an interdisciplinary examination of snow-covered ecosystems*. Cambridge: Cambridge University Press, 45-127.

Raven, P. H., Evert, R. F., and Eichhorn, S. E., 1992: *Biology of Plants*. 5th ed. New York: Worth, 944 pp.

Schroeter, B., Green, T. G. A., Kappen, L., and Seppelt, R. D., 1994: Carbon dioxide exchange at subzero temperatures. Field measurements on Umbilicaria aprina in Antarctica. *Cryptogam Botany,* 4: 233-241.

Williams, L. D., 1975: The variation of corrie elevation and equilibrium line altitude with aspect in Eastern Baffin Island, N.W.T., Canada. *Arctic and Alpine Research,* 7: 169-181.

Williams, R. S. J. and Ferrigno, J. G., 2002: *Introduction. In: Satellite Image Atlas of Glaciers of the World. Glaciers of North America - Glaciers of Canada.* Washington: U.S. Geological Survey, 405 pp.

3 CHAPTER THREE

High-resolution multispectral techniques for mapping former Little Ice Age terrestrial ice cover in the Canadian High Arctic

3.1 Introduction

Over the past few decades, persistent warming has given rise to increasing concern about the worldwide mass loss of glaciers and the accompanying rise in sea level (Dyurgerov and Meier, 1997; Church *et al.*, 2001: Arendt *et al.*, 2002). In Polar Regions, temperature increases have exceeded those elsewhere on the globe, and climate model projections indicate that this trend will continue; hence, the Arctic is a key areas in which to monitor and investigate past and present climatic variability (IPCC, 2001a,b).

In the Canadian Arctic, climate amelioration since the termination of the Little Ice Age (LIA, ~1600-1900 AD) has led to the widespread reduction of terrestrial ice cover, and the subsequent exposure of trimlines, indicating its former maximum LIA extent. Documenting the former LIA terrestrial ice extent is important, as it provides a reference against which the rate and nature of present and future changes may be compared. However, with continued warming and the inevitable change in land cover associated with arctic regions (revegetation, periglacial activity, etc.), this paleoenvironmental proxy will eventually be erased from the landscape. It is, therefore, timely and important to accurately map and monitor these potentially rapid changes (Belward *et al.*, 1999).

Investigations of LIA terrestrial ice cover have principally been conducted on the characteristically lichen covered Precambrian bedrock of Baffin Island (Ives, 1962; Andrews *et al.*, 1976; Locke and Locke, 1977). In these studies, trimlines were visually identified and recently deglaciated areas were mapped manually using panchromatic

sources (e.g., aerial photos and Landsat 1 satellite imagery) in conjunction with field verification. However, high-resolution multispectral satellite imagery (i.e., Landsat 7 ETM+ and ASTER, see below), now available for high latitude polar areas such as the Canadian High Arctic, provide the opportunity for automated and semi-automated mapping of subtle surficial features (e.g., trimlines) by means of multispectral classification. Such classification techniques provide a more objective approach than manual digitization, drastically reduce processing time, and are widely applicable across large regions (Dunn *et al.*, 1990).

Identifying trimlines surrounding recently deglaciated terrain using panchromatic sources can be difficult, perhaps impossible, in some areas of the Queen Elizabeth Islands (QEI) (Fig. 3.1). The QEI are predominantly comprised of Paleozoic and Mesozoic sedimentary rocks, upon which vegetation is sparse. Consequently, the spatial distribution of late Holocene perennial snow and ice remains, for the most part, undocumented in an area of the Canadian Arctic nearly twice the size of Great Britain. This paper presents techniques for mapping recently deglaciated terrain over broad areas of the Canadian Arctic using high-resolution multispectral satellite imagery and digital elevation models (DEMs), and addresses some of the issues involved with accurately extracting surficial information in remote polar desert environments.

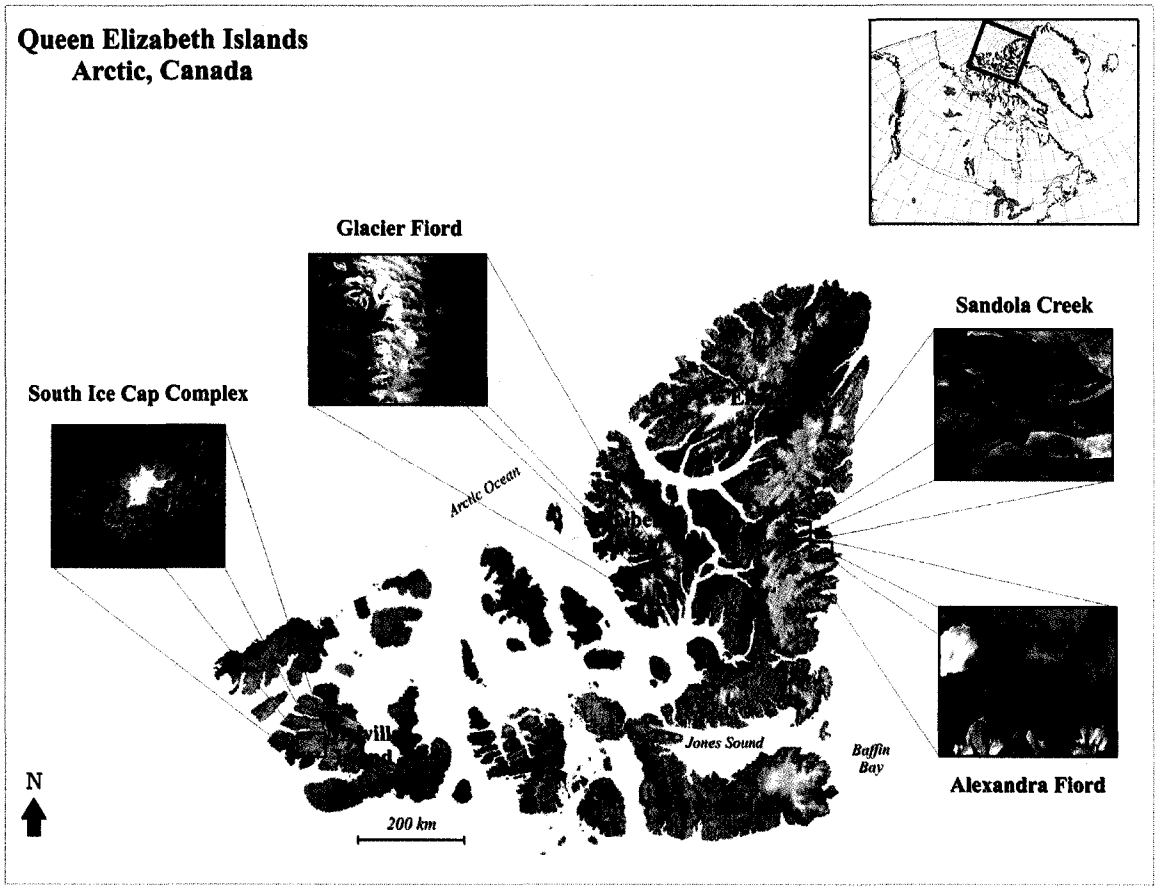

Figure 3. 1 Map of the Queen Elizabeth Islands and subset locations (Radarsat Orthomosaic of Canada courtesy of the Canadian Centre for Remote Sensing).

3.2 Study Area

The QEI are the northernmost part of the Canadian Arctic Archipelago, extending from 74 to 83° N (Fig. 3.1). Although classified as a polar desert, the QEI contain 5% of the terrestrial ice found in the Northern Hemisphere (Koerner, 1989). The eastern QEI (Devon, Axel Heiberg, and Ellesmere Islands) consist of mountains reaching 2500 m that support extensive ice caps and outlet glaciers. In contrast, the western QEI are much lower and hence tend to be largely ice-free today, with the exception of Meighen Island, which supports a small ice cap below 300 m elevation, and western Melville Island, where some plateaus above 600 m support small ice caps.

3.3 Background

Following the termination of the LIA (~1900 in Arctic Canada), a marked decrease in the areal extent of terrestrial ice was observed in glaciated regions around the globe (Grove, 1988). Throughout these glaciated regions, including Arctic Canada, the former limit of ice extent is, in many cases, delineated by lighter-toned recently deglaciated zones that display an abrupt ice-distal margin, extending back to the modern ice mass. These margins, often referred to as "trimlines," are recognized to be the result of weathering and erosion on surfaces that have been subjected to scouring by glacial flow, the recent deposition of drift, or the removal of vegetation. In the High Arctic, trimlines occur adjacent to glaciers and ice caps, and record the former position and extent of perennial snowfields. When trimlines associated with the recent retreat of thin plateau ice caps and perennial snow and ice fields are accordant, they can serve as important LIA

paleoclimatic indicators (Wolken *et al.*, 2005). Trimlines are most apparent on crystalline Precambrian terrain, where they appear as lighter-toned patches surrounded by darker terrain, on which well-developed vegetation and lichen communities exist. Although trimlines also exist on carbonate terrain, they are only subtly apparent due to the impoverished condition of the High Arctic flora on these calcareous surfaces (Fig. 3.2). Nonetheless, ground observations indicate that trimlines on carbonate substrates are discernible and are principally the product of slightly less surface weathering and less developed patterned ground within the trimline (Wolken *et al.*, 2005). This difference in the physical characteristics of the substrate results in albedo differentiation, which is detectible using high-resolution multi-spectral satellite imagery and aerial photographs.

Trimlines have commonly been used as evidence for the retreat of terrestrial ice following the LIA. Andrews *et al.* (1976) and Locke and Locke (1977) reported the first reconstructions of LIA snow and ice cover on north-central Baffin Island. Both groups of researchers used aerial photos and Landsat-1 satellite imagery, combined with field work, to manually map regionally extensive lichen-free areas that corresponded to former snow cover thought to be coeval with the LIA. Subsequently, surficial geology mapping projects on Baffin and Devon Islands included areas of lichen-free terrain in their publications, which were interpreted as areas of early plant recolonization following the removal of perennial snow and ice fields (Hodgson, 1992; Hooper and Dyke, 2000; Dyke and Hooper, 2000; Dyke, 2000a-e; 2001a-e; 2003; 2004; Bednarski, 2002; Dredge, 2004 a, b).

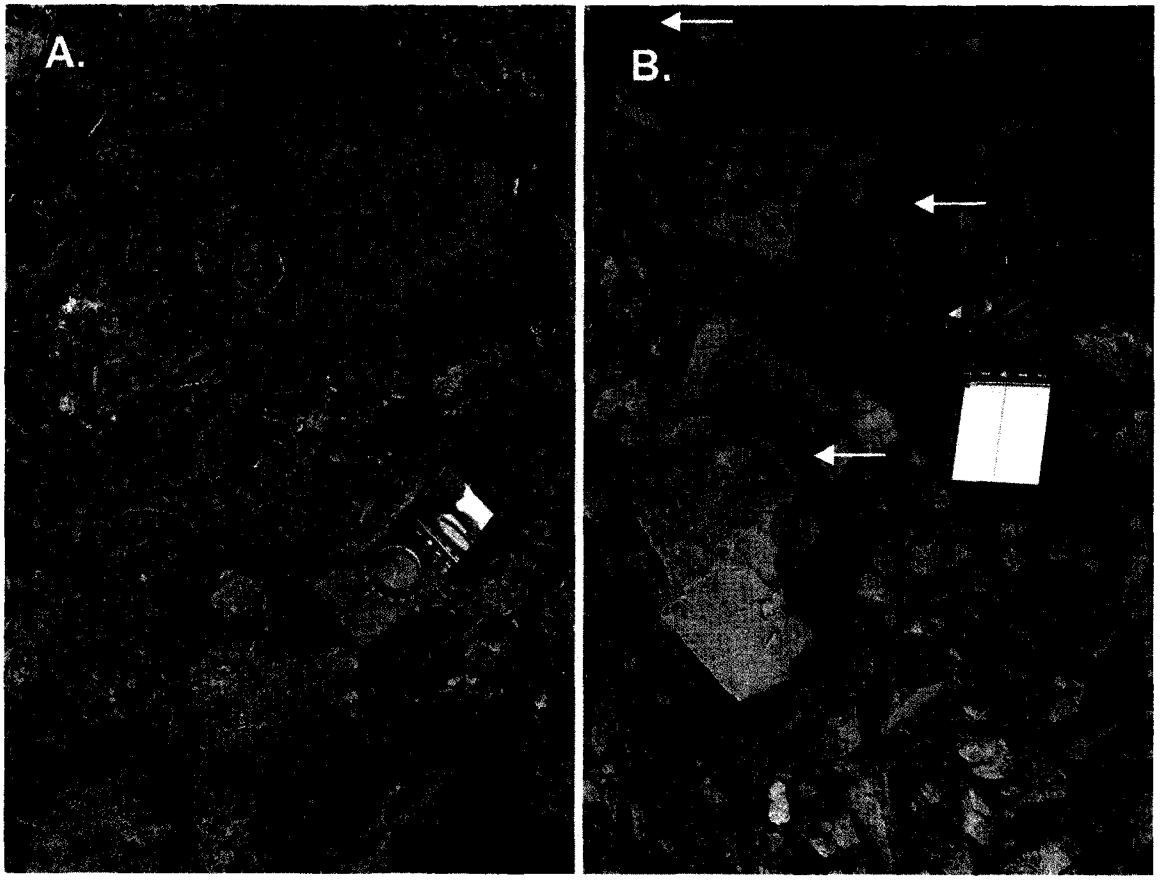

Figure 3. 2 (A) Precambrian siliceous substrate with mature plant and lichen communities, Alexandra Fiord subset, Johan Peninsula, Ellesmere Island, Canada. (B) Sparsely vegetated Paleozoic carbonate substrate; arrows point to single plants, Sandola Creek subset, Knud Peninsula, Ellesmere Island, Canada.

3.4 Methodology

3.4.1 Data sources

For this study, data from two high-resolution multispectral sensors offering the greatest coverage of the Canadian High Arctic were selected for comparison: Advanced Spaceborne Thermal Emission and Reflection Radiometer (ASTER) aboard the Terra satellite, and Enhanced Thematic Mapper Plus (ETM+) on the Landsat 7 satellite. ASTER has a swath width of 60 km and offers 14 spectral bands: Visual and Near Infrared (VNIR) (bands 1-3 nadir) with a spectral range of 520 to 760 nm and a 15 m spatial resolution; Short Wavelength Infrared (SWIR) (bands 4-9) with a spectral range of 1600 to 2430 nm and a 30 m spatial resolution; and Thermal Infrared (TIR) (bands 10-14) with a spectral range of 8125 to 11650 nm and a 90 m spatial resolution. ASTER is capable of imaging globally and has a ground track repeat cycle of 16 days (or 233 orbits); however, cloud-free summer ASTER coverage is currently incomplete (~90%) over the QEI (e.g., W Melville Island). ETM+ has a swath width of 185 km, with nearly complete cloud-free summer-time coverage of the QEI. ETM+ has seven spectral bands: VNIR and SWIR (bands 1-5 and 7) with a spectral range of 450 to 2350 nm and spatial resolution of 30 m; and a TIR band (band 6) with a spectral range of 10400 to 12500 nm and a spatial resolution of 60 m.

Four areas in the QEI were selected for conducting classification experiments on recently deglaciated terrain. Each area was selected based on different bedrock geology, surficial materials, and contrasting topographic complexity, for the purpose of creating an experimental group representative of the Canadian High Arctic (Fig. 3.1). A total of eight satellite images were obtained for this study: four ASTER and four ETM+ images,

all of which had late-summer data acquisition times, when seasonal snow cover was at a minimum (Table 3.1). Area characteristics are tabulated in Table 3.1, and procedural steps are illustrated in a workflow schematic diagram in Figure 3.3.

3.4.2 Image processing

All ETM+ images were georeferenced to 1:250,000 National Topographic System (NTS) map sheets using Universal Transverse Mercator (UTM) projection on the NAD83 datum. All ASTER images were georeferenced to the corresponding geo-registered ETM+ images using the same projection and datum definitions. All images were then orthorectified in ERDAS Imagine 8.6 using digital elevation models (DEMs), derived from the 1:250,000 Canadian Digital Elevation Data set (CDED). For each image, a minimum of 32 ground control points (GCPs) were collected from clearly identifiable features to produce a Root Mean Square Error (RMSE) of < 1.4 pixels for both ETM+ and ASTER datasets, which is equivalent to 40 m and 21 m respectively. Subsets of the experimental areas were then extracted from each ASTER and ETM+ scene.

3.4.3 Classifications

Numerous standardized techniques exist for extracting spatial information from remotely sensed data. Image classification is a common procedure for data extraction in land cover studies, whereby pixels of unknown class membership are assigned to a specific class according to their common spectral characteristics (Foody, 1992). In the Canadian High Arctic, discriminating recently deglaciated terrain from other land cover

Location	Subset Abreviation	Subset Area (km^2)	Sensor	Sensor Resolution (m)	Acquisition Date & Time/Path-Row	Topographic Complexity	Geology
Alexandra Fiord, Ellesmere Island	AF	493	ASTER	15	03-07-02 00:16:24	Medium	Precambrian; colluvial blocks and rubble with sand and silt derived from crystalline bedrock
	AF	493	ETM+	30	27-06-00 p040, r004		
Sandola Creek, Ellesmere Island	SC	493	ASTER	15	04-07-03 18:38:43	Medium	Paleozoic; colluvial rubble and silt derived from carbonate and consolidated fine clastic sedimentary rock substrate
	SC	493	ETM+	30	28-06-00 p047, r003		
Glacier Fiord, Axel Heiberg Island	GF	493	ASTER	15	03-08-01 20:00:54	High	Mesozoic; colluvial rubble and silt derived from carbonate and consolidated fine clastic sedimentary rock substrate; colluvial silt, clay, and fine sand derived from weakly consolidated shale and siltstone substrate
	GF	493	ETM+	30	22-07-99 p053r003		
South Ice Cap, Melville Island	SIC	1334	ASTER	15	11-07-03 20:24:44	Low	Paleozoic; blocks and rubble in sand or silt matrix derived from quartzitic sandstone
	SIC	1373	ETM+	30	01-08-99 p059, r006		

Table 3. 1 Subset and Image information.

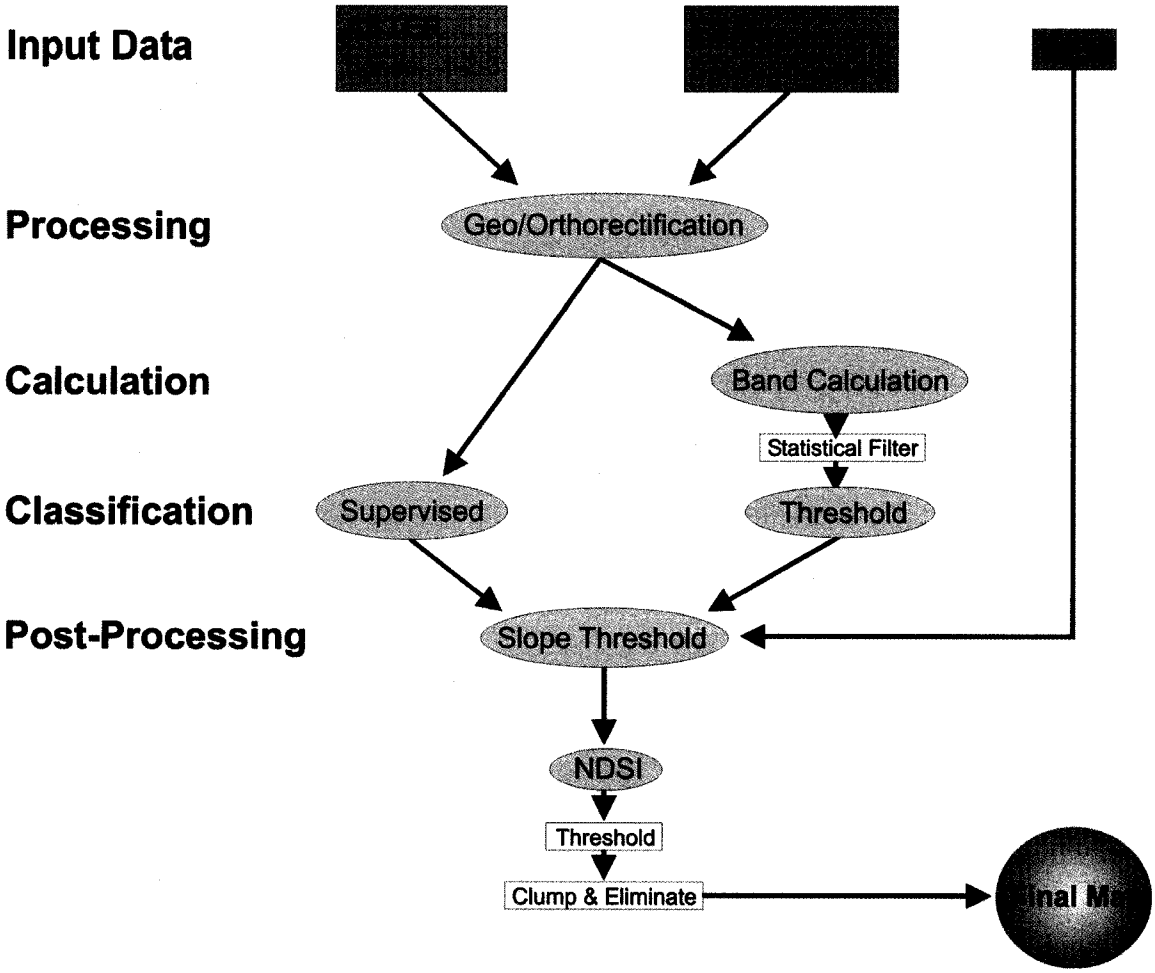

Figure 3. 3 Work flow diagram for mapping recently deglaciated LIA ice cover in the Canadian Arctic. Row headings (bold) indicate major steps in the methodology.

classes can be difficult due to the lack of vegetation, the variability of exposed lithologies, and the subsequent subtle differences between such land cover classes.

The classification approaches employed in this study were the result of judicious evaluations of land cover spectra and rigorous pre-testing (Fig. 3.4). From this pre-testing, two types of classification techniques, for each subset, were identified, which yielded the most promising results for isolating the spectral signatures of recently deglaciated terrain from other land cover categories (Table 3.2). Selections of classification types were dependent on two general requirements: accuracy and processing time. Given the large spatial extent of the Canadian Arctic, reasonable processing times associated with remotely sensed data are essential, but this limitation restricted the complexity of the classification types chosen.

Supervised classifications were conducted on each subset image by selecting training sites of known land cover, previously verified during fieldwork. Spectral characteristics were collected from recently deglaciated terrain (within trimlines) using VNIR bands for ASTER (bands 1-3) and ETM+ (bands 1-5). Following pre-testing of a range of decision rules (e.g., parallel-piped, minimum distance, and fuzzy) on each subset image, maximum likelihood parametric decision rules were used to classify the pixels. Maximum likelihood is a probabilistic classification approach that uses multivariate statistics (mean and variance-covariance) to make decisions regarding the class residence of each pixel (Maselli *et al.*, 1990).

The use of common classification indices (e.g., RVI, NDVI, SAVI, MSAVI etc.) for their intended uses was not beneficial in this study, but the detection of subtle uncorrelated bands associated with recently deglaciated terrain led to the selection of

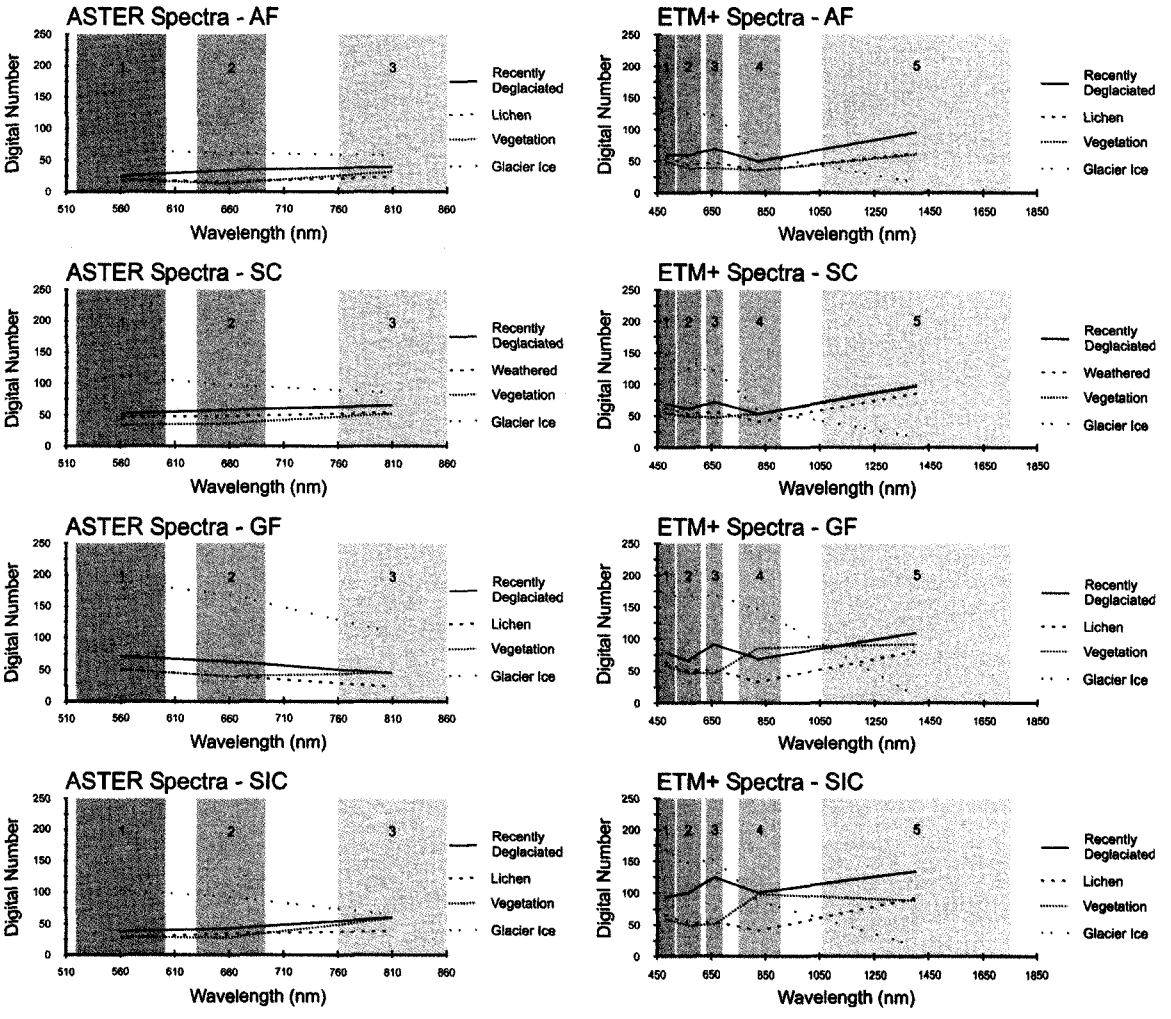

Figure 3. 4 Subset specific ASTER (bands 1-3) and ETM+ (bands 1-5) VNIR spectra of recently deglaciated terrain, lichen covered terrain, vegetation covered terrain, and glacier covered terrain. In the Sandola Creek (SC) subsets, weathered terrain replaces lichen covered terrain for land immediately distal to trimlines outlining recently deglaciated terrain.

Subset	Sensor	Band Calculation	Threshold (DN)	NDSI Threshold (DN)
AF	ASTER	(b2/b1)	191-230	-
AF	ETM+	(b3/b2)	164-198	171-255
SC	ASTER	(b2-b1)	148-163	-
SC	ETM+	(b1-b3/b1+b3)	126-137	194-255
GF	ASTER	(b2/b1)	117-129	-
GF	ETM+	(b3/b2)	191-230	174-255
SIC	ASTER	(b3/b2)	106-121	-
SIC	ETM+	(b3/b2)	158-170	161-255

Table 3. 2 Band calculation and NDSI thresholds for ASTER and ETM+ images. NDSI derived ice covers from ETM+ images were used for each corresponding ASTER image within the same subset.

simple band calculations for each image. In order to reduce the "speckled effect" and the misclassification of pixels, a 3x3 statistical filter was applied to each image. Spectral thresholds (Table 3.2), interactively determined from ground truth data, were then applied to each filtered image to produce a classified image of recently deglaciated terrain. All classification procedures were applied to both ETM+ and ASTER subset images for each experimental area, and were executed using the Spatial Modeler module in ERDAS Imagine 8.6.

3.4.4 Post-classification procedures

Following image classification, data reduction was performed on each new classified image to reduce the number of misclassified pixels. Misclassification is common on all substrates due to the mimicking spectral characteristics of such areas subjected to enhanced erosion. At high latitude locations, low sun angles produce abnormally high albedos on steep slopes, which also produce a mimicking effect, thereby, increasing the chance of pixel misclassification. To minimize this topography-induced misclassification, the slope was calculated from a Canadian Digital Elevation Data (CDED) DEM (100 m resolution), and an empirically derived slope threshold of 0-22° was applied to the data; only pixels within this slope range were used for classification. However, due to the coarse resolution of the DEM (the highest currently available), some escarpments were not eliminated during the slope thresholding process; consequently, manual digitizing and removal of these areas was necessary.

Misclassification often results from the presence of supraglacial debris (Paul *et al.*, 2004), which exhibits similar spectral properties as newly exposed terrain resulting from

recent melt. To account for this potential source of error, a normalized-difference snow index (NDSI), according to Dozier (1984), was applied to each ETM+ subset image in order to generate a mask for snow and ice cover.

$$NDSI = band\ 2 - band\ 5/band\ 2 + band\ 5$$

A threshold range specific to each ETM+ image was applied to the NDSI image in order to isolate the snow and ice class from the rest of the image (Table 3.2). A clumping procedure (ERDAS Imagine 8.6) was then applied to the snow and ice image to delineate contiguous groups of pixels, followed by an elimination procedure (ERDAS Imagine 8.6), which removed small (1-3 pixel) clumps of non-ice pixels and replaced their values with that of the snow and ice. The new snow and ice mask was then used to remove those areas from each corresponding classified image. Due to the low registration error between the ASTER and the ETM+ subset images, the same snow and ice mask was applied to each associated ASTER data set.

3.4.5 Accuracy assesment

After the classification of remotely sensed data, there is an inherent need to assess the degree of correctness and reliability of the new data. The effectiveness of the classifiers used in this study was restricted to two classes: recently deglaciated terrain and all other terrain. This was generally due to limitations in cost and accessibility to more numerous and detailed ground truth data. Classification accuracies are the basis on which image type and classification type are evaluated for mapping ability. All classifications were evaluated against training sites obtained from fieldwork and aerial photos (where applicable), and reported in the form of error matrices and kappa statistics

(Congalton and Green, 1999; Foody, 2002). In each subset, however, the recently deglaciated terrain class compared to the 'all inclusive' class represents a small percentage of the total area. Therefore, in an attempt to reduce the partiality in the calculated overall accuracy toward the larger 'all inclusive' class, the number of training sites was equalized between the two classes, effectively reducing the influence of the larger class on the overall accuracy.

3.5 Results

In this section, the results of supervised and band calculation classification approaches for each experimental subset are presented. Band calculation results have been restricted to the highest scoring (overall accuracy) classification approach for each subset (see pre-testing and screening, Methods; Classification). Table 3.3 summarizes the accuracy assessment results and total area classified with respect to each classification method, and Figure 3.5 illustrates the final classification map associated with each classification approach, applied to each subset.

Mean overall accuracies for all automated classifications were 92% (mean kappa statistic 0.76) for ETM+ and 85% (mean kappa statistic 0.58) for ASTER. Supervised classifications for ETM+ had a combined overall accuracy of 91% (mean kappa statistic 0.71) and 86% (mean kappa statistic 0.60) for ASTER. ETM+ automated classification methods (band 3/band 2) were found to be most useful on quartzitic sandstone and siliceous crystalline bedrock, with a mean overall accuracy of 98% (mean kappa statistic 0.94); whereas, semi-automated ETM+ methods (supervised classification) performed best on rubble dominated carbonate substrates, yielding a mean accuracy of 88%

Subset	Sensor	Classification Type	Overall Accuracy (%)	Kappa Statistic	Producer's Accuracy (%)	User's Accuracy (%)	Pixel Count	Area Classified (km^2)
AF	ASTER	supervised	84	0.52	100	68	25556	5.75
AF	ASTER	(b2/b1)	92	0.75	98	86	45741	10.29
AF	ETM+	supervised	96	0.85	100	92	17717	15.95
AF	ETM+	(b3/b2)	98	0.92	100	96	32109	28.90
SC	ASTER	supervised	78	0.40	97	58	141101	31.75
SC	ASTER	(b2-b1)	80	0.45	94	64	210043	47.26
SC	ETM+	supervised	88	0.66	95	80	20561	18.50
SC	ETM+	(b1-b3/b1+b3)	84	0.57	93	74	65602	59.04
GF	ASTER	supervised	99	0.96	100	98	36158	8.14
GF	ASTER	(b2/b1)	87	0.63	95	78	36088	8.12
GF	ETM+	supervised	90	0.69	98	82	20218	18.20
GF	ETM+	(b3/b2)	87	0.61	97	76	22373	20.14
SIC	ASTER	supervised	83	0.53	95	71	* 715481	* 160.98
SIC	ASTER	(b3/b2)	82	0.50	94	68	* 907557	* 204.20
SIC	ETM+	supervised	88	0.63	98	78	206173	185.56
SIC	ETM+	(b3/b2)	98	0.96	98	98	137913	124.12

Table 3. 3 Recently deglaciated terrain accuracy assessment results and area totals for each classification approach, for all subsets: Alexandra Fiord (AF); Sandola Creek (SC); Glacier Fiord (GF); South Ice Cap (SIC). Note: South Ice Cap (SIC), ASTER 'Area Classified' results (*) are only reliable for intra-sensor comparison due to cloud cover.

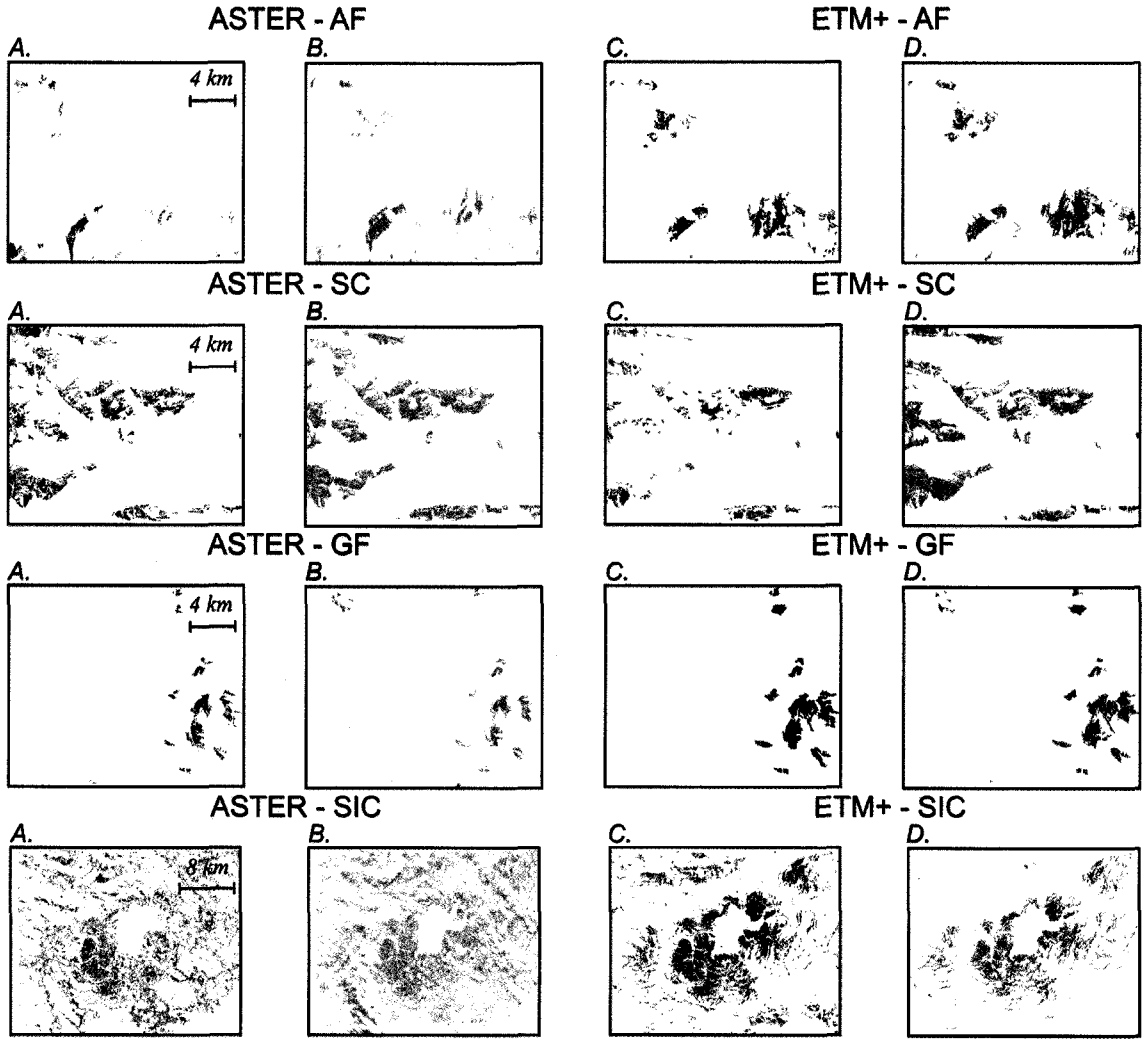

Figure 3. 5 Final maps of supervised and band calculation classification approaches for each subset. Alexandra Fiord (AF), (a) ASTER – supervised, (b) ASTER – (b2/b1), (c) ETM+ – supervised, (d) ETM+ – (b3/b2). Sandola Creek (SC), (a) ASTER – supervised, (b) ASTER – (b2-b1), (c) ETM+ – supervised, (d) ETM+ – (b31-b3/b1+b3). Glacier Fiord (GF), (a) ASTER – supervised, (b) ASTER – (b2/b1), (c) ETM+ – supervised, (d) ETM+ – (b3/b2). South Ice Cap (SIC), (a) ASTER – supervised, (b) ASTER – (b3/b2), (c) ETM+ – supervised, (d) ETM+ – (b3/b2).

(mean kappa statistic 0.66). However, carbonate derived fine grain clastic sedimentary substrates were best mapped with ASTER imagery, using supervised classification approaches (see Glacier Fiord below).

3.5.1 Alexandra Fiord, Ellesmere Island

Both classification types used for the ETM+ subset resulted in higher overall accuracies and kappa statistics, and larger areal coverages than to the ASTER classifications. The ETM+ band ratio approach (band 3/band 2) proved to have the highest overall accuracy of 98% (kappa statistic 0.92), while supervised classification had an overall accuracy of 96% (kappa statistic 0.85). For ASTER, the band ratio approach (band 2/band 1) resulted in an overall accuracy of 92% (kappa statistic 0.75), and the supervised classification of the ASTER subset resulted in an overall accuracy of 84% (kappa statistic 0.52).

3.5.2 Sandola Creek, Ellesmere Island

The spectral signatures of the land cover categories revealed only tenuous feature separation (Fig. 3.4). The automated approaches for both ASTER and ETM+ subsets (band 2-band 1; band 1-band 3/band 1+band 3) resulted in overall accuracies of 80% and 84% respectively, with low kappa statistics for each (0.45 and 0.57). Initial supervised classification attempts for both sensor types resulted in overall accuracies of less than 50%. These extremely low accuracies led to the use of n-dimensional analysis to assist in the partitioning of land cover categories. ENVI 3.6 was used to generate n-dimensional plots using ASTER (bands 1-3) and ETM+ (bands 1-5) subsets, from which, spectral

endmembers of the recently deglaciated terrain were determined interactively. This nonparametric approach was used to refine the training in a second supervised classification of these subsets, resulting in overall accuracies of 78% and 88% (0.40 and 0.66 kappa statistic), for ASTER and ETM+ respectively. Although an increase in the accuracy of the supervised classification approach occurred, it was at the expense of longer processing times.

3.5.3 Glacier Fiord, Axel Heiberg Island

Supervised classification appears to be more successful in the Glacier Fiord subset than band calculation methods. Overall accuracies for supervised classifications of ASTER and ETM+ images were 99% and 90% respectively (0.96 and 0.69 kappa statistics). Band calculations for both ASTER (band 2/band 1) and ETM+ (band 3/band 2) resulted in overall accuracies of 87% (0.63 and 0.61 kappa statistics). The area classified totals in the ETM+ image for both supervised and band calculation methods (18.20 and 20.14 km^2) were over twice those of the area classified totals for the ASTER image (8.14 and 8.12 km^2).

3.5.4 South Ice Cap Complex, Melville Island

Due to the limited availability of cloud-free ASTER imagery for this region of the Canadian Arctic, only one image with partial cloud cover was available for multispectral classification. Cloud cover and the associated shadows in this image were manually digitized, masked, and removed from the classified image. Supervised classification of the ASTER image resulted in an overall accuracy of 83% (0.53 kappa statistic), and the

band ratio approach (band 3/ band 2) resulted in an overall accuracy of 82% (0.50 kappa statistic). The removal of the cloud cover prohibits area comparisons between the two sensors, although intra-sensor comparisons may be made.

Supervised classification of the ETM+ image resulted in 185.56 km^2 classified as recently deglaciated terrain, with an overall accuracy of 88% (0.63 kappa statistic). The band ratio (band 3/band 2) approach produced an areal coverage of 124.12 km^2, with a high overall accuracy of 98% (0.96 kappa statistic).

3.6 Discussion

3.6.1 Accuracy Assessment

An error matrix is used to estimate the overall accuracy of the classification and to produce probability estimates of the producer's and user's accuracy for land cover categories. The producer's accuracy measures the omission error within the classification, that is, the percentage of pixels that should have been classified into a particular category, but were not. A low producer's accuracy indicates an under-classification of the land cover category, and thus, a source of error. The user's accuracy reflects the degree to which commission errors occur; that is, the classification of a pixel to a particular category in which the pixel does not belong. A low user's accuracy indicates that over-classification led to errors in the classified image (Table 3.3).

In this study, the kappa statistic has a strong linear relationship with the user's accuracy (Fig. 3.6). The kappa statistic is used to assess the validity of the results in the error matrix by determining whether the generated results are better than those which

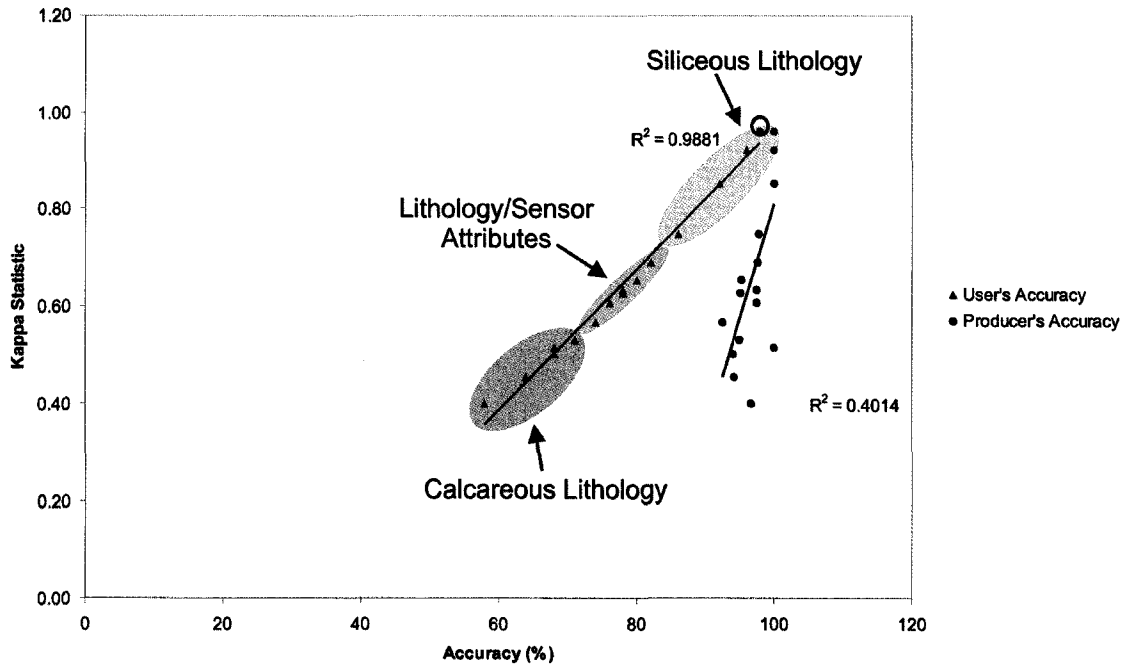

Figure 3. 6 Plot of the linear relationship between user's and producer's accuracies and the kappa statistic for all subset classifications. A direct relationship exists between the user's accuracy and the kappa statistic (expressed as over classification). Areas comprised of siliceous lithologies are found in the upper portion of the plot, while the lower portion of the plot is dominated by calcareous lithologies. A combination of surface lithology and sensor attributes control the middle section of the plot. One outlier (circle) indicates the potential benefits of higher resolution imagery in topographically complex areas (Glacier Fiord, ASTER, supervised).

may have been engendered by chance (Rosenfield and Fitzpatrick-Lins, 1986; Congalton, 1991; Pontius, 2000). The Kappa statistic can be particularly useful when comparing classification approaches, and deciding which approach may be most suited for the study (Rosenfield and Fitzpatrick-Lins, 1986). The relationship between the kappa statistic and the user's accuracy indicates that classifications (with low user's accuracies) are not markedly reducing the error that would typically occur from simple random classification of the same data. This relationship can also be generally extended to dominant substrate type; whereby, lower user's accuracies and kappa statistics tend to be representative of scenes with a high proportion of calcareous substrates, while higher figures of both variables are related to scenes with a high proportion of siliceous substrates. Classifications residing in the middle of the plot in Figure 3.6, are influenced by mixed lithologies and sensor specific attributes (see below).

The high overall accuracy of the ETM+ band ratio method is in large part due to the well-vegetated (nonglacierized) landscape associated with the Alexandra Fiord subset. This subset is mostly comprised of substrates derived from crystalline Precambrian bedrock, which facilitate the growth of lichen and vegetation. Consequently, deglaciated areas here are delineated by typically sharp vegetation trimlines. The spectral profiles of land cover categories in the Alexandra Fiord subset reveal a higher sensitivity to the distinction between former ice covered areas within trimlines and those areas surrounding them (Fig. 3.4). However, supervised classifications of both image types led to lower overall accuracies and kappa statistics compared to the band ratio techniques.

The Sandola Creek subset is characterized by plateau and fiord topography, with small plateau ice caps near or below the modern day equilibrium-line altitude (ELA), a

line that represents the boundary between the accumulation area and ablation area on a glacier. This subset is in strong contrast to the relatively well-vegetated lowlands and lichen covered uplands of the Alexandra Fiord subset. The surficial geology is dominated by rubble and silts derived from Paleozoic carbonate sedimentary rocks. As a result of this calcareous substrate, vegetation and lichen communities are extremely sparse (vegetation cover of <5%); trimline identification is dependent on the identification of slight albedo differences between the less-weathered recently deglaciated terrain and the more-weathered surrounding terrain. As a direct consequence of these minor differences in terrains, and this lithologic setting, commission errors were very high for the Sandola Creek subset; the mean user's accuracy was 77% for ETM+ and 61% for ASTER.

The Glacier Fiord subset is dominated by mountainous terrain with large icefields and numerous outlet glaciers. The surficial geology of the subset is comprised of Mesozoic sandstone, siltstone, and carbonate lithologies. Although somewhat calcareous, upland substrates, distal to recently deglaciated areas, tend to support lichen communities, which allows for greater multispectral discrimination of the land cover categories compared to the highly calcareous substrates of the Sandola Creek subset.

The South Ice Cap subset, part of the Blue Hills plateau region of western Melville Island, is dominated by resistant Paleozoic sandstone bedrock (Hodgson, 1992). The plateau surface has little topographic variability and, where not covered by ice, is largely composed of quartzose sandstone, commonly expressed as angular blocks of rubble. Large patches of lichen-free areas are widespread around the ice cap and upland surfaces; however, distal (lower elevation) to trimlines, mature lichen communities are common.

Distinct differences in the spectral profiles of recently deglaciated terrain and lichen-covered terrain, in concert with low topographic complexity, allow for high classification accuracies with the ETM+ image.

3.6.2 Sources of Error

There are many factors that contribute to the overall error in remotely sensed data (e.g., positional error, ground truth data, etc.) (Campbell, 1996). However, errors associated with classifying recently deglaciated terrain related to former LIA perennial ice cover can be largely attributed to ground surface characteristics and sensor attributes. The ground surface characteristics within each subset can influence the quality of the data. For instance, irregular terrain in the mountainous Glacier Fiord subset and the large escarpments in the South Ice Cap subset complicate the scene, leading to misclassification of the land cover categories. This misclassification is largely due to the coarse resolution of the available DEMs for the Canadian High Arctic. With the development of higher resolution digital elevation products, such classification errors will be appreciably minimized. In some instances, slopes receiving direct solar radiation have high albedos, which often mimic the spectral signature of recently deglaciated areas, causing over classification to occur. In shadowed areas, reflected radiation from the ground can be reduced, causing recently deglaciated terrain to be misidentified; hence, under classification occurs. Other sources of error are associated with the general nature of the ground environment; for example, vegetation types, lithologic types, wet or dry ground, and periglacial activity. For instance, the Sandola Creek subset is entirely composed of Paleozoic carbonate silts and rubble upon which vegetation is generally

absent. Commission errors for each classification type were exceptionally large here because land cover types are not easily differentiated (Fig. 3.4). Such "suboptimal class separability" often results in the over classification of certain classes when employing probabilistic classifiers such as maximum likelihood (Maselli *et al.*, 1990). This effect can also be observed in the Alexandra Fiord - ASTER supervised and the South Ice Cap – ETM+ supervised, where low user's accuracies coincided with carbonate outcrops occurring within siliceous crystalline and clastic dominated scenes. However, lower user's accuracy (high commission errors) associated with the Alexandra Fiord subset corresponded to less deglaciated terrain (area) classified, which is opposite to the relationship between these variables in all other subsets. The reason for this discrepancy is not clear, but is likely related to the narrow spectral range defining the trimline class.

The sensor determines the spatial resolution (or pixel size) of the produced image, and thus limits the size of the smallest identifiable feature in the scene. A pixel contains a mixture of all the ground elements within its limits; individual spectral signatures of all the elements combine to create one spectral signature representative of the pixel. High spatial resolution is particularly important in boundary areas, where the transition between land cover categories is often diffuse, resulting in a higher occurrence of mixed pixels. In this circumstance, ASTER's higher spatial resolution image has the potential for fewer classification errors compared to ETM+ (e.g., Glacier Fiord, Table 3.3). However, these errors were only found to be noteworthy in locations where exceptionally broad diffuse trimlines delineate the former perennial ice cover, typically found in the lowest and most distal sections of recently deglaciated LIA ice cover (Fig. 3.7).

Figure 3. 7 ASTER (dark grey) and ETM+ (light grey) supervised classifications in topographically complex terrain. ASTER's superior spatial resolution (15 m) achieves higher accuracies in areas such as this, where broad diffuse trimlines delineate the former perennial ice cover. ETM+ results show an over classification of the recently deglaciated LIA ice cover relative to the ASTER classification.

High spectral resolution is important when distinguishing between land cover types (Foody, 2002), and is critical in polar desert environments where land cover transitions are, in some cases, only subtly apparent. Such is the case with calcareous substrates, where distinct categories can be very difficult to determine, as the combination of numerous elements within a pixel (some likely more dominant than others) may produce a signal that allows it to become misclassified (e.g., Sandola Creek). Neither sensor performs remarkably well in areas where carbonate terrain is prevalent and vegetation and lichen communities are generally absent. However, in these settings, ETM+'s broader spectral range allows for a more detailed assessment of the spectral characteristics associated with each land cover category, which ultimately leads to more accurate classifications. Therefore, if spectral resolution becomes more important than spatial resolution in such an area, it would be beneficial to combine ASTER's VNIR and SWIR bands. Although the spatial resolution would be sacrificed with this arrangement (reduced to 30 m), the spectral resolution would be enhanced (and superior to ETM+'s), thereby, providing the opportunity for higher accuracy classifications on calcareous substrates. Nevertheless, given the large spatial extent of the Canadian Arctic, this option substantially increases the required processing time; consequently, this alternative was considered impractical for this study.

3.7 Conclusions

In the Canadian High Arctic, high-resolution multispectral imagery (e.g., ETM+ and ASTER) can be used to map recently deglaciated terrain previously covered by LIA perennial snow and ice. Automated classification methods (ETM+ band 3/band 2) were

found to be most useful on quartzitic sandstone and siliceous crystalline bedrock, while semi-automated methods (supervised classification) performed best on carbonate derived substrates (ETM+ and ASTER). ASTER's superior spatial resolution (15 m) seems to elicit higher classification accuracies in topographically complex areas and in diffuse land cover transition zones. However, ETM+'s slightly higher spectral resolution led to more accurate classifications of recently deglaciated terrain for all subsets, with an average overall accuracy of 91% compared to ASTER's 87%.

The rapid and accurate classification of recently deglaciated terrain in the Canadian Arctic is limited by a number of factors. First, the resolution of the DEMs for Arctic Canada is well below the resolution of the available imagery, which severely limits the efficacy of post-classification topographic filtering. Second, the ability to differentiate accurately between land cover types is largely dependent on the substrate type and the spectral resolution of the sensor. Sensors with higher spectral resolution would allow for more accurate classifications in polar desert environments, especially in areas dominated by calcareous substrates. Finally, the spatial resolution of sensors capable of imaging high latitude regions (ASTER: 15 m; ETM+: 30 m) is still a restriction in some cases (e.g., diffuse transitions); higher resolutions would improve the accuracy in most cases. However, when considering the areal coverage of an individual scene, ETM is favoured over ASTER, as one ETM+ scene is about nine and a half times the size of an ASTER scene; therefore, processing time is a serious consideration when taking into account the large spatial area of the Canadian High Arctic.

3.8 References

Andrews, J. T., Davis, P. T., Wright, C., 1976: Little Ice Age permanent snowcover in the Eastern Canadian Arctic: Extent Mapped from Landsat-1 satellite imagery. *Geografiska Annaler,* 58A: 71-81.

Arendt, A. A., Echelmeyer, K. A., Harrison, W. D., Lingle, C. S., Valentine, V. B., 2002: Rapid wastage of Alaska glaciers and their contribution to rising sea level. *Science,* 297: 382-386.

Bednarski, J. H., 2002: Surficial geology, northeast Bathurst Island, Nunavut. *Geological Survey of Canada, Map 2011A, scale 1:100 000.*

Belward, A. S., Estes, J. E., and Kline, K. D., 1999: The IGBP-DIS global 1-km land-cover data set DISCover: A project overview. *Photogrammetric Engineering and Remote Sensing,* 65: 1013-1020.

Campbell, J. B., 1996: *Introduction to remote sensing.* 2nd ed. London: Taylor-Francis, 621 pp.

Church, J. A., Gregory, J.M., Huybrechts, P., Kuhn, M., Lambeck, K., Nhuan, M.T., Qin, D., and Woodworth, P. L., 2001: *Changes in sea level, in Climate Change 2001: The Scientific Basis.* Cambridge, New York: Cambridge University Press, 408 pp.

Congalton, R. G. and Green, K., 1999: *Assessing the accuracy of remotely sensed data: principles and practices.* Boca Raton: CRC, 137 pp.

Congalton, R. G., 1991: A Review of Assessing the Accuracy of Classifications of Remotely Sensed Data. *Remote Sensing of Environment,* 37: 35-46.

Dozier, J., 1984: Snow Reflectance from Landsat-4 Thematic Mapper. *Ieee Transactions on Geoscience and Remote Sensing,* 22: 323-328.

Dredge, L. A., 2004: Surficial geology, Ekalugad Fiord (West half), Baffin Island, Nunavut. Geological Survey of Canada, Map 2073A, scale 1:250 000.

Dredge, L. A., 2004: Surficial geology, Lake Gillian, Baffin Island, Nunavut. Geological Survey of Canada, Map 2076A, scale 1:250 000.

Dredge, L. A., 2004: Surficial geology, McBeth Fiord (West half), Baffin Island, Nunavut. Geological Survey of Canada, Map 2074A, scale 1:250 000.

Dunn, R., Harrison, A.R., and White, J. C., 1990: Positional accuracy and measurement error in digital databases of land use: an empirical study. *International Journal of Geographical Information Systems*, 4: 385-398.

Dyke, A. S. and Hooper, J., 2000: Surficial geology, Berlinguet Inlet and Bourassa Bay, Baffin Island. Geological Survey of Canada, Map 1960A, scale 1:250 000.

Dyke, A. S., 1978: Indications of Neoglacierization on Somerset Island, District of Franklin. *Scientific and Technical Notes,,* Current Research, Part B; Geological Survey of Canada: 215-217.

Dyke, A. S., 2000: Surficial geology, Arctic Bay, Baffin Island. Geological Survey of Canada, Map 1964A, scale 1:250 000.

Dyke, A. S., 2000: Surficial geology, Milne Inlet, Baffin Island. Geological Survey of Canada, Map 1962A, scale 1:250 000.

Dyke, A. S., 2000: Surficial geology, Moffet Inlet and Fitzgerald Bay, Baffin Island. Geological Survey of Canada, Map 1963A, scale 1:250 000.

Dyke, A. S., 2000: Surficial geology, Navy Board Inlet, Baffin Island. Geological Survey of Canada, Map 1965A, scale 1:250 000.

Dyke, A. S., 2000: Surficial geology, Phillips Creek, Baffin Island. Geological Survey of Canada, Map 1961A, scale 1:250 000.

Dyke, A. S., 2001: Surficial geology, Cardigan Strait, Devon Island and Ellesmere Island. Geological Survey of Canada, Map 1974A; scale 1:250 000.

Dyke, A. S., 2001: Surficial geology, central Devon Island. Geological Survey of Canada, Map 1971A, scale 1:250 000.

Dyke, A. S., 2001: Surficial geology, eastern Devon Island. Geological Survey of Canada, Map 1970A, scale 1:250 000.

Dyke, A. S., 2001: Surficial geology, Grinnell Peninsula, Devon Island. Geological Survey of Canada, Map 1973A, scale 1:250 000.

Dyke, A. S., 2001: Surficial geology, western Devon Island. Geological Survey of Canada, Map 1972A, scale 1:250 000.

Dyke, A. S., 2003: Surficial geology, Erichsen Lake, Baffin Island, Nunavut., *Geological Survey of Canada, Open File 4484. CDROM with digital files (geology, topography, and hydrology) of Open Files 1598-1613 (previously released as paper maps at 1:50 000 scale).*

Dyke, A. S., 2004: Surficial geology, Erichsen Lake, Baffin Island, Nunavut., *Geological Survey of Canada, Map 2066A, scale 1:250 000.*

Dyurgerov, M. B. and Meier, M. F., 1997: Mass balance of mountain and subpolar glaciers: a new global assessment for 1961-1990. *Arctic and Alpine Research,* 29: 379-391.

Edlund, S. A., 1985: Lichen-free zones as neoglacial indicators on western Melville Island, District of Franklin. *Current Research, Part A, Geological Survey of Canada,* Paper 85-1A: 709-712.

England, J., Kershaw, L., LaFarge-England, C., Bednarski, J., 1981: *Northern Ellesmere Island: A natural resources inventory.* Edmonton: University of Alberta, Department of Geography, 237 pp.

Foody, G. M., 1992: On the Compensation for Chance Agreement in Image Classification Accuracy Assessment. *Photogrammetric Engineering and Remote Sensing,* 58: 1459-1460.

Foody, G. M., 2002: Status of land cover classification accuracy assessment. *Remote Sensing of Environment,* 80: 185-201.

Grove, J. M., 1988: *The Little Ice Age.* London: Methuen, 500 pp.

Hodgson, D. A., 1992: Quaternary geology of western Melville Island, Northwest Territories. *Geological Survey of Canada,* Paper 89-21: 1-35.

Hooper, J. and Dyke, A. S., 2000: Surficial geology, Agu Bay and Easter Cape, Baffin Island. Geological Survey of Canada, Map 1959A, scale 1:250 000.

IPCC, 2001: *Climate Change 2001: The Scientific Basis.* Cambridge, New York: Cambridge University Press, 408 pp.

IPCC, 2001: *Climate Change 2001: Impacts, Adaptation andVulnerability.* Cambridge, New York: Cambridge University Press, 1042 pp.

Ives, J. D., 1962: Indication of recent extensive glacierization in north central Baffin Island, N.W.T. *Journal of Glaciology,* 4: 197-205.

Koerner, R. M., 1989: *Queen Elizabeth Islands Glaciers. In: Fulton, R.J., ed. Quaternary geology of Canada and Greenland.* Ottawa: Geological Survey of Canada, 464-473 pp.

Locke, C. W. and Locke, W. W., 1977: Little Ice Age snow-cover extent and paleoglaciation thresholds: North-central Baffin Island, N.W.T., Canada. *Arctic and Alpine Research,* 9: 291-300.

Maselli, F., Conese, C., Zipoli, G., and Pittau, M. A., 1990: Use of Error Probabilities to Improve Area Estimates Based on Maximum-Likelihood Classifications. *Remote Sensing of Environment,* 31: 155-160.

Overpeck, J., K., Hughen, K., Hardy, D., Bradley, R., Case, R., Douglas, M., Finney, B., Gajewski, K., Jacoby, G., Jennings, A., Lamoureux, S., Lasca, A., MacDonald, G., Moore, J., Retelle, M., Smith, S., Wolfe, A., and Zielinski, G., 1997: Arctic environmental change of the last four centruries. *Science,* 278: 1251-1256.

Paul, F., Huggel, C., and Kaab, A., 2004: Combining satellite multispectral image data and a digital elevation model for mapping debris-covered glaciers. *Remote Sensing of Environment,* 89: 510-518.

Pontius, R. G., 2001: Quantification error versus location error in comparison of categorical maps (vol 66, pg 1011, 2000). *Photogrammetric Engineering and Remote Sensing,* 67: 540-540.

Rosenfield, G. H. and Fitzpatricklins, K., 1986: A Coefficient of Agreement as a Measure of Thematic Classification Accuracy. *Photogrammetric Engineering and Remote Sensing,* 52: 223-227.

Wolken, G. J., England, J.H., and Dyke, A. S., 2005: Re-evaluating the Relevance of Vegetation Trimlines in the Canadian Arctic as an Indicator of Little Ice Age Paleoenvironments. *Arctic,* 58 (4): 341-353.

4 CHAPTER FOUR

Climatic conditions inferred from Little Ice Age trimlines across the Queen Elizabeth Islands, Arctic Canada

4.1 Introduction

Climate change and the role of anthropogenic forcing have become focal issues in the last few decades, and concerns have escalated with regard to observed and predicted modifications to Polar Regions (ACIA, 2004). The most recognized impacts pertain to Northern Hemisphere sea ice reduction and thinning (Johanneson *et al.* 1999; Vinikov *et al.* 1999) and the associated reduction of glaciers and ice caps that are contributing to global sea level rise (Dyurgerov and Meier, 1997; IPCC, 2001). Part of the problem with accurately assessing modern climate change is the inability to differentiate between changes due to natural climatic variability from those occasioned by forcing from greenhouse gases and sulphate aerosols. This uncertainty is accentuated in the Canadian High Arctic because of the brevity of the instrumental record (~55 yrs), which precludes direct observations of climate change prior to the mid-20th century. Consequently, one must rely on paleoclimate proxies in high latitudes in order to better investigate the record of natural variability; such records can be used as a baseline to better profile modern changes. In this study, the change in the extent of perennial snow and ice between the Little Ice Age (LIA, 1600-1900 AD, Grove 1988) and 1960 is used as a measure of the impact of early 20th century warming in the Canadian High Arctic. The questions that follow concern what climatic conditions might have favoured the reported

reduction of this former snow and ice cover across this topographically and climatically diverse region (Maxwell, 1981).

A growing body of research has documented the recent cryospheric response to climate change in the Canadian High Arctic (Burgess and Sharp, 2004; Braun *et al.*, 2004; Burgess *et al.*, 2005; Mair *et al.*, 2005). Little is known, however, about the changes in terrestrial ice extent during the early to mid-20th century, and even less is known about the climatic forcing responsible for these changes. During the mid-20th century, warm conditions led to net mass loss and a decrease in the areal extent of ice caps on the Hazen Plateau (N Ellesmere Island, Hattersley-Smith and Serson, 1973). This extended period of melt, ending in the early 1960s, was followed by an interval of cooler climatic conditions eliciting a period of net mass gain and expansion of the ice caps until the mid-1970s (Hattersley-Smith and Serson, 1973; Bradley and England, 1977). Other mass balance records of glaciers and ice caps (Devon Ice Cap, Melville South Ice Cap, Meighen Ice Cap, and White Glacier on Axel Heiberg Island) in the QEI, however, show no coherent response to this mid-1970s cool episode (Dyurgerov *et al.*, 2002; 2005). Braun *et al.* (2004) extended the study of ice caps in this region by documenting the recent (1959-2001) reductions of four small plateau ice caps on the Hazen Plateau, and contrasting their modern margins with those they attributed to the LIA, as marked by lichen trimlines surrounding them.

The terrestrial ice configuration in the Canadian Arctic during the LIA is widely recognized to mark the maximum Neoglacial ice extent (post 4500 BP; Blake, 1981; Bradley, 1990; Miller *et al.*, 2005; Wolken *et al.*, 2005). Indeed, in parts of eastern Baffin Island, moraines dating from the LIA cross-cut those deposited during the early

Wisconsinan that had remained undisturbed since their formation (Marine Isotope Stage 4, Miller 1976). In addition to the widespread evidence of glaciers attaining their maximum late Holocene extents within the last few centuries (LIA), this time period in the QEI is regarded as the coldest of the entire Holocene (Bradley, 1990; Koerner and Fisher, 1990). Ice retreat since the LIA coincides with the beginning of the 20th century, when significant warming occurred in the Arctic, resulting in rapid melting of terrestrial ice, ice shelves, and sea ice (Koerner and Fisher, 1990; Overpeck *et al.*, 1997; Bengtsson *et al.*, 2004; Johanessen *et al.*, 2004). This large-scale reduction of terrestrial ice is delimited by prominent trimlines, within which the terrain is characterized by an absence of vegetation and/or a reduction in oxidized and weathered substrates. These lighter-toned surfaces are often evident on both aerial photographs and satellite imagery and are thought to mark ice retreat dating from the LIA (Ives, 1962; Wolken *et al.*, 2005). These trimlines now provide an important baseline from which paleoenvironmental information can be extracted and evaluated (Wolken *et al.*, 2005; Wolken, 2006).

4.1.1 Objectives

This study documents the magnitude and nature of terrestrial ice reduction in the QEI following the termination of the LIA, by comparing reconstructed LIA ice cover to that of 1960, when full aerial photograph coverage of the region was first established. The distribution of mapped trimlines, associated with former perennial snow/ice fields, taken to mark the position of ice margins at the end of the LIA, is then used to reconstruct trend surfaces of equilibrium-line altitude (ELA) during the LIA. These results are then compared to ELAs (1960) previously reconstructed from topographic maps (1:250,000;

Miller *et al.*, 1975). The trend surface of difference in ELA (Δh) between the end of the LIA and 1960 is then used to indicate the primary spatial changes in perennial snow/ice extent caused by post-LIA warming across the QEI. The assumption is made that all atmosphere/ocean boundary conditions occurring in the LIA and early 20th century can also occur in the modern record. Thus, patterns of ELA Δh are referenced against specific modes of variability associated with climatological variables in the modern record (1949-2002) that serve as analogs for those that might have occurred during the early 20th century in the Canadian High Arctic. Changes in the ELA (Δh) from LIA to 1960 across the QEI are used to provide first-order estimates of climate change, and identify possible patterns of atmospheric circulation that may explain the observed changes in ELA. The objective of the climatic analyses is to provide a better understanding of the synoptic scale conditions that influence the extent of terrestrial ice cover in Arctic Canada.

4.2 Study Area

The QEI comprise the northernmost part of the Canadian Arctic Archipelago (74 to 83° N, Fig. 4.1) lying north of Parry Channel. The QEI are bounded by the Arctic Ocean to the north and northwest, and by Nares Strait, Smith Sound, and Baffin Bay to the east. The total land area of the QEI is ~416,000 km^2, with the four largest islands (Ellesmere, Axel Heiberg, Devon, and Melville) accounting for ~80% of the total area. More than 25% of the land area of the QEI is covered by ice (~110,000 km^2), the largest concentration of terrestrial ice after Antarctica and Greenland (Williams and Ferrigno, 2002). The eastern QEI (Devon, Axel Heiberg, and Ellesmere Islands) have high relief

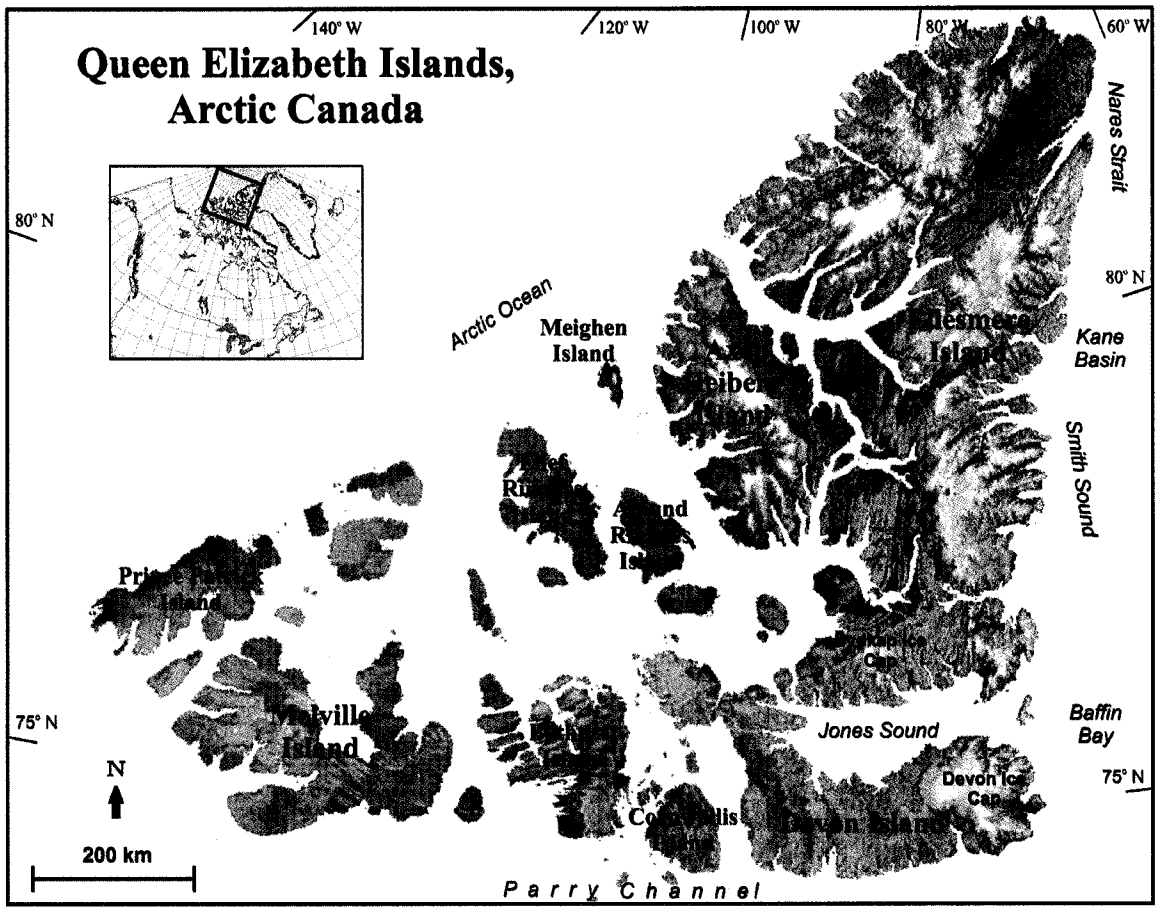

Figure 4. 1 Map of the Queen Elizabeth Islands, Arctic Canada (Radarsat Orthomosaic, courtesy of the Canadian Centre for Remote Sensing).

(reaching 2,500 meters above sea level) and support widespread ice caps and glaciers. ELAs (1960) throughout the eastern QEI range from less than 200 m along the north coast of Ellesmere Island to nearly 1,200 m in island interiors, where the climate is more continental (Miller *et al.*, 1975). Numerous plateaus occur close to the regional glaciation level in the eastern QEI and provide important surfaces where subtle changes in climate have the potential to either form new ice caps, or expand/remove existing ones. In contrast, the physiography of the western QEI is characterized by low (< 400 m asl) dissected plateaus separated by wide marine channels (Dyke, 1974). Consequently, the western QEI support only a few ice caps, which are currently restricted to higher terrain on western Melville Island (above 600 m asl) and to Meighen Island where a solitary, low elevation (<250 m asl) ice cap faces the Arctic Ocean (Koerner and Paterson, 1974).

The climate of the Canadian Arctic is strongly influenced by complex interactions between the atmosphere, ocean, sea ice, and land (Serreze and Barry, 2005). Although topographically diverse, most of the land surface of the QEI has been classified as polar desert, which is indicative of the severe aridity of this region. However, Maxwell (1981) partitions the Canadian High Arctic into climatic sub-regions, indicating high precipitation and warmer regions in the southeast bordering Baffin Bay and cold arid regions in the central and northwest QEI (Edlund and Alt, 1989). Systematic meteorological observations in the QEI began in the late 1940s, with the establishment of five (coastal) weather stations (Alert, Eureka, Mould Bay, Isachsen, and Resolute Bay). Since their establishment, observations have been at times intermittent, and two of these stations (Mould Bay and Isachsen) have been closed in recent years. However, despite the limited number of meteorological observation sites throughout the QEI, efforts have

been made to characterize the synoptic climatology of the region (Bradley, 1973; 1975; Bradley and England, 1978; 1979; Alt, 1987), revealing substantial variability in synoptic types and their influence on glaciers and ice caps in the Canadian High Arctic.

4.3 Data Sources

4.3.1 Remote Sensing Data

The reconstruction of LIA perennial snow/ice in the QEI, and its subsequent reduction up to ~1960, is based on Visual and Near Infrared (VNIR) data from two high-resolution multispectral sensors: Enhanced Thematic Mapper Plus (ETM+) on the Landsat 7 satellite (1999-2004), and Advanced Spaceborne Thermal Emission and Reflection Radiometer (ASTER) aboard the Terra satellite (2000-2004). ETM+ has nearly complete, cloud-free, summer coverage of the QEI, and offers a combined VNIR and Short Wave Infrared (SWIR) spectral range of 450 to 2350 nm in bands 1 - 5 and 7, with a swath width of 185 km and a spatial resolution of 30 m. ASTER has a swath width of 60 km and offers 14 spectral bands, with the VNIR operating on bands 1-3 (nadir) in a spectral range of 520 to 760 nm and a 15 m spatial resolution. ASTER has a ground track repeat cycle of 16 days and is capable of imaging globally; however, coverage remains incomplete in some high latitude areas (e.g., N. Ellesmere and W. Melville Islands), mainly due to a narrow window of cloud-free summer days. Other sensor details can be found in the methodological companion to this paper (Wolken, 2006).

In lieu of ETM+ and ASTER imagery, aerial photographs from the 1959/60 (here on referred to as 1960) survey of the Canadian Arctic Archipelago (acquired by the

Government of Canada) were used for N Ellesmere Island above 82.7 °N. In addition to the aerial photographs, 1960 ice margins were obtained from the National Topographic Database (NTDB) (provided by Geomatics Canada), which are thematic digital reproductions of the National Topographic System (NTS) maps derived from the 1960 aerial photographs. Digital Elevation Models (DEMs) used in this study were created from the Canadian Digital Elevation Data set, derived from the 1:250 000 NTS map series. This study utilized 149 DEMs, which were reprojected to a resolution of 100 m on a NAD83 UTM grid, and later used to create a DEM mosaic of the QEI.

4.3.2 NCEP/NCAR Reanalysis

The NCEP/NCAR reanalysis (NNR, following Bromwich *et al.*, 2002) uses historical data from 1948 to present for data assimilation conducted four times per day (every six hours starting at 0Z), with a T-62 coordinate system (horizontal resolution of ~208 km) at 28 levels vertically (Kalnay *et al.*, 1996; Kistler *et al.*, 2001). As per standard procedure, these four times daily values are averaged, and the daily means are compiled to monthly means, which are then output to a global grid with a spatial resolution of 2.5° latitude by 2.5° longitude. The monthly mean data for the study period (1949-2002) were obtained for this study from the NCEP/NCAR Reanalysis Project (http://www.cdc.noaa.gov/cdc/reanalysis/reanalysis.shtml) and include: 2 m temperature (hereafter referred to as surface air temperature, SAT); surface precipitation rate (SPR); sea level pressure (SLP); and 850, 500, and 200 hPa geopotential heights. Gridded NNR variables are ranked according to the relative influence of observational data versus model output, where a rank of *A* indicates that the variable selected is most reliable, based

strongly on observational data, whereas rank *B* indicates less reliability due to diminished observational influence on the variable and a greater dependence on the model. Rank *C* indicates a variable that is fully model dependent, i.e., direct observational data associated with the variable are unavailable (Kalnay *et al.*, 1996). For the variables used in this study, NNR ranks the pressure level variables as *A*, SAT as *B*, and SPR as *C*.

Gridded reanalysis allows for a more comprehensive assessment of climate in remote regions than individual station analysis and is generally preferred in climate studies of the Arctic (Bromwich *et al.*, 2002). Some high latitude studies, however, have revealed inaccuracies in certain NNR variables selected for use in this study. For example, topographic smoothing related to the low resolution of gridded NNR oversimplifies mountainous terrain, which leads to inaccuracies in the derived modelled temperatures (Bromwich *et al.*, 2002). In the QEI, the potential for this error is greatest in its eastern alpine sector, where topographic complexity is greatest. Compounding this problem is the paucity and variable quality of observational climate data from this region, which causes inhomogeneities in the assimilation data, especially in the early part of the record (pre-1958) when only limited radiosonde coverage occurred (Serreze and Barry, 2005: 257). Still, only two long-term weather stations exist in the mountainous eastern sector of the QEI (Alert and Eureka), both of which are located in isolated coastal lowlands, thereby limiting their climatic representation of this area (Maxwell, 1981).

Additional inaccuracies are associated with NNR modelled precipitation in the Arctic. Over land areas, NNR tends to overestimate summer precipitation, an effect resulting from excessive (modelled) convective precipitation (Serreze and Hurst, 2000).

For the time period of interest in this study, however, summer precipitation rate over the QEI is very low and any overestimation inherent to this variable is believed to have little impact on subsequent analyses (discussed later). NNR generated spatial patterns of precipitation rate has also been shown to be too simplistic, especially in its inability to produce observed interannual variability in snow cover (Serreze and Maslanik, 1997; Cullather *et al.*, 2000). Serreze *et al.* (2003) report consistent NNR underestimation of precipitation variability in Arctic regions, and similar accounts of underestimated precipitation variability are also noted by Bromwich *et al.* (2002) in their work over Baffin Island; nevertheless, they noted that the normalized, long-term record still captures the relative variability in SPR, which is also true over the QEI.

4.3.3 ERSST Data

Climate variability is strongly linked to variations in oceanic boundary conditions (Hansen and Bezdek, 1996). Thus, the influence of Sea Surface Temperatures (SSTs) in high latitude regions on variations in atmospheric circulation is considered. The Extended Reconstructed Sea Surface Temperature (ERSST v.2) data set (Smith and Reynolds, 2004) was obtained from the National Oceanic and Atmospheric Administration's Cooperative Institute for Research in Environmental Sciences (NOAA-CIRES), Climate Diagnostic Center (CDC) (http://www.cdc.noaa.gov/cdc/data.noaa.ersst.html). The ERSST v.2 was developed using the SST data and enhanced statistical techniques provided by the International Comprehensive Ocean-Atmosphere Data Set (ICOADS). The ERSST v.2 has a 2° latitude by 2° longitude grid, and was designed to manage regions with weak-variance

more effectively while improving high-latitude SST analyses by using sea-ice concentration data (Smith and Reynolds, 2004).

4.4 Methods

4.4.1 Trimline Mapping: Fieldwork

Trimlines are distinct transitions on a glaciated landscape resulting from differential weathering and erosion of a surface formerly covered by a perennial snow/ice mass. Trimlines record the former extent of glaciers, ice caps, and perennial snowfields and can be used for paleoenvironmental reconstruction (Wolken *et al.*, 2005). In the QEI, trimlines are most visible when expressed as vegetation trimlines, typically occurring on siliceous substrates that are well vegetated, but they are also detectable on calcareous substrates, where they are much subtler in appearance due to the lack of vegetation on such terrains (Fig. 4.2). Trimlines can be used for paleoenvironmental reconstruction. Where trimlines surrounding former perennial snowfields and thin plateau ice caps are accordant, their common elevation is used here to represents the lowest Neoglacial multi-year ELA. Although the specific age of the perennial snow/ice expansion event that produced these trimlines is not known, the existing age determinations associated with trimlines in Arctic Canada place their creation in the late Neoglacial (Wolken *et al.*, 2005). Hence, it is hypothesized that this expansion occurred during the LIA.

4.4.2 Trimline Mapping: Remote Sensing

Reconstructing the extent of former perennial snow/ice cover in the QEI using remotely sensed data poses numerous challenges due to the size, topographic and

Figure 4. 2 Trimlines (arrows) surrounding recently exposed terrain associated with (A) former perennial snowfields on siliceous terrain, central Axel Heiberg Island, and (B) a small plateau ice cap on calcareous terrain, Knud Peninsula, Ellesmere, Island.

lithologic diversity, and sparsity of vegetation in this region. These challenges are augmented by the amount of time required to process the remotely sensed data and to determine what classification techniques are most appropriate for each sector investigated. Wolken (2006) applied several different classification methods to both ASTER and ETM+ images for areas of the QEI with the most representative lithologies and topographic settings. He found that automated classification methods (band calculations) were most effective on terrains derived from quartzitic sandstone and siliceous crystalline rock, whereas semi-automated methods (supervised classification) were most effective on carbonate-derived substrates. Furthermore, ETM+ was found to be a better all-around sensor for classifications of recently deglaciated terrain, due primarily to its slightly higher spectral resolution in its combined VNIR and SWIR bands, and to its superior areal coverage (9.5 times larger than ASTER). Image processing and classification procedures presented here follow Wolken (2006).

ETM+ (LANDSAT 7, spatial resolution 30 m) was the primary sensor used for this study. Automated and semi-automated classifications were applied according to the estimated ratio of siliceous (automated) *versus* calcareous (semi-automated) terrain in each image. This effort was guided by the use of surficial and bedrock geology maps, ground observations (where available), and extensive examination of the images. For example, if an image was comprised mostly ($\geq$~75%) of igneous (siliceous) Precambrian bedrock, then an automated classification was employed. However, if an image was comprised of nearly equal parts of siliceous and calcareous terrains, then both automated and semi-automated classifications were applied separately to the image, followed by masking and elimination of classified pixels on the unsought terrain (either siliceous or

calcareous) of each new classified image. To reduce over-classification of the imagery, caused by the inclusion of features that mimic trimlines (e.g., lithological contacts, talus slopes, and escarpments), data reduction procedures were applied to each classified image, thus identifying and removing these areas from the final classified maps (Wolken, 2006).

In the northernmost part of Ellesmere Island, where multispectral coverage is either missing or unusable due to extensive cloud cover, the former coverage of perennial snow/ice was mapped manually from aerial photographs scanned at high-resolution (spatial resolution ~5 m). On-screen, three-dimensional mapping from aerial photograph stereo-pairs (using ERDAS Stereo Analyst), minimized errors associated with the inadvertent mapping of features similar in appearance to trimlines. The raster data from the classified images were then converted into vector coverages and merged with the manually digitized sections of N Ellesmere Island. This produced a single vector coverage comprised of polygons demarcating recently deglaciated terrain (inside designated trimlines).

4.4.3 ELA Reconstruction

The DEM mosaic of the QEI was used to extract low point elevation and coordinate data from each polygon of recently deglaciated terrain. Where trimlines outlining the former margins of thin plateau ice caps are accordant with trimlines marking former perennial snowfields, their common elevation is interpreted to record the former ELA for that locality (Wolken *et al.*, 2005). Point data meeting this criterion were selected manually from the trimline data set to create a new data set consisting of 4,334 elevation

points representing the altitude of the equilibrium-line throughout the QEI. A three-dimensional LIA ELA trend surface, with 250 m resolution, was then created from the array of elevation points using Topogrid in ArcInfo 8.0, and was later resampled to a one-kilometre resolution grid for trend surface analysis (discussed below). Topogrid uses ANUDEM, a DEM interpolation program that calculates elevations using finite difference interpolation on a discretized smooth surface regular grid (Hutchinson, 1989). Topogrid is effective in modeling surface topography where steep gradients occur locally in the data, and for this reason, was chosen to model the variable ELA trend surface over the QEI. Although some uncertainty in the reconstructed LIA ELA trend surface can be attributed to low image classification accuracy and errors associated with other image processing procedures, most of the error can be ascribed to the vertical accuracy of the DEMs, which is estimated to be ±20 m over bedrock to ±90 m over complex terrain and ice covered regions (Centre for Topographic Information, 2000; Burgess and Sharp, 2004). Another source of uncertainty in the LIA ELA trend surface stems from uneven LIA ELA point distribution which is largely a function of lithology (see above); some areas in the QEI have better LIA ELA representation than others. Figure 4.3 shows qualitative uncertainties associated with the LIA ELA trend surface over the QEI.

4.4.4 LIA and 1960 Ice Covers

The polygon coverage of recently ice-free terrain provides a minimum measure of former LIA ice extent, because many formerly ice-covered sites have been obscured by periglacial processes or are otherwise undetectable with available sensors. Consequently, the interpolated ELA trend surface (250 m resolution) for the LIA was used to estimate

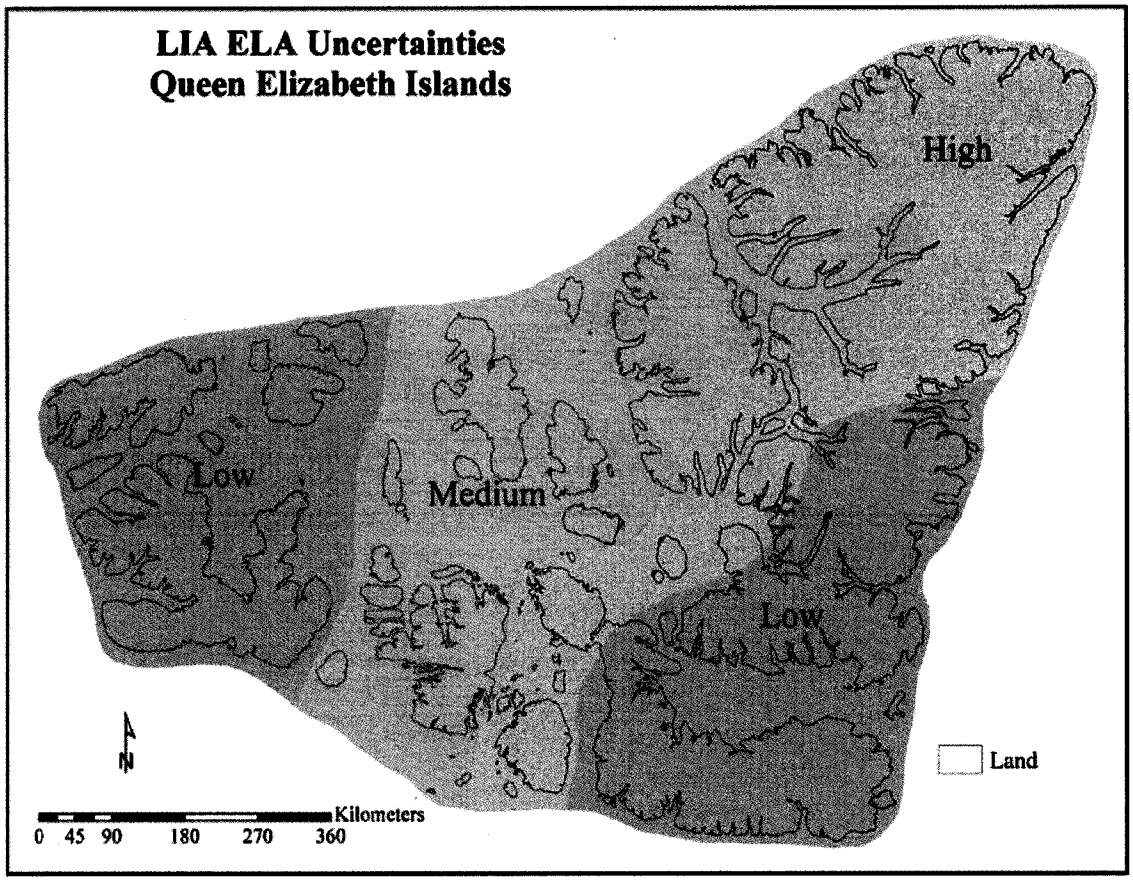

Figure 4. 3 Uncertainties (qualitative) associated with the LIA ELA trend surface over the QEI. These uncertainties are largely a function of lithology, and hence the distribution of LIA ELA points.

the total area formerly covered by perennial snow/ice. The land area above the LIA ELA trend surface (corresponding to the LIA accumulation area) was determined by subtracting the ELA trend surface from the DEM mosaic of the study area. Positive pixel values in the new raster data set represent areas above the ELA, and hence ice-covered land during the LIA. However, this data set only includes perennial snow/ice cover above the LIA ELA and does not account for outlet glaciers that would have extended below the ELA. In his investigation into Neoglaical fluctuations of glaciers in SE Ellesmere Island, Blake (1981) reported widespread evidence indicating that outlet glaciers were (in the late 1970s) at their maximum Neoglacial extent, or slightly retreated from this position, which they likely reached within the last 100 years. For glaciers elsewhere in the QEI, it is likely that only minimal marginal retreat would have occurred by the 1960 aerial photography survey; in fact, it is possible that some glaciers at this time were still advancing in response to LIA cooling (Miller *et al.*, 1975). Consequently, in order to obtain a more realistic estimate of LIA perennial snow/ice cover, 1960 glacier outlines extending below the LIA ELA trend surface were amalgamated with the LIA ice cover above the ELA. Area calculations of LIA and 1960 ice covers were performed by converting each ice cover into raster grids (30 m resolution), then multiplying the total pixel count for each grid by 900 m^2 (the area of one pixel).

4.4.5 1960 ELAs

ELAs for the QEI (1960; Fig. 4.4) were derived from a map by Miller *et al.* (1975). The map was georeferenced and the ELA contours were digitized manually in point form.

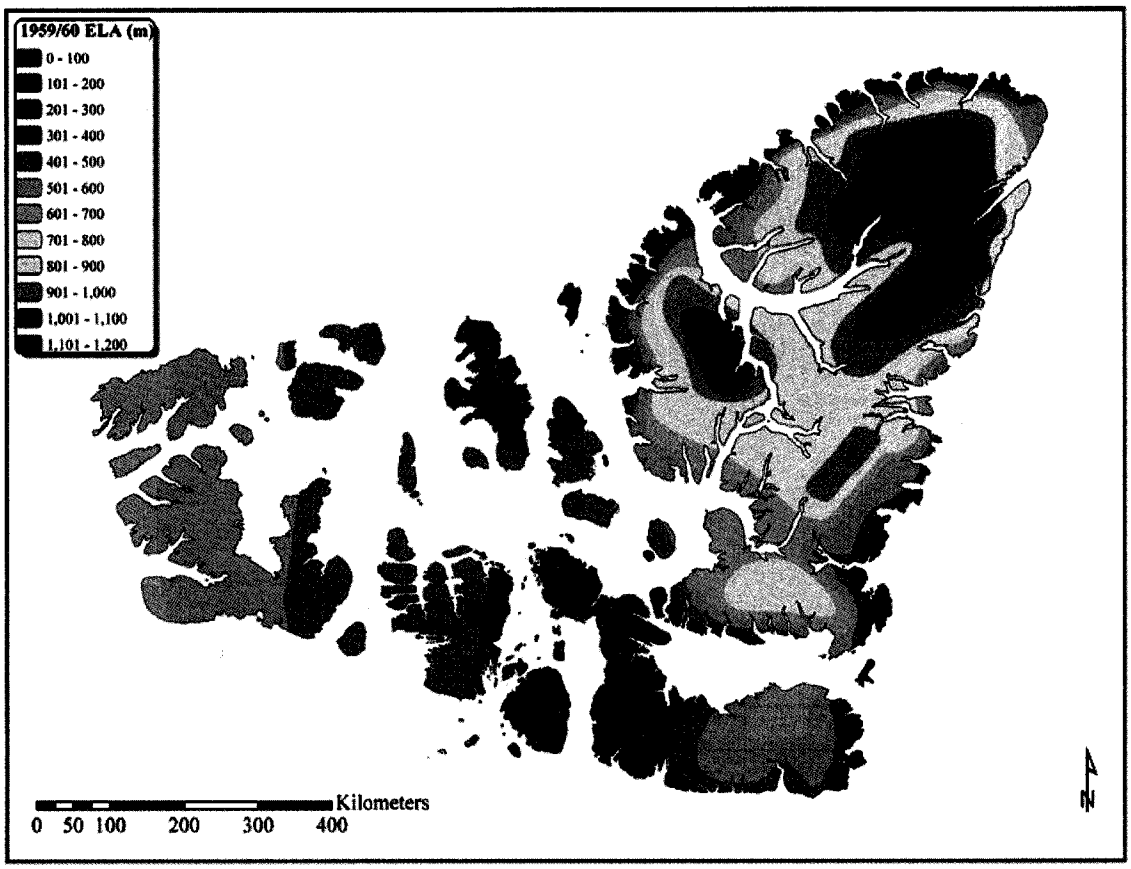

Figure 4. 4 1959/60 ELA trend surface recreated from Miller et al. (1975).

The ELA points were then used to create a DEM (or ELA trend surface) by interpolating the points onto a one-kilometer resolution grid using Topogrid in ArcInfo 8.0 (see above).

Miller *et al.* (1975) determined "steady-state" ELAs throughout the QEI (based on at least one point per 2,500 km^2) using one of three different methods: (i) Accumulation Area Ratio (AAR; 0.65) on the lowest small cirque glacier; (ii) AAR (0.65) on the lowest small ice cap; and (iii) elevation of the change of contour inflection from convex to concave down-glacier. Although the AAR method performed on cirque glaciers was preferred, in the absence of cirque glaciers the second method was used where only ice caps existed, and the third option was used in extensively glacierized areas. Overall, 1960 ELA estimates produced from the first method are generally consistent with multi-year ELA estimates derived from mass balance records from a limited number of glaciers throughout the QEI (Dyurgerov *et al.*, 2002; 2005), but the second method systematically underestimates the ELA by using ice masses that are not in equilibrium with the contemporary climate. During the 1960 aerial photography surveys, many small plateau ice caps were entirely below the ELA, as evidenced by their missing accumulation area and local ELA estimates determined from mass balance records (Dyurgerov *et al.*, 2002; 2005). Therefore, under these conditions, the use of the AAR method on the lowest small ice cap in a given area would produce an erroneously low ELA. Based on an extensive photogrammetric evaluation of the study area using the 1960 aerial photographs and the QEI DEM mosaic, it is inferred that there are two areas in the QEI where the 1960 ELA is seriously underestimated: (*i*) central and western Devon Island; and (*ii*) S Ellesmere Island. For this area of the QEI, long-term mass balance monitoring exists only on the Devon Ice Cap, with records from 1961 to present. In order to estimate the multi-year

ELA for the early 1960s, a fourth-order polynomial was used to statistically fit the observed ELA data. Based on this "best-fit" model, the multi-year ELA for the Devon Ice Cap during the early-1960s was determined to be ~1200 m, which is >400 m above the estimates produced by Miller *et al.* (1975) for this area. To account for the underestimated ELAs over the southern QEI, the multi-year ELA for the Devon Ice Cap was used to create a grid of correction values, which was then applied to the original 1960 ELA trend surface. The correction area was delineated according to two assumptions: (*i*) the 1960 ELA trend surface is correct in areas where cirque glaciers existed in 1960; (*ii*) the 1960 ELA trend surface on Melville Island is correct (Fig. 4.1). In the SE QEI, a correction value of 400 m was assigned to both the Devon and Sydkap ice caps (Fig. 4.1), and a value of 0 m was assigned to areas containing small cirque glaciers (i.e., central and E Ellesmere Island and E Devon Island), as well as to all points distal to these glaciers and those to the west beyond the underestimated region. These correction values were used as fixed limits in a tensional spline interpolation on a one-kilometre resolution grid to create an elevation model of correction values over the QEI (Fig. 4.5). As an independent evaluation of the validity of the 1960 ELA corrections, NNR was used to model the height of the mean July 0 °C isotherm over the QEI on a 2.5° resolution regular grid for the period 1958-1962 (Fig. 4.6). Bradley (1975) showed that in the Canadian High Arctic a strong positive correlation exists between the height of the July 0 °C isotherm and the ELA; high July 0 °C isotherm heights in the SE QEI suggest a correspondingly high ELA trend surface, which includes the area of underestimated ELAs (1960). Furthermore, the decreasing trend in isotherm heights to the northwest corresponds to the tendency of correction values determined for the area of

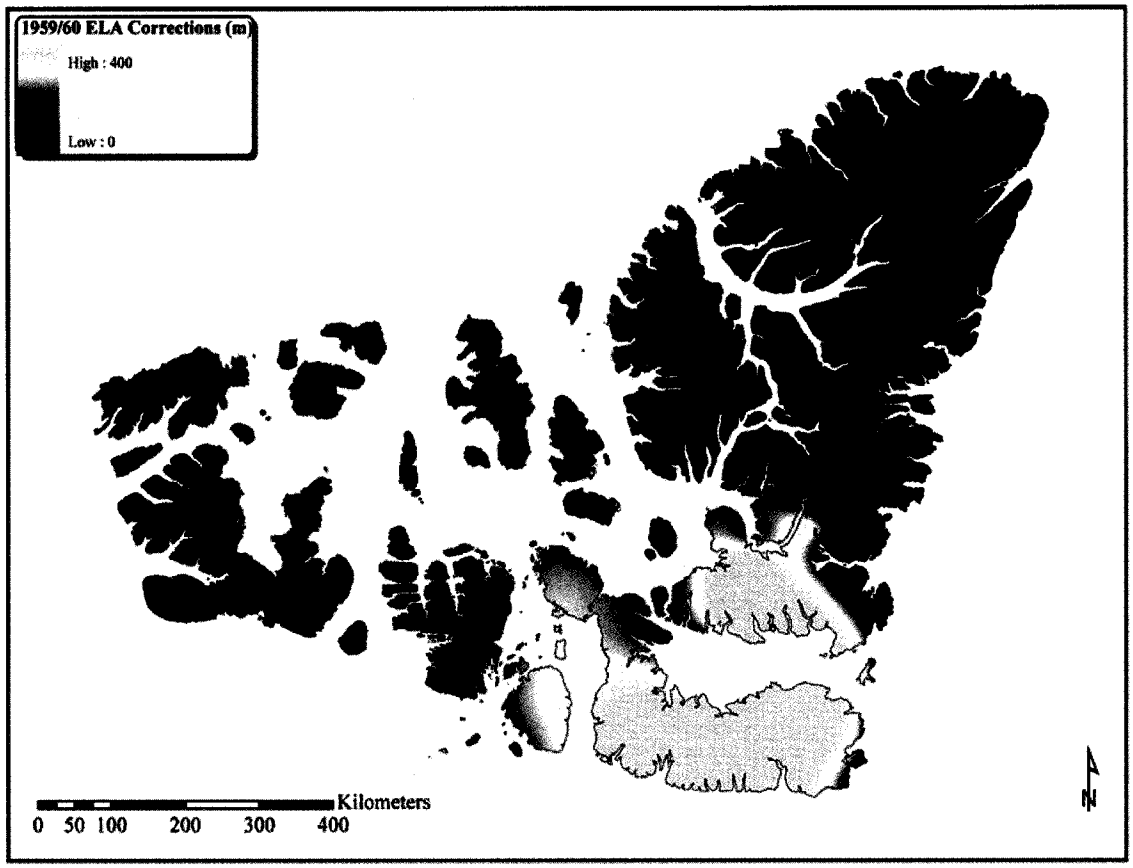

Figure 4. 5 Correction values for 1959/60 ELAs. Values were interpolated over underestimated areas of the SE QEI based on the early 1960s multi-year ELA on the Devon Ice Cap.

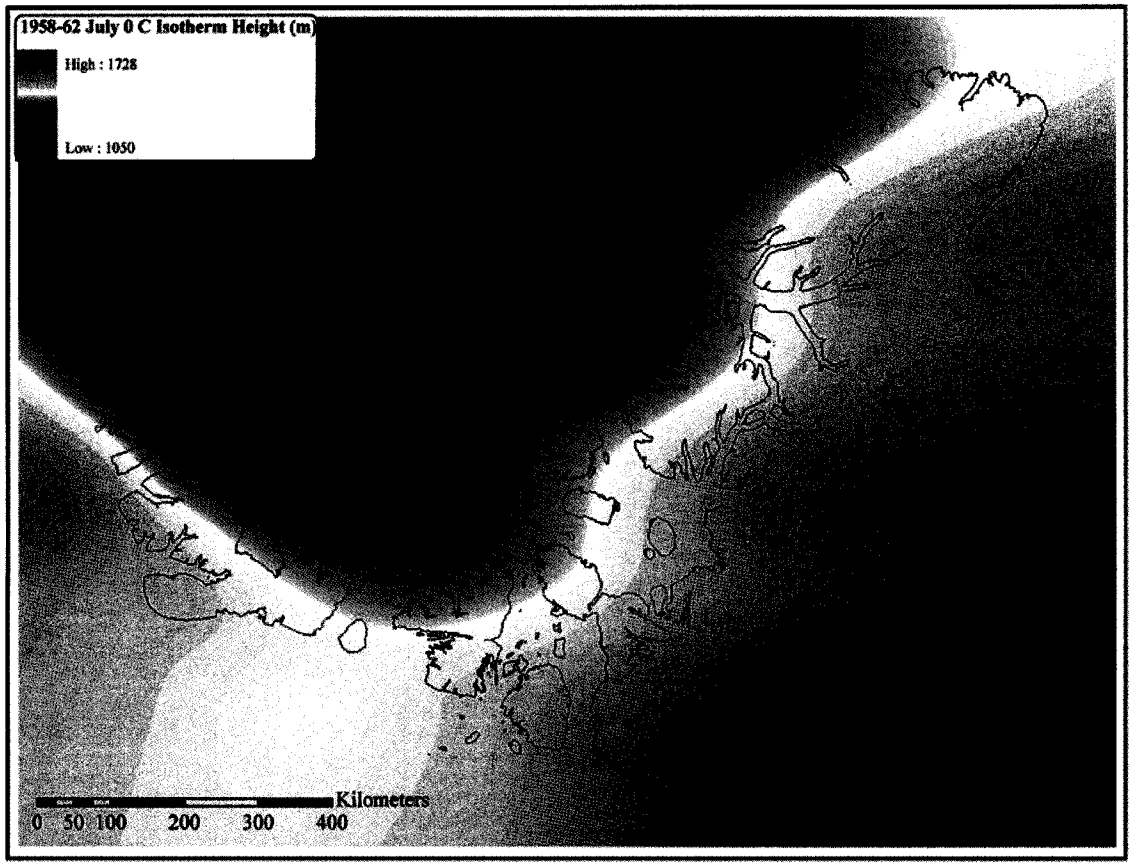

Figure 4. 6 Mean July 0 °C isotherm heights over the QEI for the period 1958-1962. The multi-year average height, centered on 1960, shows the trend in the 0 °C isotherm, which has been shown to be positively correlated with height of the equilibrium-line in the Canadian High Arctic (Bradley, 1975).

underestimated ELAs. The correction grid was added to the original 1960 ELA grid to produce a corrected 1960 ELA trend surface across the QEI (ELA.2, Fig. 4.7). The map of corrected 1960 ELAs (ELA.2) replaces the original 1960 ELA trend surface map (from Miller *et al.*, 1975) for all analyses in forthcoming sections. The contrast between the 1960 and LIA ELA trend surfaces is used as a basis for interpreting differences in climatic conditions between the LIA and the mid-20th century, which led to post-LIA changes in perennial snow/ice extent across the QEI.

4.5 Post-LIA Changes in Perennial Ice Cover and ELAs

Between the termination of the LIA and 1960, the area of the QEI covered by perennial snow/ice decreased by 37% or 62,387 km^2 (Fig. 4.8 and Table 4.1). Most of this ice cover loss (94%, 58,677 km^2) occurred on the three largest islands (Ellesmere, Axel Heiberg, and Devon Islands) where most of the ice in the QEI is concentrated today. Area changes for individual islands ranged from 20 to 40% for the eastern QEI (Ellesmere, Axel, Devon, and Coburg). With the exception of Meighen Island (~40%), reductions in the low-lying central and western QEI (Bathurst, Cornwallis, Cornwall, Amund Ringnes, Ellef Ringnes, and Melville Islands) ranged from 90 to 100%.

Collectively, the ELA trend surface (1 km resolution) during the LIA shows a significant departure from the corrected 1960 ELA trend surface (Fig. 4.9). The LIA ELA trend surface indicates lower elevations along coasts and increasing heights inland. For example, exceptionally low ELAs (0-200 m) are found along the coasts of SE Ellesmere and E Devon Islands that face Baffin Bay (Koerner, 1977; Maxwell, 1981). In the northwest QEI a lower ELA (0-200 m) also characterizes the coastlines extending

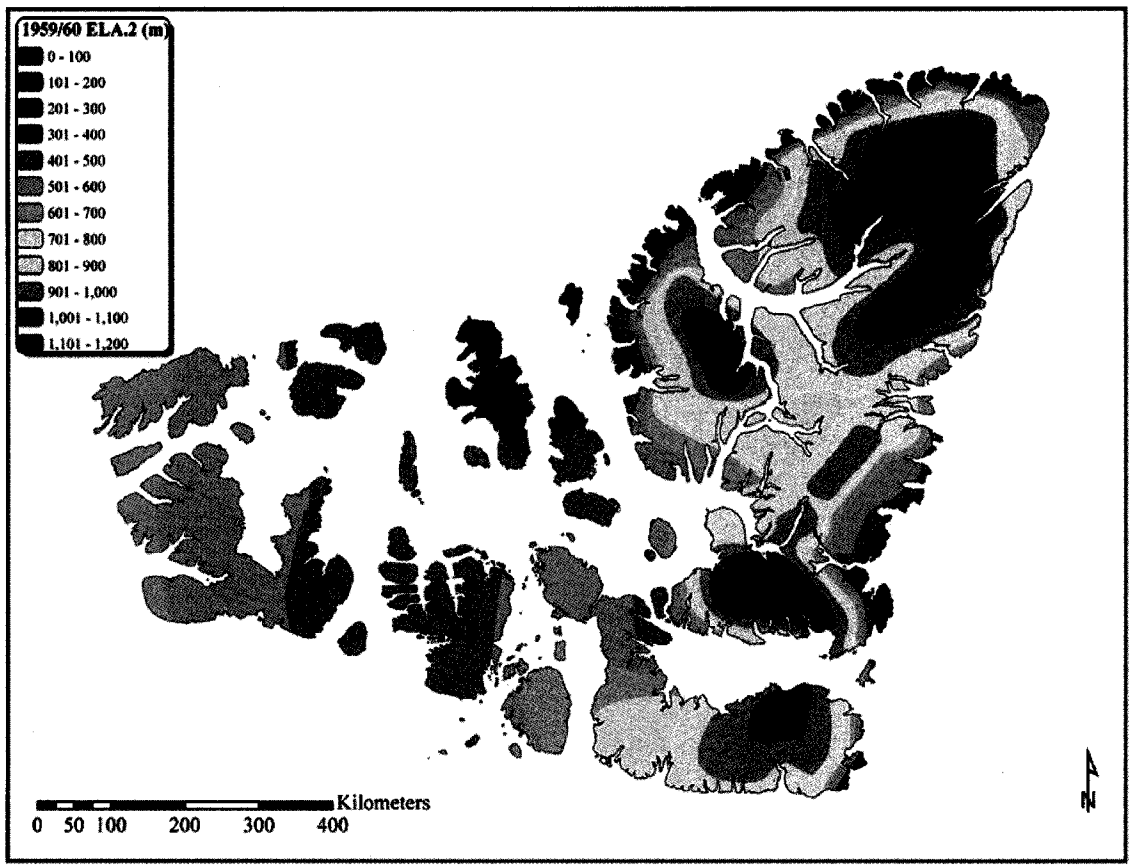

Figure 4. 7 Corrected 1959/60 ELA trend surface (ELA.2); interpolated correction values (see Fig. 4.5) added to original 1960 ELAs (Fig. 4.4; Miller *et al.*, 1975).

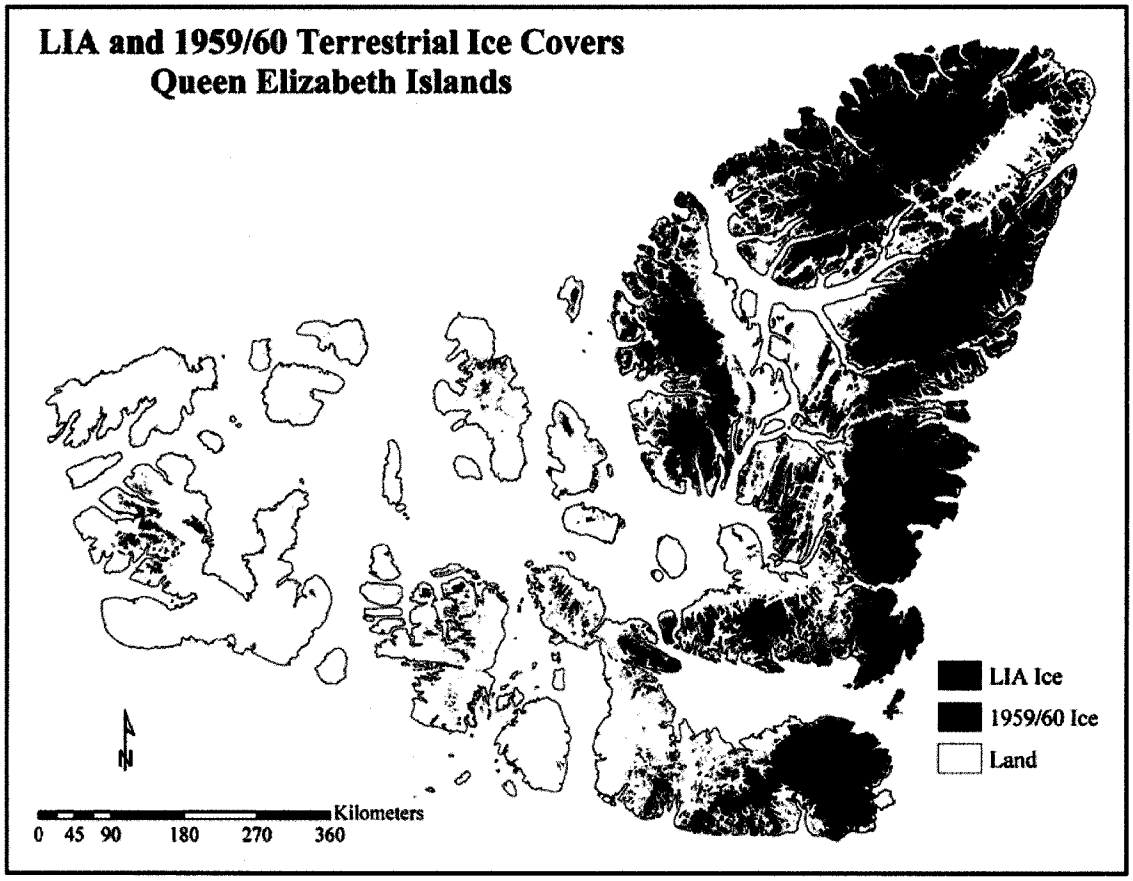

Figure 4. 8 Reconstructed LIA and 1959/60 perennial snow/ice cover for the QEI.

Island	LIA (km^2)	1959/60 (km^2)	Area Change (km^2)	% Area Change
Ellesmere	122993.0	79317.5	-43675.6	-35.5
Axel Heiberg	20039.4	11987.2	-8052.2	-40.2
Devon	22942.8	15993.1	-6949.7	-30.3
Melville	1860.8	153.2	-1707.6	-91.8
Bathurst	1065.4	0.0	-1065.4	-100.0
Ellef Ringnes	497.1	0.0	-497.1	-100.0
Amund Ringnes	246.7	0.0	-246.7	-100.0
Cornwall	69.4	0.0	-69.4	-100.0
Meighen	155.6	93.1	-62.5	-40.1
Coburg	226.9	188.0	-39.0	-17.2
Cornwallis	22.8	0.0	-22.8	-100.0

Table 4. 1 LIA and 1959/60 ice area and area change totals (LIA-1959/60) for the QEI.

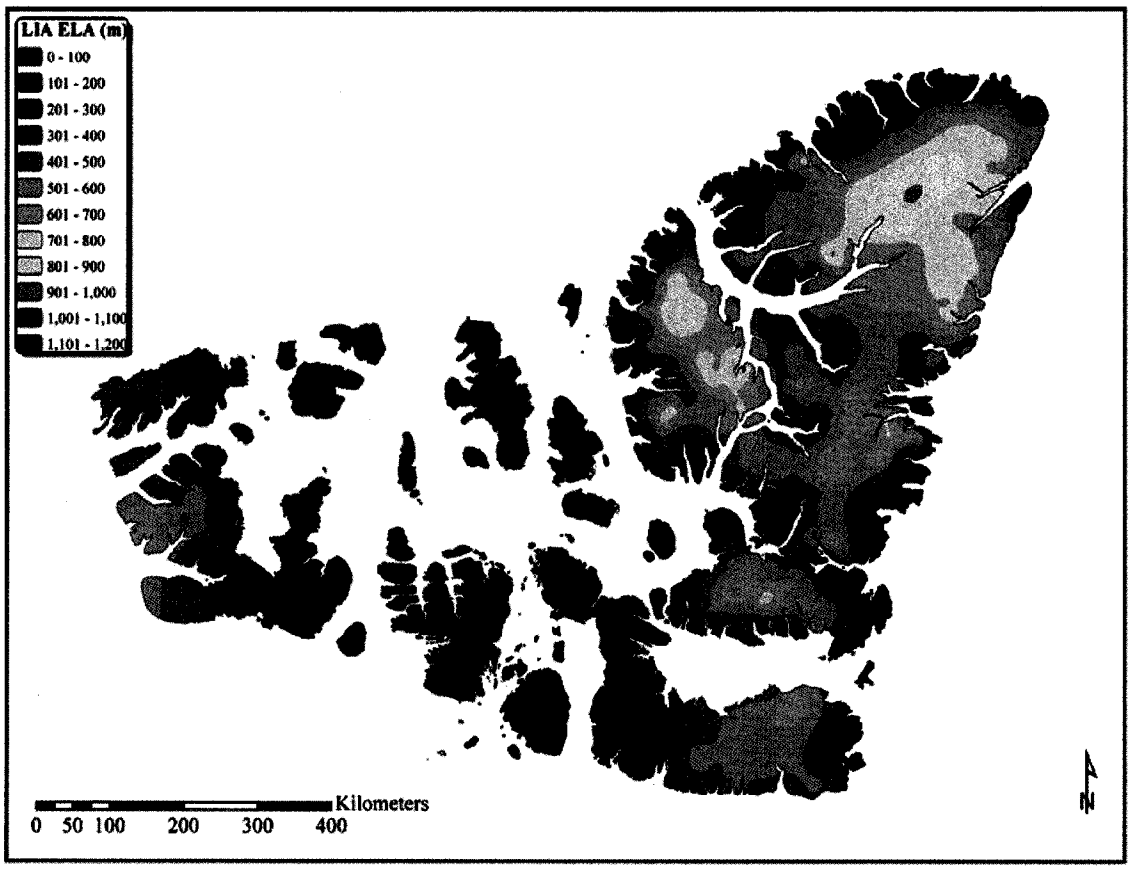

Figure 4. 9 Reconstructed LIA ELA trend surface over the QEI.

from Ellef Ringnes Island to N Ellesmere Island (Fig. 4.9). ELAs gradually increase towards the southwest QEI where higher ELAs (400-600 m) are found on western Melville Island. Higher ELAs (> 1,000 m) can also be found in the interiors of Axel Heiberg and Ellesmere Islands.

In their mapping of ELAs and glaciation levels (GL) in the QEI, Miller *et al.* (1975) identified the existence of sharp gradients in the GL in coastal areas, in particular along the north coast of Ellesmere Island (Fig. 4.4). Although the trend surfaces for both intervals exhibit similar spatial patterns, LIA ELA gradients, however, tend to be much shallower along the coasts of Devon and SE Ellesmere Islands bordering Baffin Bay and along the north coasts of Axel Heiberg and Ellesmere Islands. For instance, LIA ELA gradients along the north coast of Ellesmere Island to inland locations were ~6 m km^{-1} compared to ELA gradients of ~14 m km^{-1} for the same area in 1960. Shallower LIA ELA gradients in these areas may be due to high precipitation rate during the LIA (i.e., a change in the lifting condensation level (LCL) or more frequently occurring storms), and hence a modulation of the ELA trend surface.

ELA Δh throughout the QEI from the LIA to 1960 are shown in Figure 4.10. The region of greatest change (~300->600 m) extends from Devon Island, into S Ellesmere and S Axel Heiberg Islands and north into the lowlands separating Axel Heiberg and Ellesmere Islands and the high plateaus and mountains of northern Ellesmere Island. The smallest change (<100 m) occurred in coastal localities, especially along northern Axel Heiberg Island, northwest Ellesmere Island, the southeast sector of the QEI bordering Baffin Bay, and western Melville Island.

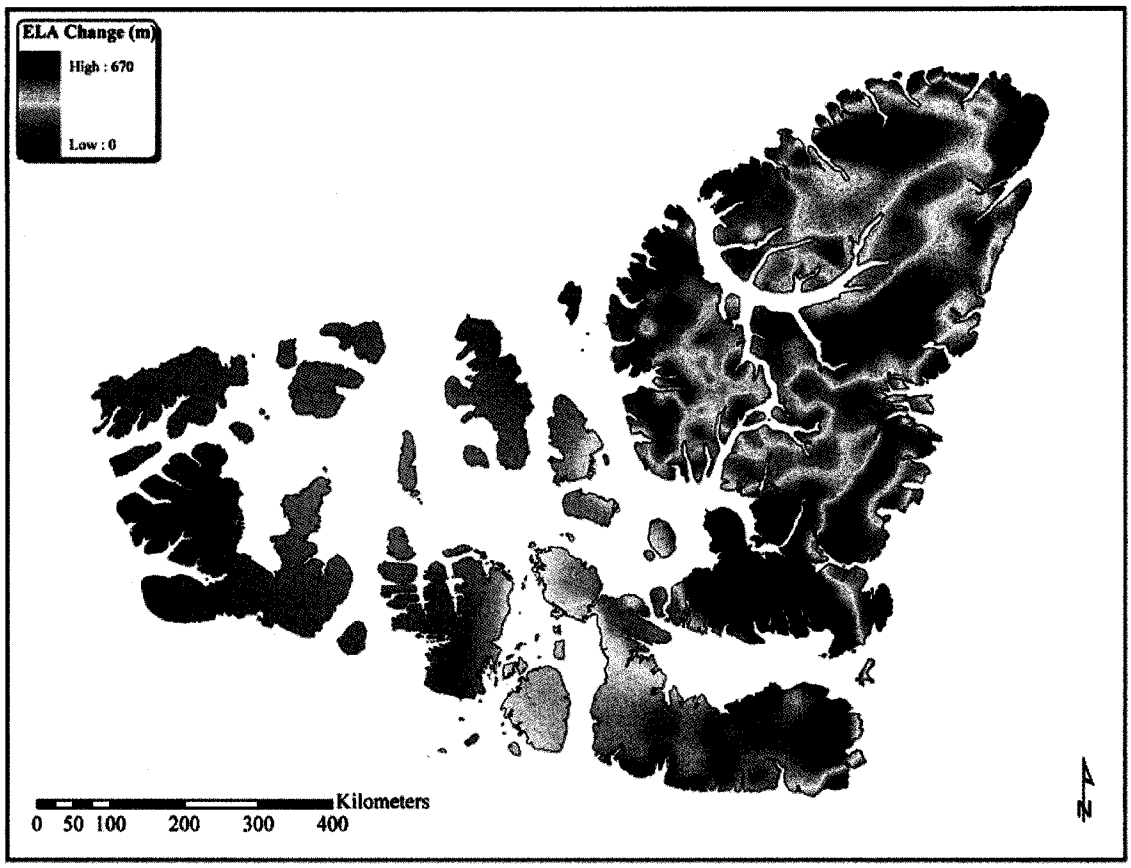

Figure 4. 10 ELA change (Δh) between the LIA and 1960.

4.6 Analysis and Discussion

This section presents a four-part analysis and discussion of the results from the previous section. The first section investigates the spatial changes in perennial snow/ice extent between the LIA and 1960. The second section analyses NCEP/NCAR reanalysis and identifies extreme cold and warm decades and specific modes of variability associated with climatological variables in the modern record (1949-2002) that serve as possible analogs for those that might have occurred between the LIA and early 20th century in the QEI. In the third section, important atmosphere-ocean interactions related to modern analogs of LIA and the early 20th century climates (cold and warm decades) are identified and discussed. The fourth section identifies important connections between the pattern of ELA Δh and the primary modes of variability of climatological variables found in the modern record, and provides a spatial reconstruction of post-LIA to 1960 temperature change across the QEI.

4.6.1 Ice Cover Distribution

Throughout the QEI, a rise in the ELA following the LIA resulted in a substantial decrease in ice cover and a considerable exposure of predominantly unoxidized and unvegetated bedrock and/or unconsolidated substrates (Fig. 4.2). This reduction in snow and ice area has also resulted in a change in the pattern of ice distribution. Figure 4.11 shows area-elevation relationships for the LIA and 1960 ice covers. During the LIA, the maximum areal coverage of perennial snow/ice in the QEI was centred on an elevation of ~700 m. By 1960, this had increased to ~1100 m. Consequently, the greatest reduction of ice cover following the LIA was on intermediate elevation plateaus (700-1000 m asl)

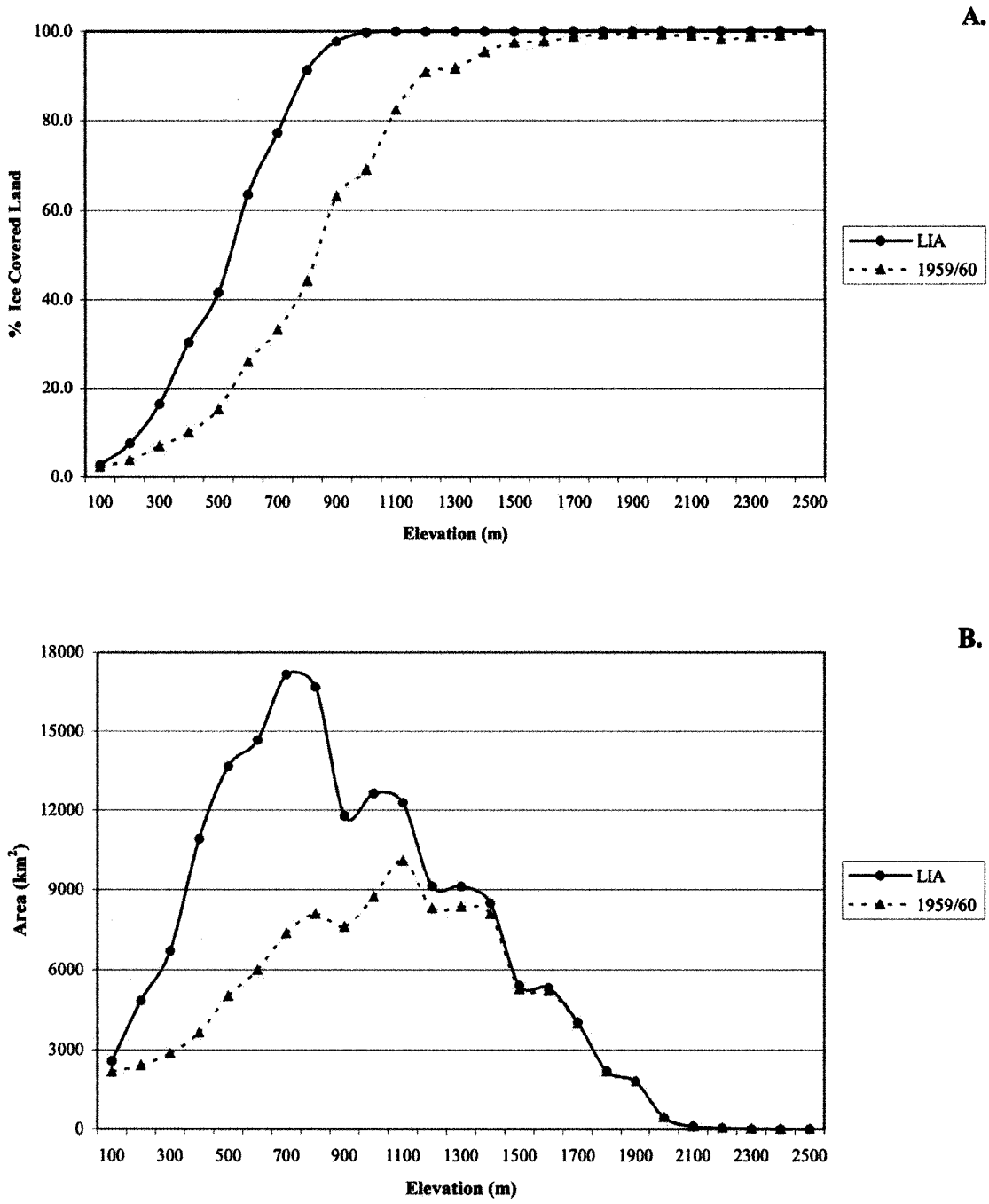

Figure 4. 11 Area-elevation (hypsometric) relationships for LIA and 1960 ice covers in the QEI. (A) shows the distribution of ice covered land with respect to elevation, and (B) shows ice area with respect to elevation.

rather than in surrounding mountains where higher accumulation zones have helped to maintain many outlet glaciers close to their LIA margins.

A change in the distribution of ice cover in the QEI with respect to the position of the ELA is dependent not only on the prevailing climatic conditions but also on the hypsometry (area-elevation distribution) of the land. Climatically induced lowering (rising) of the ELA will result in an increase (decrease) in ice-covered area as more land is added to the accumulation area (ablation area). This effect is enhanced if ELA lowering (or rising) occurs in areas where topographic complexity is low (i.e., few large undulations) and orographic amplitude is high (i.e., high land elevation), such as in intermediate and high plateau regions. Such areas may provide the most suitable setting for glacial inception (Oerlemans, 2002), but they are also the most vulnerable to large-scale reductions in perennial snow/ice cover as a result of a small increase in the ELA. For instance, on western Melville Island, extensive high plateaus rise abruptly from sea level to >700 m in the west and descend gently eastward to >400 m over ~100 km. Between the LIA and 1960, an average increase in the ELA of only ~50 m over the plateaus of W Melville led to a 92% reduction in ice cover (Fig. 4.8 and 4.10). Substantial reductions in ice cover since the LIA are characteristic of many of the plateaus in the central and western QEI, where orographic range is limited to only a few hundred meters over hundreds of square-kilometers, and the change in ELA was generally <100 m. By 1960, most of these islands were devoid (or nearly so) of perennial snow/ice (Fig. 4.8 and Table 4.1). In contrast, the least amount of areal change in perennial snow/ice cover, coincident with the largest change in Δh, occurred in the mountains of Axel Heiberg and Ellesmere Islands, where large ice caps and many

glaciers persist today. In these highly glacierized areas, large changes in the ELA have little short-term (10^1-10^2 yr) impact because the ice coverage is already substantial.

4.6.2 Climate Variability in the QEI

In the QEI, variability in net mass balance is dominated by climate conditions during the summer (i.e., temperature and precipitation), because winter accumulation is low and relatively consistent, allowing inter-annual variability in ablation to predominantly control variations in the height of the equilibrium-line (Dowdeswell *et al.*, 1997). It is, therefore, assumed that the reduction of perennial snow/ice extent since the LIA has been dominated by changes in summer climate; if this is so, this area reduction provides a proxy record of summer climate. Hence, the variability in summer temperature and precipitation in the QEI between the end of the LIA and 1960 is of primary interest for this study. However, because the instrumental record in the QEI (~56 yr) extends only a decade into the time period of interest (pre-1960), the contemporary record was searched for potential modern analogs of climatic conditions that would have favoured, and hence help to explain, the high summer ablation and the large spatial differences in Δh in the QEI during the early twentieth century noted above.

4.6.3 Climate Data

All NNR variables were spatially averaged across the QEI based on a 2.5° resolution grid. All climate variables used in this study (NNR and ERSST) span the interval 1949-2002 and annual, summer (JJA), and winter (DJF) averages were obtained

for each year. Long-term seasonal means (1949-2002) and standard deviations were calculated, and used to compute normalized anomalies from the long-term mean by,

$$X_N = (X_i - X_m)/S_x,$$

where X_i is the mean of a meteorological variable (annual or seasonal) for a particular year, X_m is the long-term mean (annual or seasonal), and S_x is the long-term standard deviation (annual or seasonal) for a meteorological variable.

4.6.4 1949 - 2002

The NNR time series (1949-2002) of QEI normalized mean summer SAT and SPR anomalies are shown in Figure 4.12. Both temperature and precipitation records show substantial inter-annual variability, and only a slight negative correlation (r = -0.09) is found between the two variables. Summer SAT anomalies in the time series range from -2.5 to 2.3 standard deviations, equivalent to -1.0 to 0.9 °C. The highest (warmest) anomalies in the period occurred in the late 1950s to early 1960s, before a step-like change to the lowest (coldest) anomalies from the mid-1960s to mid-1970s. The period from the late 1970s to the present is characterized by less inter-annual variability with more positive temperature anomalies resulting in a gradual increase in mean summer temperature. The time series contains nine extreme cold years (those exceeding one standard deviation: 1964, 1965, 1967, 1969, 1970, 1972, 1974, 1992, and 1996) and five extreme warm years (1954, 1957, 1960, 1981, and 1998). Seven of the cold years occurred during the mid-1960s to mid-1970s, with the coldest mean summer temperature (1972) dropping -0.9 °C below the 1949-2002 mean (-0.8 °C). Three of the five warm years occurred during the warmer than normal part of the record, from the late 1950s to

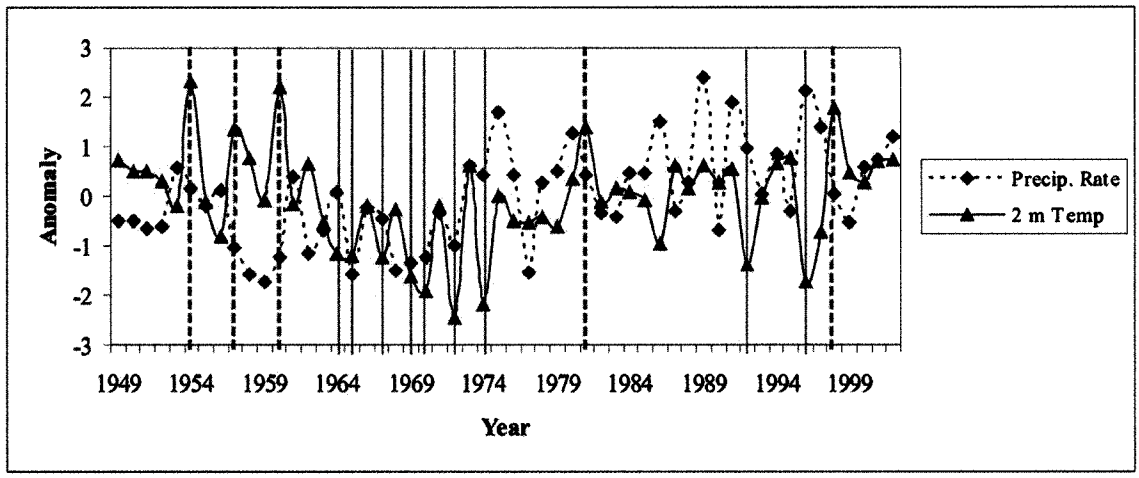

Figure 4. 12 Normalized anomaly time series of summer 2 m temperature (SAT; red) and surface precipitation rate (SPR; blue) for the period 1949-2002. Solid (dashed) vertical lines denote extreme (exceeding one standard deviation) cold (warm) years.

early 1960s; the warmest mean summer SAT for the entire record (0.1 °C; 1954) reached 0.9 °C above the 1949-2002 mean. QEI averaged summer SPR anomalies in the time series range from -1.7 to 2.4 standard deviations, and trends in the time series show drier than normal conditions in the first half of the record (1949-1974), with several extreme dry (1957-60, 1962, 1965, 1968-70, and 1972) and no extreme wet summers occurring during this time. The latter half of the record (1975-2002), however, shows wetter than normal conditions, with several extreme wet (1975, 1980, 1986, 1989, 1991-92, 1996-97, and 2002) and only one extreme dry summer (1977).

4.6.4.1 Patterns of Variability

Empirical Orthogonal Functions (EOFs) provide a compressed description of the variability of a spatially distributed time series, often referred to as a mode of variability. Principal Components (PCs) associated with these modes of variability demonstrate how the EOFs oscillate in time. In this study, EOFs were used to describe the main modes of variability of NNR meteorological variables over the QEI for the 1949-2002 (summer) period. EOFs were computed using Climate Explorer from the Royal Netherlands Meteorological Institute (http://climexp.knmi.nl) to a cumulative explained variance of 80% for the following meteorological variables: SAT, precipitation, sea surface temperature, sea level pressure, and geopotential heights at 850, 500, and 200 hPa levels.

Figure 4.13 shows the leading mode of variability (EOF-1) for summer SAT for the QEI and the corresponding PC time series from 1949-2002. EOF-1 explains 55% of the variance (EOFs 2 and 3 explain 12 and 8%, respectively) and illustrates a strong pattern of variability over the E QEI. The largest values of variance occur in the southeast part

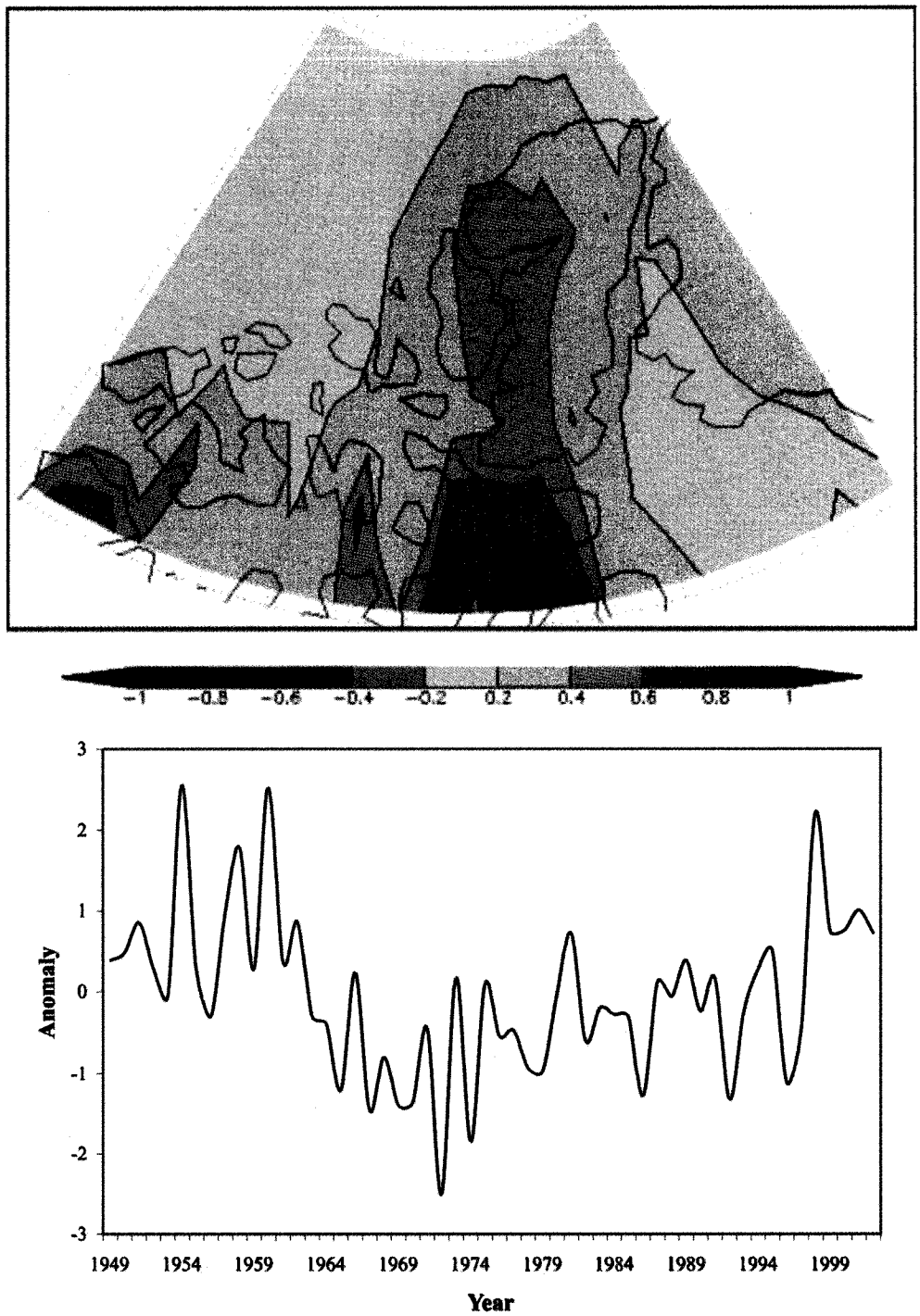

Figure 4. 13 The first Empirical Orthogonal Function (EOF-1) of SAT (top), centered over the QEI, and corresponding principal component (PC-1) time series (bottom) for the period 1949-2002.

of the islands (principally Devon Island) and extend north into the intermontane basin between Axel Heiberg and Ellesmere Islands. The pattern of variability illustrated by EOF-1 coincides with the pattern of ELA Δh (Figs. 4.13 and 4.10). The principal component time series associated with EOF-1 shows how this preferred temperature pattern evolves over time (Fig. 4.13). The positive phase of this pattern was strongly established during the early part of the record, concomitant with the highest summer temperatures during the period. Conversely, negative scores (PC-1) of this mode are dominant from the mid-1960s to the late 1970s, indicating cool summer temperatures in the same spatial pattern.

EOF-1 of SPR (1949-2002) explains 40% of the variability in the period (Fig. 4.14). The spatial pattern of variability shows a band of positive variance values (loadings) extending from the north-central to east-central QEI, with the high values over the Arctic Ocean and running through Meighen Island and Amund and Ellef Ringnes Islands. The associated PC time series (Fig. 4.14) shows high inter-annual variability, with the first half of the record showing mainly negative anomalies in the SPR (1949-1974), whereas positive anomalies are prevalent during the latter part of the record (1975-2002). EOFs 2 and 3 (not shown) explain another 16 and 11% of the variability within the period of record, respectively.

4.6.4.2 Correlations and Decadal Trends

Variations in summer temperature and precipitation in the QEI (1949-2002) are due in part to fluctuations in the distribution of atmospheric mass in the Arctic. Correlation coefficients for linear regression analysis indicate positive correlations between PC-1

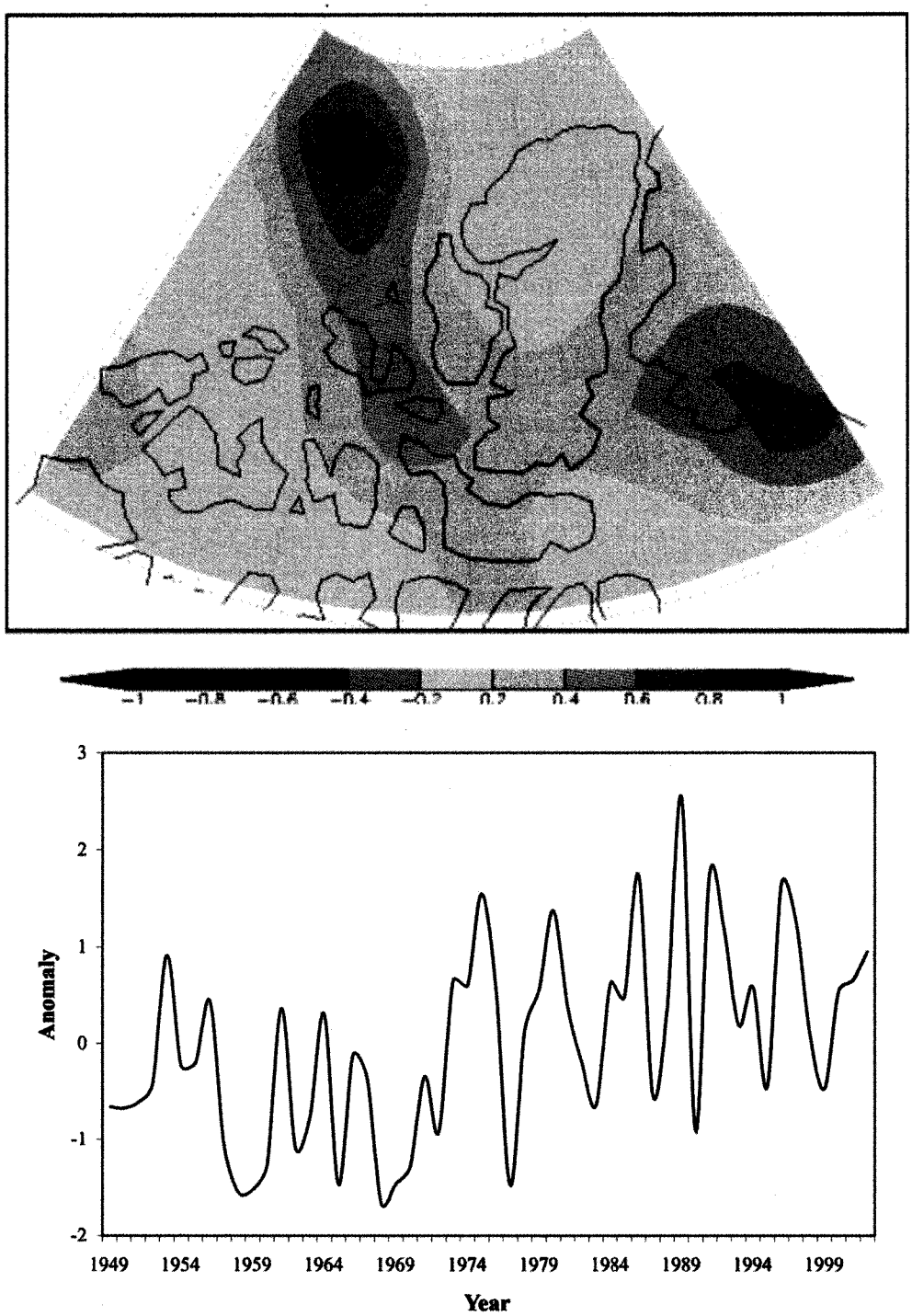

Figure 4. 14 EOF-1 of SPR (top), centered over the QEI, and corresponding PC-1 time series (bottom) for the period 1949-2002.

(summer SAT) and summer geopotential height at the 500z and 200z levels (r = 0.57 and 0.59, respectively), and also exhibits a negative correlation with the summer North Atlantic Oscillation (NAO) index (r = -0.48). Only slight correlations, however, are apparent with other climate indices (e.g., Pacific North American pattern (PNA), r = 0.19; Southern Oscillation Index (SOI), r = 0.17; Arctic Oscillation (AO), r = 0.03). PC-1 of summer QEI precipitation rate is negatively correlated with fluctuations in the height of the summer 500 hPa geopotential surface (r = -0.64) and positively correlated with the summer AO index (r = 0.53).

Figure 4.15 shows five-year running mean time series of the first principal components of QEI averaged summer SAT and summer geopotential height at the 500z and 200z levels, and the NAO index for the period 1949-2002. Decadal scale fluctuations in PC-1 of summer SAT are strongly coupled to changes in both the upper troposphere (500z) and lower stratosphere (200z). Moreover, decadal shifts in the phase of the NAO are coincident with decadal-scale modifications in PC-1 of summer SAT, which suggests regional scale influences on summer surface temperature fluctuations in the QEI. Distinct trends in the time series in approximately the first half of the record illustrate contrasting periods of warm and cold conditions, which will serve as the basis for the following analyses.

4.6.5 Warm and Cold Decades

Two decadal episodes representing extreme (exceeding one standard deviation of the decadal mean for the period 1949-2002) warm (1953-1962) and cold (1965-1974) periods are recoded in the NNR spatially averaged time series for the QEI. The warm

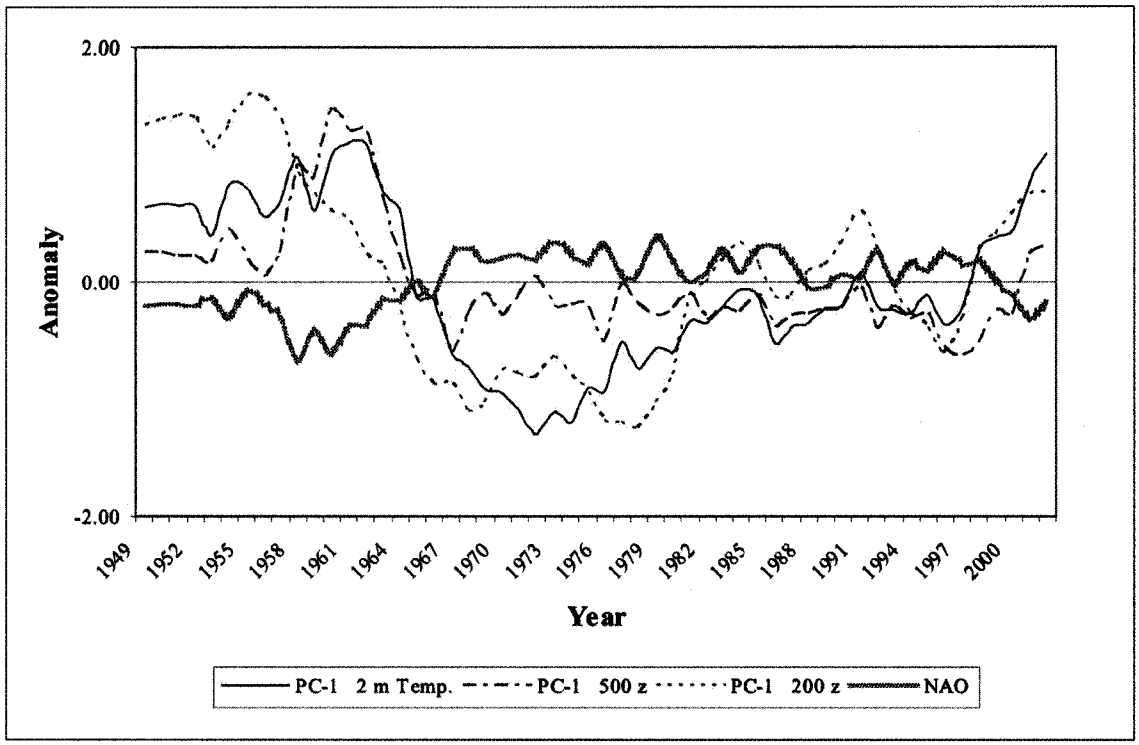

Figure 4. 15 5-year running mean time series of the first principal components of SAT and 500 and 200 hPa geopotential heights, and normalized anomalies of the NAO index (1949-2002). In the early part of the record, strong decadal extremes are evident as each of the time series co-vary. During the latter part of the record decadal trend are much weaker, and inter-annual variability dominates.

decade is consistent with reports of net ablation on glaciers on the Hazen Plateau, E Ellesmere Island (Hattersley-Smith and Serson, 1973), and the cold decade is characterized by a lowering of the ELA and positive mass balance on some QEI glaciers and ice caps (Bradley and Miller, 1972; Bradley, 1973; Bradley, 1975; Bradley and England, 1978; Alt, 1987; Braun *et al.*, 2004). These contrasting temperature regimes are examined and analyzed in order to identify potential modern analogs for LIA and early 20th century climates.

4.6.5.1 Patterns of Variability

EOFs of SAT and SPR for the QEI were calculated for both warm and cold decades separately (above), and the leading EOFs for each extreme decade are shown in Figure 4.16. EOF-1 of SAT for the warm decade explains 62% of the variation over the QEI for this interval. The positive phase of this pattern describes anomalously high temperatures over most of the QEI, with the greatest warming found in the east-southeast QEI and normal temperatures over the north central islands bordering the Arctic Ocean. For the cold decade, EOF-1 of SAT explains 65% of the variability, with the negative phase of this pattern depicting anomalously low temperatures encompassing the entire QEI. This pattern shows the largest variance values extending from the south, particularly over Melville Island with an elongated spur extending north over Devon, Axel Heiberg, and southwest Ellesmere Island (Fig. 4.16).

The leading EOFs of summer SPR for both the warm and cold decades (Fig. 4.16, explaining 52% and 48% of the variability, respectively) are structurally similar to the leading mode of variability for the entire study period (1949-2002; Fig. 4.14), with

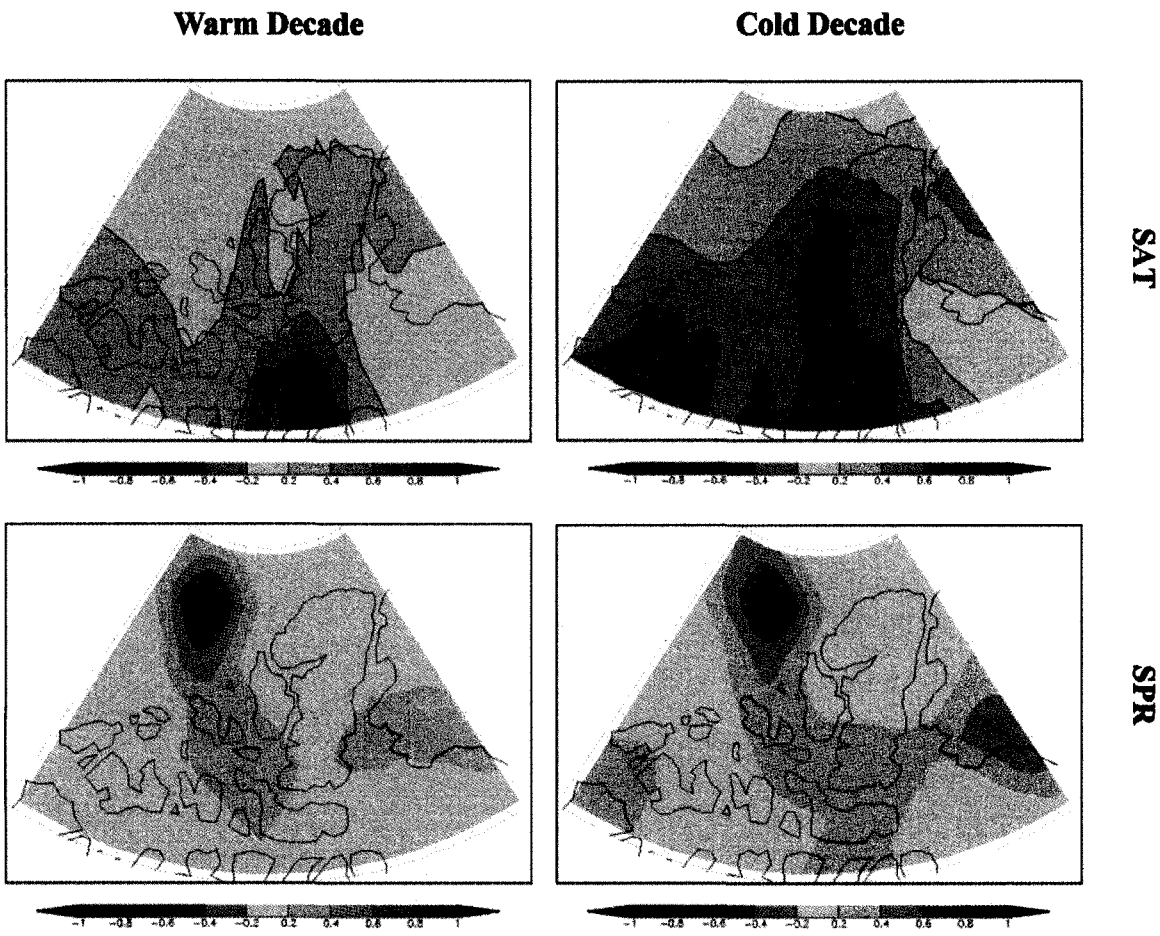

Figure 4. 16 EOF-1 of SAT and SPR for both warm (1953-1962) and cold (1965-1974) decades.

positive values of variance extending from the Arctic Ocean, south-southeasterly through the central QEI. The spatial pattern of variation is mostly in its negative phase during both warm and cold decades (PC-1, Fig. 4.14), indicating more frequently occurring low SPR anomalies in the QEI during this time. During the second half of the study period, EOF-1 (SPR) is mostly in its positive phase and its amplitude generally increases with time, concomitant with temperature increases across the QEI (Fig. 4.13).

The distinct pattern of variability that is expressed in each of the leading EOFs of precipitation (Fig. 4.14 and 4.16) represents the dominant storm track through the QEI. The QEI is situated between relatively high SLP associated with the perennially ice-covered Arctic Ocean and low SLP in the commonly open waters of Baffin Bay (Alt, 1987). This configuration causes cyclones to take a S-SE track through the QEI towards Baffin Bay, where there is an increase in cyclone frequency and cyclogenesis (Serreze and Barry, 2005:98). Higher than normal precipitation occurs in the QEI when there is an increase in the frequency of cyclones along this track (i.e., the positive phase of the leading EOF of SPR); however, anomalously low SPR during both warm and cold decades suggests a decrease in the frequency of cyclones following this S-SE trajectory through the QEI.

4.6.5.2 Relation to Atmospheric Circulation

In order to examine the influence of atmospheric circulation patterns on summer SAT in the QEI during both warm and cold decades, PC-1 of QEI averaged summer SAT was regressed upon mean summer sea-level pressure and 850, 500 and 200 hPa geopotential height fields at each grid point north of 45 °N (Fig. 4.17). For the warm

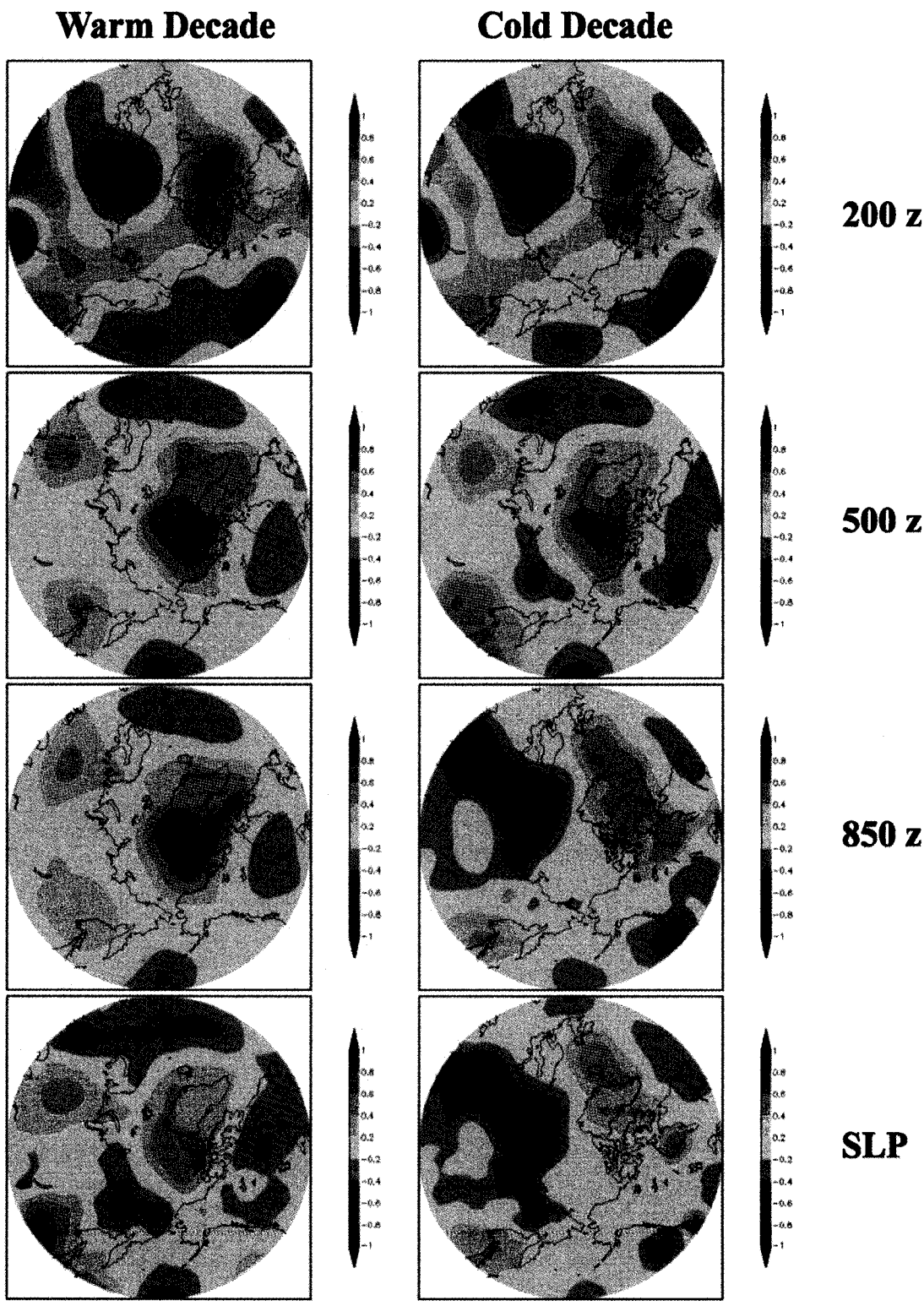

Figure 4. 17 Correlation coefficients for linear regression of PC-1 of QEI averaged SAT with SLP and 850, 500, and 200 hPa geopotential height surfaces (1949-2002) at each grid point north of 45 °N.

decade, anomalously high temperatures in the QEI are positively correlated with higher than normal SLP (Fig. 4.18) and elevated geopotential heights up to 200z over the Canadian Arctic, most of the Arctic Basin and southeastwardly over Iceland, the western North Atlantic Ocean and the Labrador Sea (i.e., a warm core high). In this region, a barotropic structure exists, that is, the positive geopotential anomaly occurs from the surface to the lower stratosphere, which coincides with a weak summer polar vortex, the centroid of which lies northwest of the QEI near the centre of the Arctic Ocean (Fig. 4.19). This barotropic structure is similar to that associated with the negative phase of the AO (Thompson and Wallace, 1998), and to a lesser extent with the NAO. Hence, a negative correlation exists between warm decade PC-1 of QEI averaged summer SAT and both the AO and NAO indices ($r = -0.38$ and -0.57, respectively). During the cold decade, PC-1 of QEI averaged summer SAT is positively correlated with geopotential height at the 200 and 500 hPa levels over the QEI (Fig. 4.17). In the lower troposphere, however, only a slight negative correlation exists between geopotential height (850 hPa to surface) and PC-1 (summer SAT) in the Arctic Basin and the western QEI, whereas, in the eastern Canadian Arctic, Greenland, and Iceland a positive correlation occurs between these variables. In the Arctic basin and western QEI, a core of cold dense air resides in the lower troposphere, resulting in high SLP and anomalously high geopotential heights below ~850 hPa (i.e., a cold core high; Fig. 4.18). Above this surface high, a strong, QEI-proximal summer polar vortex occurs in the upper troposphere and lower stratosphere (Fig. 4.19). From northern Ellesmere Island to southern Hudson Bay and eastwards across the North Atlantic, the negative geopotential anomaly occurs consistently from the lower troposphere to the lower stratosphere, while in the mid-

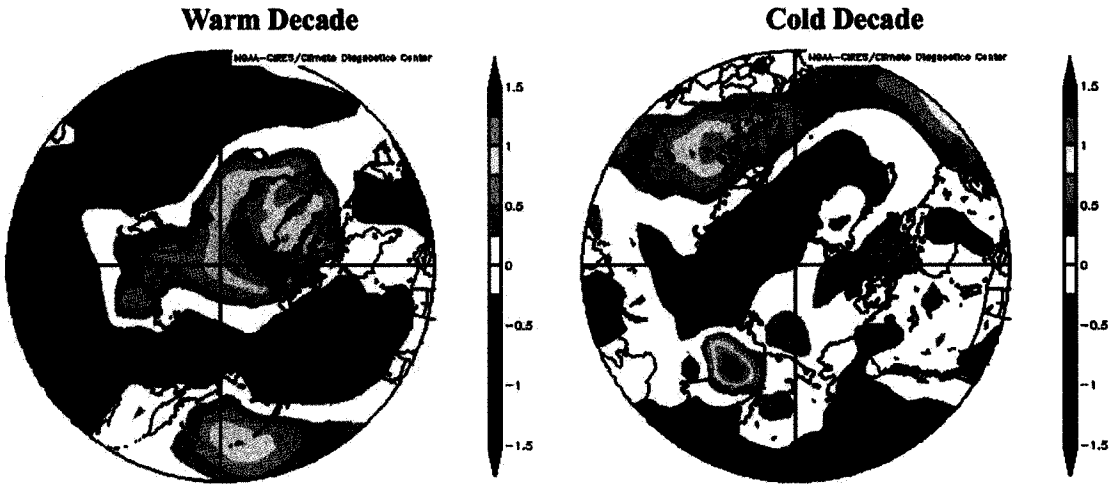

Figure 4. 18 Summer mean SLP anomalies (45-90 °N) during warm (1953-1962) and cold (1965-1974) decades in the QEI. Anomalies are in reference to the 1949-2002 climatology period.

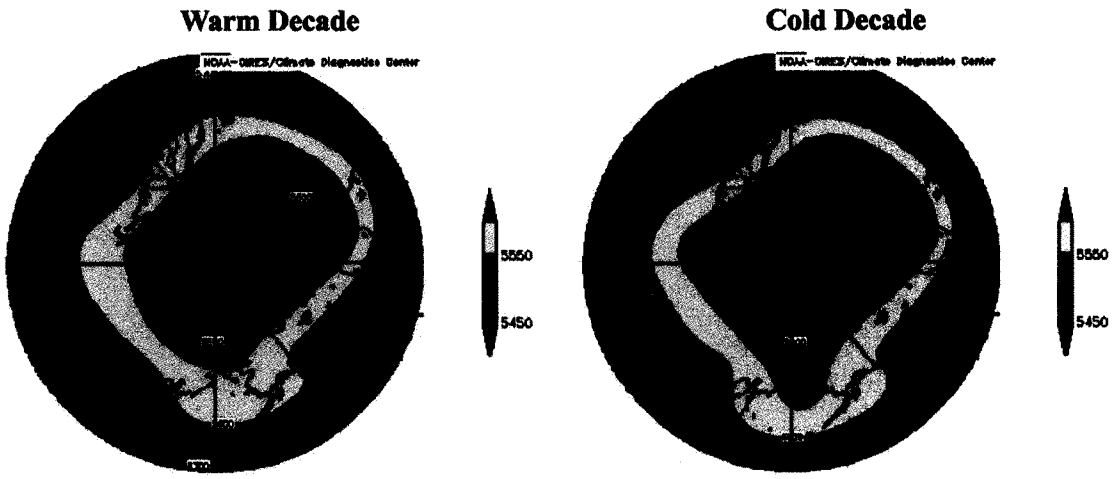

Figure 4. 19 Mean 500 hPa geopotential height surface indicating a weak, QEI-distal (strong, QEI-proximal) polar vortex during the warm (cold) decade.

Atlantic, areas of negative correlation represent positive geopotential anomaly (Fig. 4.17). Anomalously low pressure in the North Atlantic relative to high pressure in the mid-Atlantic during the cold decade, is characteristic of a positive NAO (Fig. 4.18); a negative correlation exists between PC-1 of QEI averaged summer SAT and the NAO index (Fig. 4.15), but the correlation is weak (r = -0.32).

4.6.5.3 Atmosphere-Ocean Interactions

In high latitude regions, complex energy exchanges between the atmosphere and ocean can bring forth positive feedbacks affecting atmospheric circulation, SSTs, and SATs (Hansen and Bezdek, 1996; Mysak *et al.*, 1996; Rogers *et al.*, 1998). To investigate the influence of SST on temperature changes during the warm and cold decades across the QEI, PC-1 of mean summer SAT was regressed upon mean summer SST (using the ERSST reanalysis) at each grid point for the extended circumpolar region north of 45° N (Fig. 4.20). During the warm decade, PC-1 of QEI averaged SAT is positively correlated with SST in the central and western North Atlantic, Labrador Sea and Hudson Bay and north into Baffin Bay and along the east coast of Greenland. In these areas, the correlation is robust (r = 0.65) and the variation in summer SST explains approximately 42% of the variability in the mean summer temperature for the QEI. Additional areas of positive correlation also occur in the Bering Sea, extending northward through Bering Strait, as well as in the Gulf of Alaska. During the cold decade, PC-1 of QEI averaged SAT is positively correlated with SST across the North Atlantic, with the most robust correlation located in the east-central North Atlantic (r = 0.70), where variation in summer SST accounts for about 50% of the variation in summer temperature

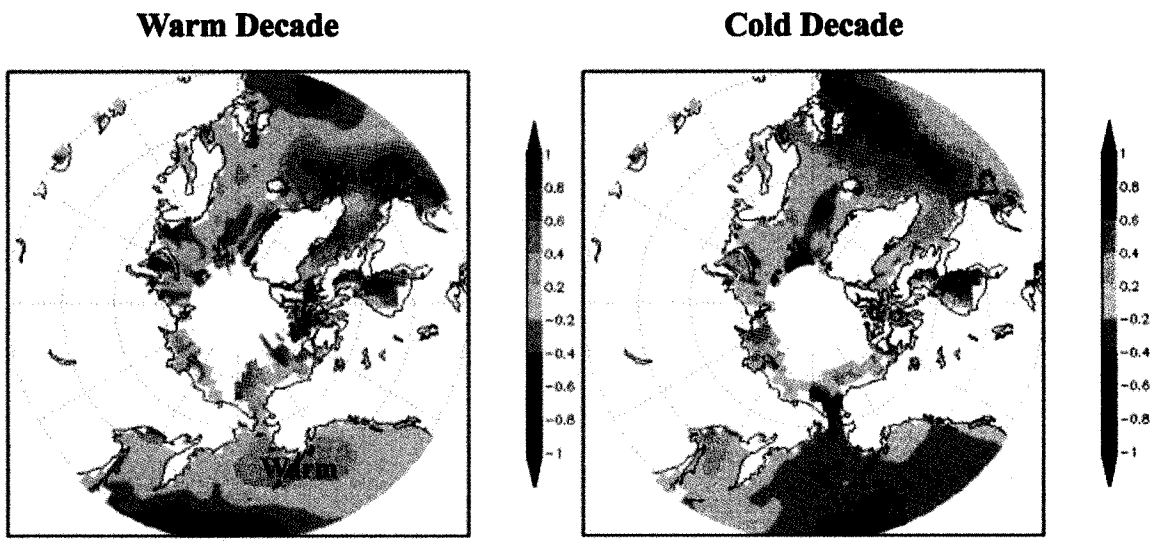

Figure 4. 20 Figure 4. 20 Correlation coefficients of linear regression of PC-1 of QEI averaged SAT with SST (1949-2002) at each grid point north of 45 °N.

in the QEI. Other areas of positive correlation are shown in Hudson Bay and the Labrador Sea, extending north into Davis Strait. Anomalously cool SAT in the QEI during this decade is negatively correlated with a broad area of warm SST in the North Pacific, as well as a much smaller area along the northeast coast of Greenland.

EOFs of summer SST were computed for the area north of 45 °N for the period 1949-2002. Figure 4.21 shows the leading two EOFs and their corresponding principal component time series. EOF-1 accounts for 29% of the variance and depicts a spatial pattern of variability whereby positive loadings are in the North Pacific and Bering Strait and lesser positive values are in the North Atlantic. For the full period of record, a positive correlation is revealed between PC-1 of SST and PC-1 of QEI summer SAT ($r = 0.32$), with a positive correlation during the warm decade ($r = 0.32$) and a weak negative correlation during the cold decade ($r = -0.10$). EOF-2 explains 18% of the variance in the data set and shows strongly positive values of variance in the North Atlantic, Davis Strait and Hudson Bay, and slightly negative values in the Bering Sea, Bering Strait and the Gulf of Alaska. A positive correlation was found between PC-2 of SST and PC-1 of QEI summer SAT for the period 1949-2002 ($r = 0.54$), with stronger positive correlations during both the warm and cold decades ($r = 0.65$ and 0.76, respectively), explaining 42% (warm) and 58% (cold) of the variance in PC-1 of QEI SAT. Strong coupling in these time series reflects the influence of changes in SSTs in the North Atlantic on SAT in the QEI during both extreme decades (Fig. 4.22).

The distribution of SST is largely influenced by surface winds resulting from strong gradients in the sea-level pressure fields. During the cold decade, anomalously low SSTs across the North Atlantic were influenced by enhanced westerly winds across the North

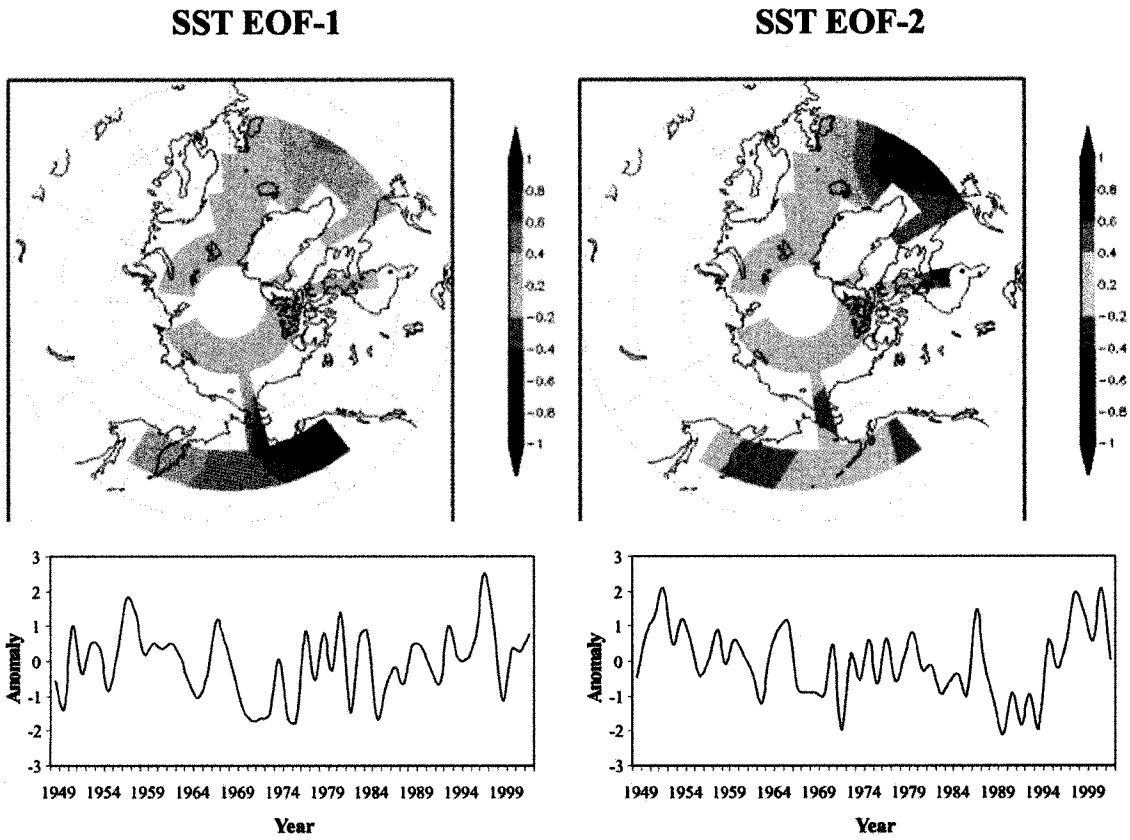

Figure 4. 21 First and second EOFs of summer SST (1949-2002) north of 45 °N for the period 1949-2002.

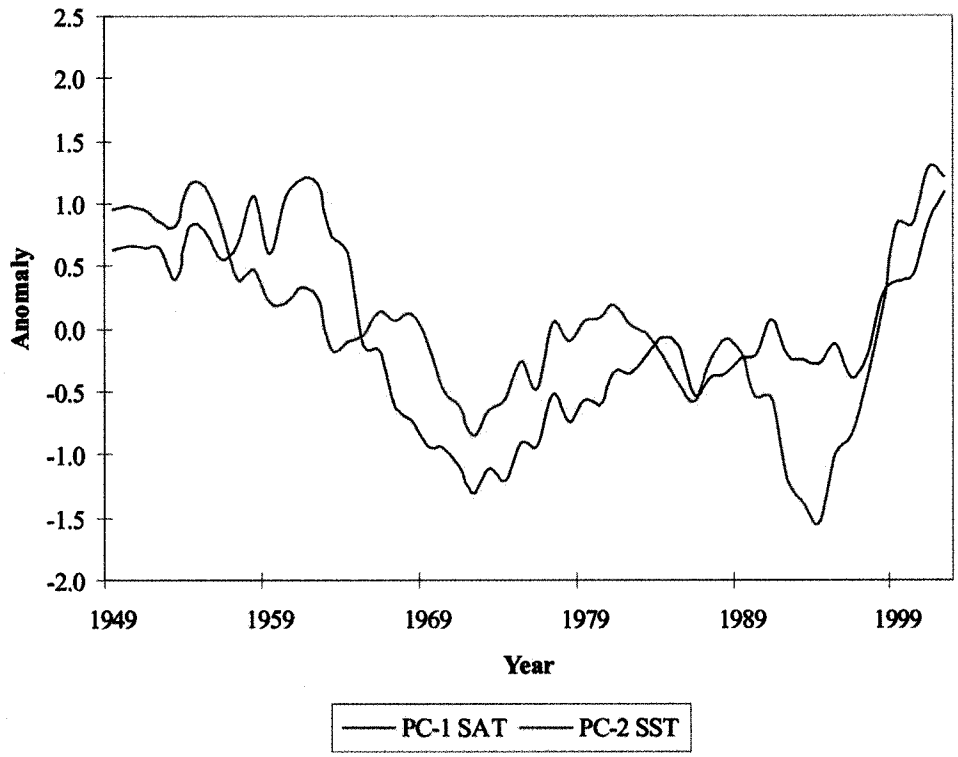

Figure 4. 22 5-year running mean time series of PC-1 of summer QEI SAT and PC-2 of summer SST (1949-2002) north of 45 °N showing strongly coupled variation during warm (1953-1962) and cold (1965-1974) decades in the QEI.

Atlantic, resulting from lower than normal pressure near Iceland (extending northeast into the Greenland and Barents seas) in combination with anomalously high pressure in the central Atlantic (Fig. 4.20 and 4.18). Although less intense, the cold decade atmospheric circulation pattern is similar to that of the 1972 extreme cold year described by Bromwich *et al.* (2002) (Fig. 4.23), where strong westerly winds across the North Atlantic increased the stress on the Ekman layer causing enhanced divergence and upwelling (lower SSTs) in the North Atlantic (Fig. 4.20). In both patterns (cold decade and 1972, Figs. 4.18 and 4.23), a deeper than normal Icelandic low was coupled with anomalously high pressure over the Arctic Ocean and the Canadian Arctic Archipelago, which created an intense zonal pressure gradient across the central and eastern QEI and Greenland and caused strong northerly airflow over this region. This persistent high pressure also serves as an effective obstruction to cyclones that typically track through this region (Alt, 1987), thereby reducing the precipitation during such cold intervals. Low SSTs in the North Atlantic increase low-level mid-latitude baroclinicity, resulting in enhanced low pressure over Iceland and stronger than normal cold northerly flow over the eastern Canadian Arctic (Bromwich *et al.*, 2002). In 1972, this northerly flow resulted in exceptionally low snowlines and positive summer mass balances on QEI glaciers (Alt, 1987), as well as one of the lowest percentages of summer open water on record throughout the QEI (Koerner, 1977). It has been hypothesized that the anomalous SSTs during the summer of 1972 were related to transient pools of cold water associated with the Great Salinity Anomaly (1968-1982; Dickson *et al.*, 1988; Rogers *et al.*, 1998; Bromwich *et al.*, 2002); it is possible that the migration of the salinity anomaly through the North Atlantic may have had an influence on the anomalous SSTs that were recorded

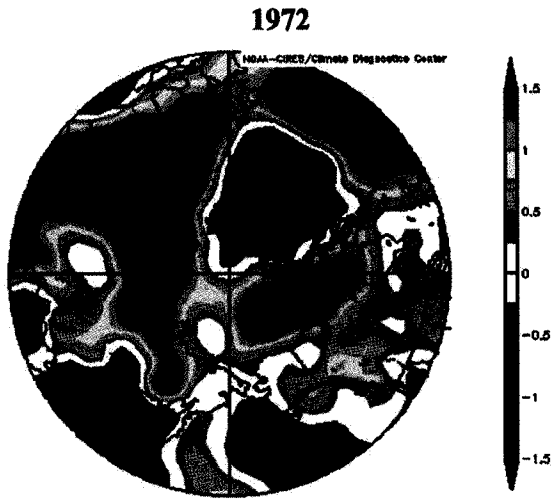

Figure 4. 23 Mean SLP anomalies (45-90 °N) for extreme cold summer 1972. Anomalies are in reference to the 1949-2002 climatology period.

during the cold decade, and ultimately, the low SATs throughout the QEI during this time. However, anomalously low SSTs in the North Pacific may also have influenced QEI SATs during the cold decade by modifying the Northern Hemisphere atmospheric circulation, which has also been credited for the abrupt lowering of summer freezing level heights over the QEI in 1963 (Bradley, 1973). Changes in the freezing level height in the atmosphere have been shown to be directly related to fluctuations in the ELA in the High Arctic (Bradley, 1975). Another influence on the low SAT across the QEI during the cold decade may have been the injection of volcanic aerosols into the stratosphere in response to increased volcanic activity during the 1960s and 1970s, starting with the massive eruption of Mt. Agung (Indonesia, 1963) (Hansen *et al.*, 1978; Bradley and England, 1978a; 1978b).

During the warm decade, high SSTs in the W North Atlantic Ocean and the Labrador Sea coincided with lower than normal pressure over northern Quebec, and anomalously high pressure over Greenland and most of the Canadian Arctic Archipelago (Fig. 4.20 and 4.18). The anomalous circulation pattern resulted in the cessation of typically strong westerly winds in the W North Atlantic, which, to first order, would have decreased the evaporative heat loss from the ocean surface layer. In addition, a pressure gradient reversal led to anomalous easterly wind stresses on the Ekman layer in this region, which would have caused a convergence of flow, leading to downwelling and a thickening of the warm surface layer in the western North Atlantic and Labrador Sea. Advection of warm water into Davis Strait and Baffin Bay would have significantly reduced sea-ice extent and increased the thermodynamic efficiency of warm south-

easterly winds directed into the QEI, effectively increasing the ELA and enhancing ablation on perennial snow/ice masses in this region.

Temperature variability in the Arctic has also been linked to fluctuations in sea-ice extent (Chapman and Walsh, 1993; Parkinson *et al.*, 1999; Bengtsson *et al.*, 2004; Johannessen *et al.*, 2004). In order to examine the role of sea-ice extent in variations in QEI SAT during the extreme warm and cold decades, the 100 yr 'Zakharov' data set is used. This includes observations of Arctic sea-ice extent within the ice-ocean margin (Zakharov, 1997; Johannessen *et al.*, 2004). Figure 4.24 shows time series of PC-1 of summer SAT for the QEI compared with mean annual sea-ice extent (1900 to 1999) using 5 yr running means. SAT and sea-ice extent time series are negatively correlated ($r = -0.31$) for the overlapping period of record (1949-1999), with stronger negative correlations occurring during both warm and cold decades ($r = -0.52$). Thus, on a decadal time-scale, it is evident that QEI SAT and sea-ice extent co-vary. During the cold decade (1965-1974), the QEI experienced anomalously low mean summer temperatures (~ -0.42 °C cooler), corresponding to the largest increase in sea-ice extent in the Arctic since the end of the LIA. In contrast, however, a pronounced decrease in sea-ice extent corresponds to the warm decade, when the mean summer SAT throughout the QEI was ~0.24 °C warmer than the 1949-2002 mean. These trends are also apparent in the early 20th century, when anomalously low Arctic mean annual SATs (~1900-1919) correspond to the largest sea-ice area during the century-long record, and anomalously high SATs (~1920-1939) match a significant decrease in sea-ice extent (Johannesson *et al.*, 2004, Fig. 5). This sizeable decrease in sea-ice extent is coincident with an increase (~0.5-1.0

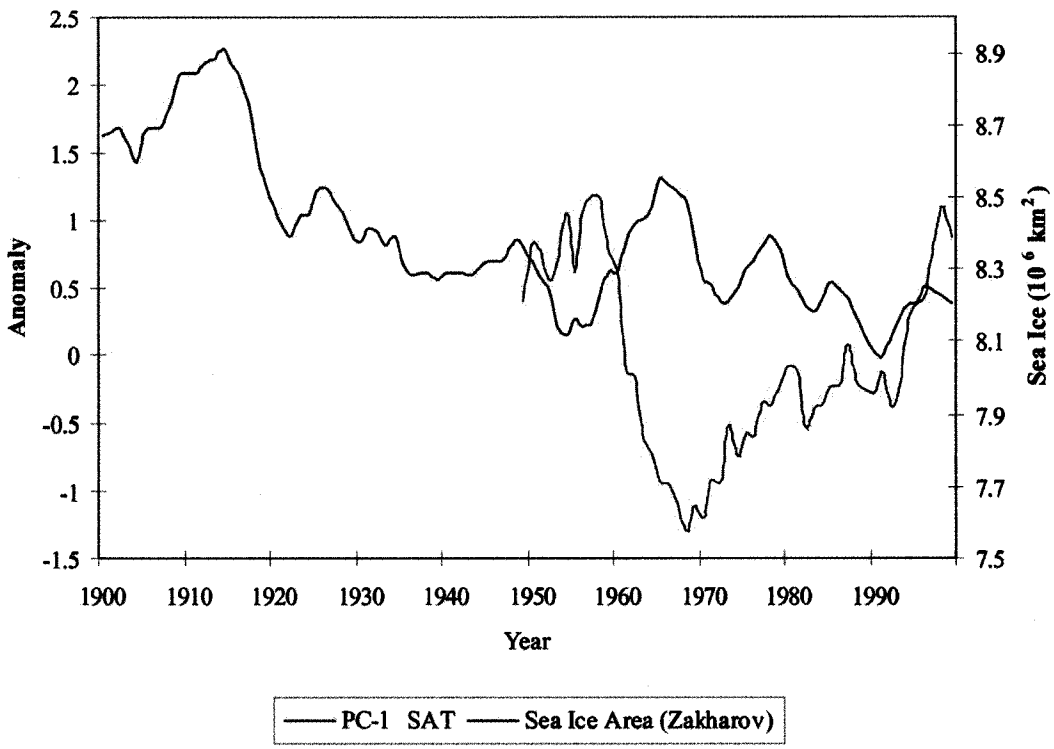

Figure 4. 24 5-year running mean time series of sea-ice area (1900-1999) (Zakharov, 1997; Johannessen, 2004) and PC-1 of QEI averaged SAT (1949-1999).

°C) in the observed spring/summer/fall SAT across the QEI, likely marking the end of the LIA there (Johannesson *et al.*, 2004, Fig. 2).

4.6.6 ELA changes and 20th Century Analogs

The above analyses of climatic conditions in the QEI during the extreme cold and warm decades of the modern record, lead to the hypothesis that these decades can be used as analogs for describing climatic conditions that could be linked to LIA cooling and early 20th century warming in the QEI. Regional spatial variations in 20th century climate across the QEI are reflected in the change in the distribution of perennial snow/ice cover and ELA Δh between the end of the LIA and 1960. Although the spatial distribution of Δh shows substantial meso- and micro-scale variability across the QEI, especially in the mountainous regions (where orographic effects are amplified), the data set also exhibits distinctive synoptic scale patterns, indicative of regional climate forcing. For example, the area of greatest change in the ELA (Fig. 4.10) is qualitatively similar to the pattern of the primary mode of summer temperature variability in the QEI (EOF-1, 1949-2002, Fig. 4.13). This pattern shows the greatest amount of variability occurring in the eastern QEI, extending from central Devon Island northward across SW Ellesmere Island through the axis of Eureka Sound. The positive phase of EOF-1 (PC-1, summer SAT, Fig. 4.13) characterizes the warm decade (1953-1962), when the mean temperature rose 1.5 standard deviations over the 1949-2002 mean (Fig. 4.12). Strong qualitative similarities between EOF-1 (summer SAT) during the warm decade and the pattern of ELA Δh indicate that the warm decade may serve as a suitable analog for climatic conditions during the early 20th century that caused an increase in melt of perennial snow/ice masses

across the QEI. Furthermore, dry conditions dominated throughout the QEI during the warm decade (Fig. 4.12, 4.14, and 4.16), and paleo-precipitation proxy records from the central QEI suggest that similar dry conditions persisted during the early 20th century (Lamoureux, 2000). While the effect of low summer precipitation on net mass balance in the QEI is important (Dowdeswell *et al.*, 1997), such dry conditions indicate that the regional pattern of ELA Δh is largely a reflection of the variation in summer temperature.

Reconstructed temperature change across the QEI from the end of the LIA to 1960 is shown in Figure 4.25. This reconstruction is calculated from ELA Δh based on a summer near-surface temperature lapse rate of -4.4 °C km^{-1}, which was empirically derived from an observational network on Prince of Wales Icefield, Ellesmere Island (Marshall *et al.*, in press). Resulting mean temperature change for the QEI was 1.1 °C (stdv. = 0.4 °C), ranging from <0.5 °C along NW Axel Heiberg and Ellesmere Islands and W Melville Island, to >2.9 °C in localized areas of Ellesmere and Devon Islands. The ELA-derived temperature changes are in agreement with QEI averaged mean summer temperature anomalies for extreme years in the modern record (e.g., 1954), and they are also consistent with changes derived from circum-Arctic gridded surface air temperatures (MJJASO) dating back to 1900 (Johannessen *et al.*, 2004; Fig. 2). The derived temperature changes are also in broad agreement with other temperature reconstructions from the High Arctic. For instance, based on proxy data from lakes, ice cores, wetlands, and marine sources Overpeck *et al.* (1997, Fig. 3) reported an average summer-weighted Arctic warming of ~1.5 °C from the end of the LIA to ~1960, with changes in the Canadian Arctic between 1 and 3 °C. Also in the Canadian High Arctic, melt layer and $\delta^{18}O$ analyses from ice cores extracted from the Devon and Agassiz ice

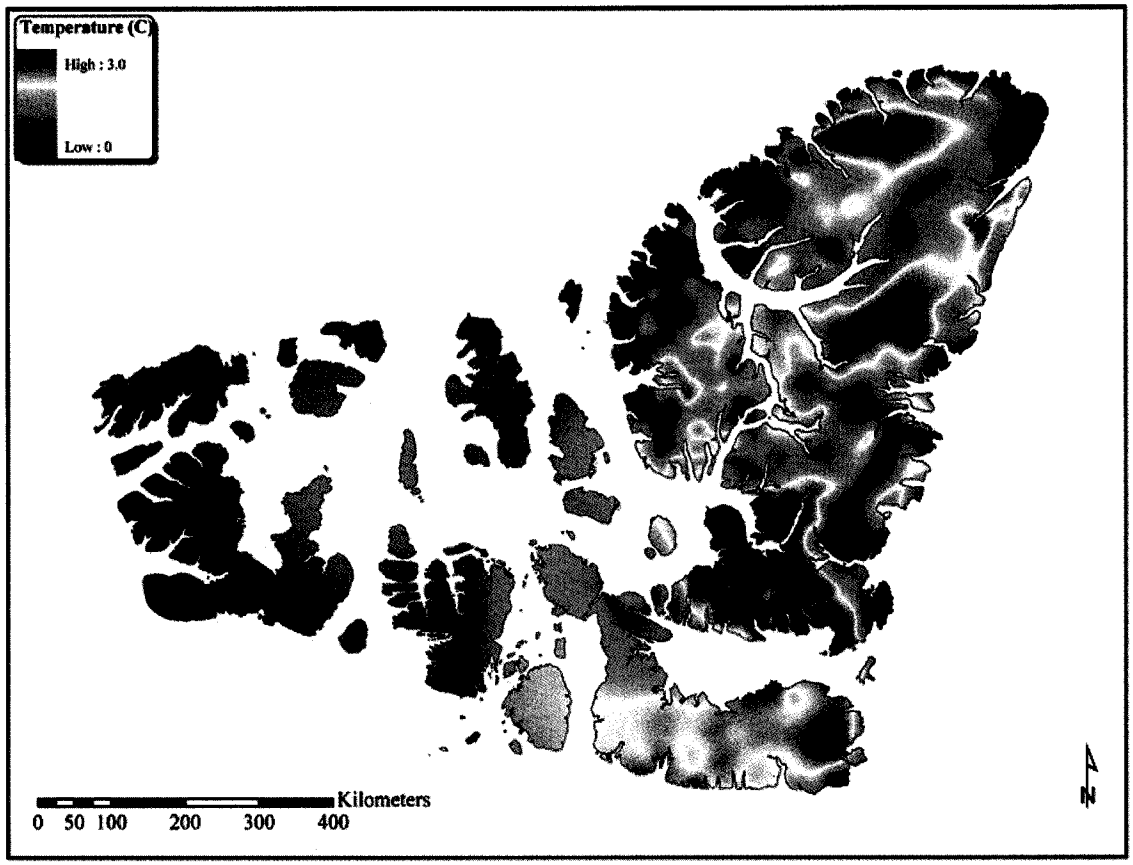

Figure 4. 25 Temperature change between the LIA and 1960, estimated from ELA Δh using a summer near-surface temperature lapse rate of -4.4 °C km^{-1} (Marshall *et al.*, 2006).

caps (both in the QEI) reveal marked warming in summer temperatures (~0.5 to 1.5 °C) between the end of the LIA and modern times (Koerner, 1977; Koerner and Fisher, 1990), which is consistent with abrupt warming between the mid-19th century and mid-20th century, as indicated by high sedimentation rates seen in lake core records from the QEI (Lamoureux and Bradley, 1996; Gajewski *et al.*, 1997; Lamoureux and Gilbert, 2004; Smith *et al.*, 2004) and by a rapid colonization of diatoms in QEI lakes in response to a reduction in lake-ice cover (Perren *et al.*, 2003).

Large-scale atmospheric circulation patterns during the cold and warm decades can also be used as analogs for those patterns that may have occurred during the LIA and the early 20th century. Atmospheric circulation causing strong northerly flow into Arctic Canada during the cold decade is responsible for producing temperature anomalies in the QEI similar to those estimated from temperature reconstructions noted above. This atmospheric circulation pattern is similar to the synoptic types producing "cool and dry" conditions (types 1, 4, 6, and 9) described by Bradley and England (1979), as well as the synoptic type *I* suggested by Alt (1987), which produces strong northerly flow through the QEI and is associated with melt suppression on QEI ice caps. Although the seasonal atmospheric circulation patterns characterizing the cold decade produced temperatures comparable to those reported to have occurred during the LIA, other patterns observed in the contemporary record are capable of producing similar cool episodes, some of which are accompanied by increased precipitation (Bradley and England, 1979; Alt, 1987; Bromwich *et al.*, 2002). Indeed, some paleoclimatic reconstructions for the central QEI suggest enhanced summer precipitation in these areas during the LIA (Lamoureux, 2000);

some precipitation events during this time may have been related to increased volcanic activity (Lamoureux *et al.*, 2001).

One of the characteristic atmospheric circulation features during the warm decade in the Arctic is the strong S-SE flow across the QEI, which undoubtedly played a major role in the spatial distribution of positive SAT anomalies throughout this region. The similarity in the spatial pattern of temperatures reconstructed from ELA Δh, indicates that this circulation feature may also have been important during the post-LIA to 1960 period. However, other elements of high latitude atmospheric circulation have also been suggested to contribute to circum-Arctic warming during the early 20th century. For instance, Bengtsson *et al.* (2004) propose that enhanced winter oceanic and atmospheric heat transport into the Arctic, initiated by an increase in the S-SW winds into the Barents Sea between Spitsbergen and Norway, was associated with regional warming that provided the main contribution to Arctic SAT anomalies from 1920-1940. While this feature does not appear during the winter months (NDJFMA) of the warm decade, there is indication of a possible winter atmospheric circulation pattern, which would have favoured warmer temperatures in the QEI during the warm decade summers. During the winter months (warm decade), a weakened pressure gradient between the Icelandic low and central Atlantic high would have resulted in substantially reduced westerly winds across the North Atlantic and decreased evaporative heat loss and upwelling in the W North Atlantic, thereby, allowing higher than normal SSTs to persist in the W North Atlantic, and augmenting summer SST anomalies linked to warmer than normal summers in the QEI.

4.7 Conclusions

The areal extent of perennial snow/ice in the QEI underwent a massive reduction between the end of the LIA and 1960 as a consequence of early 20th century warming. Trimlines were used to map former LIA perennial snow/ice extent throughout the QEI, revealing a 37% (62,387 km^2) reduction in snow and ice cover between the end of the LIA and 1960. The largest areal reduction in snow and ice extent occurred in the E QEI where most ice persists today; however, the most substantial reductions occurred on intermediate and high plateaus where small increases in the ELA caused vast areas of land to enter the ablation zone. On several of the central and western islands, a 100% reduction in snow/ice cover occurred by 1960, which was largely controlled by the low relief of these islands, which in turn makes them especially vulnerable to a rise in the ELA. ELA changes (Δh) between the LIA and 1960 range from 0 to >600 m; the spatial distribution of Δh reveals a high degree of local variability in the mountains of the eastern QEI, but it exhibits a strong regional-scale pattern of change over the QEI as a whole.

Warm (1953-1962) and cold (1965-1974) decades of summer SAT in the QEI were identified in the 1949-2002 NNR as potential modern analogs of LIA (cold) and early 20th century (warm) climates. The spatial pattern of Δh between the LIA and 1960 is qualitatively similar to the primary mode of variability for mean summer SAT in the modern record (i.e., EOF-1, 1949-2002, Fig. 4.13), the positive (negative) phase of which is strongly in place during the warm (cold) decade. During the cold decade, lower than normal SATs are associated with atmospheric circulation patterns producing strong northerly winds over the study region. Warmer than normal SATs during the warm decade are linked to warm south-easterly flow through the QEI resulting from a pressure

gradient reversal in the W North Atlantic, caused by anomalously high pressure over Greenland and the Canadian Arctic Archipelago coupled with lower than normal pressure over N Quebec and NW mainland Canada. SAT anomalies in the QEI during the warm (cold) decade are positively correlated with a weak (strong) polar vortex, higher (lower) than normal SSTs in the North Atlantic, and one of the lowest (highest) periods of sea-ice extent during the 20th century.

Due to the low precipitation in the QEI during both warm and cold decades, and its minimal influence on the pattern of ELA Δh compared to temperature, Δh is considered to reflect regional changes in summer SAT between the end of the LIA and 1960. Estimates of temperature change between the LIA and 1960 are calculated from Δh based on a summer near-surface temperature lapse rate of -4.4 °C km^{-1}. The mean estimated temperature change in the QEI from the LIA to 1960 is 1.1 °C, and ranges from <0.5 °C near the northwest coasts of Axel Heiberg and Ellesmere Islands and the west coast of Melville Island, to >2.9 °C in localized mountainous areas of Ellesmere Island. While the large-scale atmospheric circulation changes required to produce this warming are not clear, plausible circulation patterns based on modern analogs have been proposed.

This research demonstrates the usefulness of LIA trimlines for reconstructing former perennial snow/ice extent and ELAs in the Canadian High Arctic. LIA ELA reconstructions from the QEI present an important proxy of LIA climate in a region with limited observational data, and thereby, serve as an important extension of the climatic record. Reconstructed ELAs have been used here to assess climate variability on longer time scales and provide a comprehensive reconstruction of the spatial variability of temperature and precipitation change in the QEI between the end of the LIA and 1960.

This study also highlights the rapid change in terrestrial ice extent occasioned by early 20^{th} century warming; such modifications to terrestrial ice masses in response to past warming events provide an important reference, against which, modern changes may be evaluated.

4.8 References

ACIA, 2004: *Arctic Climate Impacts Assessment.* Cambridge: Cambridge University Press, 1046 pp.

Alt, B. T., 1987: Developing synoptic analogs for extreme mass balance conditions on Queen Elizabeth Island ice caps. *Journal of Climate and Applied Meteorology,,* 26,: 1605-1623.

Bengtsson, L., Semenov, V. A., and Johannessen, O. M., 2004: The early twentieth-century warming in the Arctic - A possible mechanism. *Journal of Climate,* 17: 4045-4057.

Blake, W. J., 1981: Neoglacial fluctuations of glaciers, Southeastern Ellesmere Island, Canadian Arctic Archipelago. *Geografiska Annaler,* 63: 201-218.

Bradley, R. S., 1973: Recent freezing level changes and climatic deterioration in the Canadian Arctic archipelago. *Nature,* 243: 398-400.

Bradley, R. S., 1975: Equilibrium-line altitudes, mass balance, and July freezing-level heights in the Canadian High Arctic. *Journal of Glaciology,* 14: 267-274.

Bradley, R. S. and England, J., 1977: The Simmonds Ice Cap. *In* Bradley, R. S. and England, J. (eds.), *Past glacial activity in the High Arctic.* Amherst: University of Massachusetts, 184.

Bradley, R. S. and England, J., 1978a: Volcanic dust influences on glacier mass balance at high latitudes. *Nature,* 271: 736-738.

Bradley, R. S. and England, J., 1978b: Recent climatic fluctuations of the Canadian High Arctic and their significance for glaciology. *Arctic and Alpine Research,* 10: 715-731.

Bradley, R. S. and England, J., 1979: Synoptic climatology of the Canadian High Arctic. *Geografiska Annaler,* 61: 187-201.

Bradley, R. S., 1990: Holocene paleoclimatology of the Queen Elizabeth Islands, Canadian High Arctic. *Quaternary Science Reviews,* 9: 365-384.

Bradley, R. S. and Jones, P. D., 1992: *Records of explosive volcanic eruptions over the last 500 years*. London: Routledge, 679 pp.

Braun, C., Hardy, D. R., and Bradley, R. S., 2004: Mass balance and area changes of four High Arctic plateau ice caps, 1959-2002. *Geografiska Annaler Series a-Physical Geography,* 86A: 43-52.

Bromwich, D. H., Toracinta, E. R., and Wang, S. H., 2002: Meteorological perspective on the initiation of the Laurentide Ice Sheet. *Quaternary International,* 95-6: 113-124.

Burgess, D. O. and Sharp, M. J., 2004: Recent changes in areal extent of the Devon Ice Cap, Nunavut, Canada. *Arctic, Antarctic, and Alpine Research,* 36: 261-271.

Burgess, D. O., Sharp, M. J., Mair, D. W. F., Dowdeswell, J. A., and Benham, T. J., 2005: Flow dynamics and iceberg calving rates of Devon Ice Cap, Nunavut, Canada. *Journal of Glaciology,* 51: 219-230.

Centre for Topographic Information, C. S. G., 2000: *Canadian Digital Elevation Data Standards and Specifications*. Sherbrooke: Natural Resources Canada, 15 pp.

Chapman, W. L. and Walsh, J. E., 1993: Recent Variations of Sea Ice and Air-Temperature in High-Latitudes. *Bulletin of the American Meteorological Society,* 74: 33-47.

Cullather, R. I., Bromwich, D. H., and Serreze, M. C., 2000: The atmospheric hydrologic cycle over the Arctic basin from reanalyses. Part I: Comparison with observations and previous studies. *Journal of Climate,* 13: 923-937.

Dickson, R. R., Meincke, J., Malmberg, S. A., and Lee, A. J., 1988: The Great Salinity Anomaly in the Northern North-Atlantic 1968-1982. *Progress in Oceanography,* 20: 103-151.

Dowdeswell, J. A., Hagen, J. O., Bjornsson, H., Glazovsky, A. F., Harrison, W. D., Holmlund, P., Jania, J., Koerner, R. M., Lefauconnier, B., Ommanney, C. S. L., and Thomas, R. H., 1997: The mass balance of circum-Arctic glaciers and recent climate change. *Quaternary Research,* 48: 1-14.

Dyke, A. S., 1974: Deglacial chronology and uplift history: Northeastern sector, Laurentide Ice Sheet. *Arctic and Alpine Research,* Occasional Paper: 113.

Dyurgerov, M. B. and Meier, M. F., 1997: Mass balance of mountain and subpolar glaciers: a new global assessment for 1961-1990. *Arctic and Alpine Research,* 29: 379-391.

Dyurgerov, M. B., Meier, M. and Armstrong, R. L., 2002: *Glacier Mass Balance and Regime: Data of measurements and analysis*: Institute of Arctic and Alpine Research, University of Colorado, Boulder, 275 pp.

Dyurgerov, M., 2005: Mass balance of mountain and sub-polar glaciers outside the Greenland and Antarctic ice sheets. *Supplement to Occasional Paper No. 55, Institute of Arctic and Alpine Research, University of Colorado (distributed by National Snow and Ice Data Center, Boulder, CO).*

Edlund, S. A. and Alt, B. T., 1989: Regional congruence of vegetation and summer climate patterns in the Queen Elizabeth Islands, Northwest Territories, Canada. *Arctic,* 42: 3-23.

Gajewski, K., Hamilton, P. B., and McNeely, R., 1997: A high resolution proxy-climate record from an arctic lake with annually-laminated sediments on Devon Island, Nunavut, Canada. *Journal of Paleolimnology,* 17: 215-225.

Grove, J. M., 1988: *The Little Ice Age.* London: Methuen, 500 pp.

Hansen, J. E., Wang, W.C., and Lacis, A. A., 1978: Mount Agung eruption provides test of a global climatic perturbation. *Science,* 199: 1065-1068.

Hansen, D. V. and Bezdek, H. F., 1996: On the nature of decadal anomalies in North Atlantic sea surface temperature. *Journal of Geophysical Research-Oceans,* 101: 8749-8758.

Hattersley-Smith, G. and Serson, H., 1973: Reconnaissance of a small ice cap near St. Patrick Bay, Robseson Channel, Northern Ellesmere Island, canada. *Journal of Glaciology,* 12: 417-421.

Hutchinson, M. F., 1989: A New Procedure for Gridding Elevation and Stream Line Data with Automatic Removal of Spurious Pits. *Journal of Hydrology,* 106: 211-232.

IPCC, 2001: *Climate Change 2001: The Scientific Basis*. Cambridge, New York: Cambridge University Press, 408 pp.

Ives, J. D., 1962: Indication of recent extensive glacierization in north central Baffin Island, N.W.T. *Journal of Glaciology,* 4: 197-205.

Johannessen, O. M., Shalina, E.V. and Miles M.W., 1999: Satellite evidence for an Arctic sea ice cover in transformation. *Science,* 286: 1937-1939.

Johannessen, O. M., Bengtsson, L., Miles, M. W., Kuzmina, S. I., Semenov, V. A., Alekseev, G. V., Nagurnyi, A. P., Zakharov, V. F., Bobylev, L. P., Pettersson, L. H., Hasselmann, K., and Cattle, A. P., 2004: Arctic climate change: observed and modelled temperature and sea-ice variability. *Tellus Series a-Dynamic Meteorology and Oceanography,* 56: 328-341.

Johannesson, T., Raymond, C. F., Waddington, E. D., 1989: Time-scale adjustments of glaciers to changes in mass balance. *Journal of Glaciology,* 35: 355-369.

Kalnay, E., Kanamitsu, M., Kistler, R., Collins, W., Deaven, D., Gandin, L., Iredell, M., Saha, S., White, G., Woollen, J., Zhu, Y., Chelliah, M., Ebisuzaki, W., Higgins, W., Janowiak, J., Mo, K. C., Ropelewski, C., Wang, J., Leetmaa, A., Reynolds, R., Jenne, R., and Joseph, D., 1996: The NCEP/NCAR 40-year reanalysis project. *Bulletin of the American Meteorological Society,* 77: 437-471.

Kistler, R., Kalnay, E., Collins, W., Saha, S., White, G., Woollen, J., Chelliah, M., Ebisuzaki, W., Kanamitsu, M., Kousky, V., van den Dool, H., Jenne, R., and Fiorino, M., 2001: The NCEP-NCAR 50-year reanalysis: Monthly means CD-ROM and documentation. *Bulletin of the American Meteorological Society,* 82: 247-267.

Koerner, R. M. and Paterson, W. S., 1974: Analysis of a Core through Meighen Ice Cap, Arctic Canada, and Its Paleoclimatic Implications. *Quaternary Research,* 4: 253-263.

Koerner, R. M., 1977: Ice thickness measurements and their implications with respect to past and present ice volumes in the Canadian High Arctic ice caps. *Canadian Journal of Earth Sciences,* 14: 2697-2705.

Koerner, R. M. and Fisher, D. A., 1990: A record of Holocene summer climate from a Canadian high-Arctic ice core. *Nature,* 343: 630-631.

Lamoureux, S. F. and Bradley, R. S., 1996: A late Holocene varved sediment record of environmental change from northern Ellesmere Island, Canada. *Journal of Paleolimnology,* 16: 239-255.

Lamoureux, S., 2000: Five centuries of interannual sediment yield and rainfall-induced erosion in the Canadian High Arctic recorded in lacustrine varves. *Water Resources Research,* 36: 309-318.

Lamoureux, S. F., England, J. H., Sharp, M. J. and Bush, A. B. G., 2001: A varve record of increased 'Little Ice Age' rainfall associated with volcanic activity, Arctic Archipelago, Canada. *The Holocene,* 11: 243-249.

Lamoureux, S. F. and Gilbert, R., 2004: A 750-yr record of autumn snowfall and temperature variability and winter storminess recorded in the varved sediments of Bear Lake, Devon Island, Arctic Canada. *Quaternary Research,* 61: 134-147.

Mair, D., Burgess, D., and Sharp, M., 2005: Thirty-seven year mass balance of Devon Ice Cap, Nunavut, Canada, determined by shallow ice coring and melt modeling. *Journal of Geophysical Research-Earth Surface,* 110, F01011, doi:10.1029/2003JF000099.

Marshall, S. J., Sharp, M.J., Burgess, D.O. and Anslow, F. S., 2006: Near-surface temperature lapse rates on the Prince of Wales Icefield, Ellesmere Island, Canada: Implications for regional downscaling of temperature. *International Journal of Climatology, In Press.*

Maxwell, J. B., 1981: Climatic regions of the Canadian Arctic islands. *Arctic,* 34: 225-240.

Miller, G. H., Bradley, R. S. and Andrews, J. T., 1975: The glaciation level and lowest equilibrium line altitude in the High Canadian Arctic: maps and climatic interpretation. *Arctic and Alpine Research,* 7: 155-168.

Miller, G. H., 1976: Anomalous Local Glacier Activity, Baffin Island, Canada - Paleoclimatic Implications. *Geology,* 4: 502-504.

Miller, G. H., Wolfe, A. P., Briner, J. P., Sauer, P. E., and Nesje, A., 2005: Holocene glaciation and climate evolution of Baffin Island Arctic Canada. *Quaternary Science Reviews,* 24: 1703-1721.

Mysak, L. A., Ingram, R. G., Wang, J., and van der Baaren, A., 1996: The anomalous sea-ice extent in Hudson Bay, Baffin Bay and the Labrador Sea during three simultaneous NAO and ENSO episodes. *Atmosphere-Ocean,* 34: 313-343.

Oerlemans, J. and Klok, E. J., 2002: Energy balance of a glacier surface: Analysis of automatic weather station data from the Morteratschgletscher, Switzerland. *Arctic Antarctic and Alpine Research,* 34: 477-485.

Overpeck, J., K., Hughen, K., Hardy, D., Bradley, R., Case, R., Douglas, M., Finney, B., Gajewski, K., Jacoby, G., Jennings, A., Lamoureux, S., Lasca, A., MacDonald, G., Moore, J., Retelle, M., Smith, S., Wolfe, A., and Zielinski, G., 1997: Arctic environmental change of the last four centruries. *Science,* 278: 1251-1256.

Parkinson, C. L., Cavalieri, D. J., Gloersen, P., Zwally, H. J., and Comiso, J. C., 1999: Arctic sea ice extents, areas, and trends, 1978-1996. *Journal of Geophysical Research-Oceans,* 104: 20837-20856.

Perren, B. B., Bradley, R. S., and Francus, P., 2003: Rapid lacustrine response to recent High Arctic warming: A diatom record from Sawtooth Lake, Ellesmere Island, Nunavut. *Arctic Antarctic and Alpine Research,* 35: 271-278.

Rogers, J. C., Wang, C. C., and McHugh, M. J., 1998: Persistent cold climatic episodes around Greenland and Baffin Island: Links to decadal-scale sea surface temperature anomalies. *Geophysical Research Letters,* 25: 3971-3974.

Serreze, M. C. and Maslanik, J. A., 1997: Arctic precipitation as represented in the NCEP/NCAR reanalysis. *Annals of Glaciology,* 25: 429-433.

Serreze, M. C. and Hurst, C. M., 2000: Representation of mean Arctic precipitation from NCEP-NCAR and ERA reanalyses. *Journal of Climate,* 13: 182-201.

Serreze, M. C., Clark, M. P., and Bromwich, D. H., 2003: Monitoring precipitation over the Arctic terrestrial drainage system: Data requirements, shortcomings, and applications of atmospheric reanalysis. *Journal of Hydrometeorology,* 4: 387-407.

Serreze, M. C. and Barry, R. G., 2005: *The Arctic climate system.* Cambridge: Cambridge University Press, 402 pp.

Smith, S. V., Bradley, R. S., and Abbott, M. B., 2004: A 300 year record of environmental change from Lake Tuborg, Ellesmere Island, Nunavut, Canada. *Journal of Paleolimnology,* 32: 137-148.

Smith, T. M. and Reynolds, R. W., 2004: Improved extended reconstruction of SST (1854-1997). *Journal of Climate,* 17: 2466-2477.

Thompson, D. W. J. and Wallace, J. M., 1998: The Arctic Oscillation signature in the wintertime geopotential height and temperature fields. *Geophysical Research Letters,* 25: 1297-1300.

Vinnikov, K. Y., Robock, A., Stouffer, R. J., Walsh, J. E., Parkinson, C. L., Cavalieri, D. J., Mitchell, J. F. B., Garrett, D. and Zakharov, V. F., 1999: Global warming and northern Hemisphere sea ice extent. *Science,* 286: 1934-1937.

Williams, R. S. J. and Ferrigno, J. G., 2002: *Introduction. In: Satellite Image Atlas of Glaciers of the World. Glaciers of North America - Glaciers of Canada.* Washington: U.S. Geological Survey, 405 pp.

Wolken, G. J., England, J.H. and Dyke, A. S., 2005: Re-evaluating the Relevance of Vegetation Trimlines in the Canadian Arctic as an Indicator of Little Ice Age Paleoenvironments. *Arctic,* 58: 341-353.

Wolken, G. J., 2006: High-resolution multispectral techniques for mapping former Little Ice Age terrestrial ice cover in the Canadian High Arctic. *Remote Sensing of Environment,* 101: 104-114.

Zakharov, V. F., 1997: Sea ice in the climate system, *WMO Tech. Doc. 782. World Climate Research Programme, Arctic Climate System Study*. Geneva, Switzerland, 80.

5 CHAPTER FIVE

Summary and Conclusions

5.1 Summary

This study has demonstrated the usefulness of trimlines for paleoenvironmental reconstruction in the Canadian High Arctic. Based on observations and extensive mapping in the Queen Elizabeth Islands (QEI), the formation of trimlines was re-examined and the validity of conflicting hypotheses related to their origin was reevaluated (paleoclimatic versus ecological; Ives (1962) and Koerner (1980), respectively). The ecological hypothesis, as proposed by Koerner (1980), does not adequately account for the existence of sharp trimlines, especially on carbonate terrain, and fails to consider lichens' ability to endure short growing seasons. On the other hand, the paleoclimatic hypothesis (Ives, 1962), explains the existence of both diffuse and sharp trimlines resulting from perennial snow/ice expansion. Further credence is added to this hypothesis from the prevalence of accordant trimlines, associated with the former limits of perennial snow/ice fields and small plateau ice caps, the altitude of which represents the position of the former equilibrium-line.

This thesis has led to the development of new methods for mapping trimlines surrounding recently deglaciated terrain on complex topography with diverse surficial geology. Two remote sensors were used for this study, ASTER and Landsat ETM+, both chosen for their high-resolution and multispectral imaging capabilities. Automated (band calculation) and semi-automated (supervised classification) techniques were employed for classifying recently deglaciated terrain using both ASTER and ETM+ sensors.

Automated techniques were most effective on substrates derived from siliceous crystalline rock and quartzitic sandstone, whereas, semi-automated techniques were found to be more effective on calcareous substrates with high incidences of carbonate lithologies. ASTER yielded higher classification accuracies in highly complex terrain, but ETM+ achieved higher accuracies on a larger variety of substrate types and topographic settings. The techniques developed offer a quick and accurate alternative to conventional photogrammetric approaches when conducting regional-scale mapping of subtle landscape features in arid settings.

Using these techniques, LIA terrestrial ice extent was reconstructed and the nature and magnitude of ice reduction in the QEI between the LIA and 1960 was examined. Between the end of the LIA and 1960, the area of terrestrial ice in the QEI decreased by 37% (62,387 km^2). Most of this reduction (94%) occurred in the eastern QEI where the majority of the ice exists today; however, a 100% reduction in ice cover occurred on many of the western islands by 1960, an effect largely controlled by the subtle relief and the low topographic complexity of these islands. LIA equilibrium-line altitude (ELA) trend surfaces were also reconstructed and used with the 1960 mapped ELAs (Miller *et al.*, 1975) to calculate spatial variations in the height (h) of the equilibium-line throughout the QEI during the first half of the 20th century. ELA changes (Δh) between the LIA and 1960 ranged from 0 to >600 m. The spatial distribution of Δh reveals a high degree of local variability in the mountainous regions, but a strong regional-scale pattern of change over the QEI as a whole.

Regional-scale spatial variation in the change in ELA trend surfaces between the end of the LIA and 1960 corresponds to Empirical Orthogonal Functions (EOFs)

representing specific patterns of climate variability found in the modern record. Extreme warm (1953-1962) and cold (1965-1974) decades in the modern record were used as modern analogs of climatic conditions during the early 20th century and the LIA, respectively. Temperature anomalies during the warm decade were positively correlated with pressure fields over the study area from the surface to the lower stratosphere. Temperature anomalies during the cold decade were positively correlated with geopotential height surfaces from the mid-troposphere to lower stratosphere (i.e., a strong polar vortex); however, the pressure distribution in the lower troposphere indicated anomalously low pressure over the eastern QEI, with anomalously high pressure over the western QEI. High pressure prevailed over the central QEI during both warm and cold decades and weakened the dominant storm track through the region, resulting in below normal precipitation rates in the QEI during both extreme decades. Because of the minimal influence of precipitation during both extreme decades, temperature becomes the variable upon which the fluctuation of the ELA is dependent. Hence, the ELA Δh pattern describes the spatial pattern of change in SAT across the QEI between the LIA and 1960. This pattern is consistent with the primary mode of variability of mean summer SAT in the modern record (i.e., EOF-1, 1949-2002), the positive (negative) phase of which is strongly in place during the extreme warm (cold) decade. SAT anomalies in the QEI during the warm (cold) decade are positively correlated with a weak (strong) polar vortex, higher (lower) than normal SSTs in the North Atlantic, and one of the lowest (highest) periods of sea-ice extent during the 20th century. The climatic conditions during the cold decade are believed to describe conditions, which if sustained, would lead to a LIA-type cold episode capable of long-term snowline lowering and perennial snow/ice

expansion. The climatic conditions during the warm decade represent possible modern analogs for those that might have occurred during the early 20th century in the Canadian High Arctic, which led to a considerable reduction in perennial snow/ice.

5.2 Conclusions

This thesis further clarifies our understanding of the influence of late Neoglacial (i.e., the LIA) climate on the terrestrial cryosphere in the Canadian Arctic, the pattern of temperature change during the early 20th century in the QEI and its impact on perennial snow/ice, and the complex interactions associated with ocean-atmosphere-ice-land feedbacks in high latitude northern regions.

Data presented in this thesis significantly advance our knowledge about the configuration and extent of perennial snow/ice across the QEI during the LIA. Until now, our awareness of LIA perennial snow/ice cover in the QEI has been very limited; either restricted to observations noted in research reports or simply included as thematic items on surficial geology maps of only a few areas (Dyke, 1978; Edlund, 1985; Bednarksi, 2002). In other regions of the Canadian Arctic, however, Quaternary geologists have regularly mapped and interpreted trimlines surrounding perennial snow/ice fields, glaciers, and ice caps as evidence of an expanded former ice cover (Ives, 1957, 1962; Andrews *et al.*, 1975, 1976; Locke and Locke, 1977; Dyke, 1978; Edlund, 1985; Evans and England, 1992; Hooper and Dyke, 2000; Dyke and Hooper, 2000; Dyke, 2000a-e; 2001a-e; 2003; 2004; Dredge, 2004 a-c). However, these studies were mostly limited to areas where trimlines are best expressed, that is, on terrain where siliceous

crystalline rock is exposed at the surface (i.e., on the Canadian Shield of E Arctic Canada).

The spatial distribution of LIA perennial snow/ice across the QEI provides a valuable dataset for modeling past and future environmental change. These data are an important contribution to glacial onset and ice nucleation studies, as much still remains unknown about the climatic conditions necessary for long-term lowering of the snowline and the development of perennial snow/ice fields across vast expanses of land, which are inherent to glacial/ice sheet inception. Patterns of atmospheric variability capable of producing such conditions have been reported in the modern record, but the events are rare and the necessary frequency of them is not known (Bromwich *et al*, 2002). Furthermore, it is not known whether the atmospheric circulation patterns occurring today offer useful insight into those that may have produced the glacial periods of the past, as they may be very different (Stroeven *et al.*, 2002). The reconstructed LIA perennial snow/ice extent for the QEI, however, provides physical evidence of former ice nucleation centres during what some have termed an "abortive" glaciation (Flohn, 1974), and paleoclimate reconstructions derived from former LIA ELAs offer renewed insight into the climatic conditions necessary for glacial onset. Hence, the reconstructed LIA snow/ice extent and the attendant climatologies presented here can be used to validate coupled glacier-climate models used in investigations of the pattern and timing of interglacial-glacial transitions (e.g., the late Sangamon-early Wisconsinan).

The reduction of perennial snow/ice in the QEI between the end of the LIA and 1960 reflects the terrestrial crysospheric response to early 20th century warming following the cooler climatic conditions of the 19th century. Similar responses to this

transition have been recorded in the observational record of circum-Arctic SAT (Johannessen *et al.*, 2004) and sea ice extent (Zakharov, 1997; Johannessen *et al.*, 2004), and in temperature proxy records, such as ice cores that show an increase in the frequency and thickness of melt layers and predominantly negative mass balance records for glaciers throughout the Arctic (Grove, 1988; Koerner and Fisher, 1990; Mayewski *et al.*, 1993; Dowdeswell *et al.*, 1997) and ground surface temperature records from boreholes (Taylor *et al.*, 2006), as well as nearly all other circum-polar proxy records (Overpeck *et al.*, 1997). Indeed, a broadly synchronous pattern of glacier retreat occurred around the globe at the close of the 19th century and the beginning of the 20th century (Porter, 1981; Grove, 1988; Dyurgerov and Meier, 2000; IPCC, 2001; Bradley *et al.*, 2003).

ELA trend surfaces modelled throughout the QEI represent important proxies of climate in a region with limited or no observational data during the late 19th and early 20th centuries. This study presents a coherent regional-scale pattern of ELA change across the QEI between the LIA and 1960, which is linked to variations in summer SAT. Within this pattern of change are spatial complexities reflecting strongly developed differences in local climate, which are likely modulated by various combinations of orographic, maritime and continental influences. This finding is important because it emphasizes the impact of local-scale spatial variability on point specific reconstructions from typically sparse High Arctic proxy records (e.g., ice cores, lake sediment cores, shrub dendrochronology). However, a multi-proxy approach, combining the high-resolution (spatial) pattern of summer temperature change produced in this study with high-

resolution (temporal) proxy records of summer temperature (above), may help present a clearer picture of the climatic variability during the early 20th century in the QEI.

Synthesis of the spatial patterns associated with climatic variability and the cryospheric response to such changes provides an important reference and an essential contribution to glaciological and climatological models of the Arctic. Data presented in this thesis help to advance our understanding of the links between spatial patterns of variability and physical processes in the climate system on decadal and multi-decadal time scales. For instance, ocean-atmosphere feedback processes related to specific patterns of atmospheric circulation were shown to be associated with variations in sea ice extent and distinct periods of warm and cold conditions in the QEI during the modern record, which corresponded to similar spatial patterns of temperature change in the QEI during the early 20th century that led to a substantial reduction in perennial snow/ice. While it is beyond the scope of this investigation to speculate about the causal mechanisms (external and internal climate forcings) associated with changes in large-scale atmospheric circulation, this study does provide a glimpse into the tremendous influence of atmosphere-ocean-ice-land energy exchanges and positive feedback mechanisms in high latitude regions, the effects of which are far reaching and predicted to intensify as a result of global warming (Overpeck *et al.*, 1997; IPCC, 2001).

Investigating and understanding ice mass responses to past changes in climate is imperative to our understanding of future modifications to the cryosphere. Data presented in this thesis demonstrate the extent to which ice reduction occurred in the QEI, in response to an average estimated temperature increase of 1.1 °C between the end of the LIA and 1960. These data are particularly important for placing the recent increased

warming and melt in the Arctic (Krabill *et al.*, 2000; Arendt *et al.*, 2002; Abdalati *et al.*, 2004; Burgess and Sharp, 2004) and the accelerated warming trend seen globally (Mann *et al.*, 1998) into perspective. Predicted temperature increases for the Arctic will cause an increase in the length of the snow-free season (Chapin III *et al.*, 2005) and further mass loss of glaciers, ice caps and ice sheets, as well as higher ground surface temperatures and a deepening of the permafrost active layer (Taylor *et al.*, 2006). These cryospheric responses will likely result in a positive feedback effect of sustained melt; as land surfaces are exposed, decreases in terrestrial albedo will promote additional increases in land surface temperature and a subsequent rise in the ELA. One of the first responses to a rising ELA in the QEI will be the accelerated retreat of plateau ice caps, many of which are currently on the threshold of rapid decay due to their precarious position at or below the modern ELA (England *et al.*, 1981; Braun *et al.*, 2004). Continued melt of Arctic terrestrial ice masses will inevitably have an impact on global sea level (Meier, 1984; Van de Wal and Wild, 2001; Meier and Dyurgerov, 2002; Arendt *et al.*, 2002; Burgess and Sharp, 2004), and increased discharge of melt water into high latitude oceans could have dramatic far reaching consequences for the climate system through global teleconnections.

5.2.1 Future Research

This thesis contributes to our understanding of the cryospheric response to late Holocene climate variability in the Canadian Arctic. Three areas of future research stemming from this project are identified.

First, natural extensions to this project include mapping the areal extent of LIA perennial snow/ice and reconstructing the ELA trend surface throughout the remainder of Arctic Canada. Although some efforts have been made to document the former extent of perennial snow/ice in a number of areas of the southern Canadian Arctic Archipelago and N Labrador (references above), regional scale reconstructions of perennial snow/ice extent are nonexistent and previous reconstructions of the LIA ELA trend surface were restricted to parts of Baffin Island (Locke and Locke, 1977). A thorough systematic mapping of this area is needed. Expanding LIA perennial snow/ice mapping to this region would provide the opportunity to investigate spatial patterns of LIA extent and early 20th century ice cover reduction over a larger area, thereby, allowing for an assessment of the controls on this former perennial snow/ice cover and a quantitative evaluation of the changes in areal extent since the LIA. After mapping the former extent of perennial snow/ice, these data could then be used to guide the reconstruction of the LIA ELA trend surface across the southern archipelago. Data presented in this thesis describing the spatial pattern of change in the ELA trend surface throughout the QEI between the LIA and 1960 were found to be a proxy of early 20th century temperature change. Modeling this change over the southern archipelago would extend our knowledge of the spatial pattern and magnitude of temperature change during the early 20th century, and allow further analysis of ocean-atmosphere-ice-land interactions over a larger area of the Arctic. This could be particularly important on Baffin Island, as it is adjacent to Baffin Bay and therefore, sensitive to changes in this part of the North Atlantic Ocean. In addition, integrating former perennial snow/ice cover data from Arctic Canada with those from other Arctic locations (e.g., Yukon, Alaska, Greenland,

Iceland, Svalbard, and Russia) would provide a circum-Arctic perspective on the extent of LIA perennial snow/ice cover and the impact of early 20th century warming.

Second, the timing of the event that produced the expanded former snow/ice cover needs to be better constrained. At this time only a couple dates exist (none from the QEI) that relate to former snow/ice cover. These only provide maximum age estimates that simply indicate the expanded snow/ice cover occurred in the late Neoglacial. It is imperative to explore new methods of dating over a broad sampling area in order to refine the temporal constraints of the cold episode that produced this former perennial snow/ice cover.

Third, because the Arctic is particularly sensitive to changes in climate, the biotic response to global warming in this region is critically important (IPCC, 2001). This thesis quantifies the areal reduction of snow/ice in the QEI between the LIA and 1960, and in effect provides an estimate of the amount of "new" land available for recolonization by lichens and plants. Incipient lichen and plant recolonization can be found in distal regions of such areas formerly covered by perennial snow/ice, with estimated recolonization times on the order of about a century (Wolken *et al.*, 2005). However, continued warming in the Arctic raises questions about the change in the rate of recolonization, as well as the abundance and diversity of recolonization species. Hence, it is important to monitor the evolution of these areas in order to gauge and interpret modifications resulting from modern and future climatic changes (Belward *et al.*, 1999).

5.3 References

Abdalati, W., Krabill, W., Frederick, E., Manizade, S., Martin, C., Sonntag, J., Swift, R., Thomas, R., Yungel, J., and Koerner, R., 2004: Elevation changes of ice caps in the Canadian Arctic Archipelago. *Journal of Geophysical Research-Earth Surface,* 109, doi:10.1029/2003JF000045.

Andrews, J. T., Barry, R.G., Davis, P.T., Dyke, A.S., Mahaffy, M, Williams, L.D. and Wright, C., 1975: The Laurentide Ice Sheet: Problems of the mode and speed of inception. *World Meteorological Publication,* 421: 87-94.

Andrews, J. T., Davis, P. T., Wright, C., 1976: Little Ice Age permanent snowcover in the Eastern Canadian Arctic: Extent Mapped from Landsat-1 satellite imagery. *Geografiska Annaler,* 58A: 71-81.

Arendt, A. A., Echelmeyer, K. A., Harrison, W. D., Lingle, C. S., Valentine, V. B., 2002: Rapid wastage of Alaska glaciers and their contribution to rising sea level. *Science,* 297: 382-386.

Bednarski, J. H., 2002: Surficial geology, northeast Bathurst Island, Nunavut. *Geological Survey of Canada, Map 2011A, scale 1:100 000.*

Belward, A. S., Estes, J. E., and Kline, K. D., 1999: The IGBP-DIS global 1-km land-cover data set DISCover: A project overview. *Photogrammetric Engineering and Remote Sensing,* 65: 1013-1020.

Bradley, R. S., Briffa, K. R., Cole, J., Hughes, M. K. and Osborn, T. J., 2003: The climate of the last millennium. In: Paleoclimate, Global Change and the Future, *Paleoclimate, Global Change and the Future.* Berlin: Springer, 105-141.

Braun, C., Hardy, D. R., and Bradley, R. S., 2004: Mass balance and area changes of four High Arctic plateau ice caps, 1959-2002. *Geografiska Annaler Series a-Physical Geography,* 86A: 43-52.

Bromwich, D. H., Toracinta, E. R., and Wang, S. H., 2002: Meteorological perspective on the initiation of the Laurentide Ice Sheet. *Quaternary International,* 95-6: 113-124.

Burgess, D. O. and Sharp, M. J., 2004: Recent changes in areal extent of the Devon Ice Cap, Nunavut, Canada. *Arctic, Antarctic, and Alpine Research,* 36: 261-271.

Chapin, F. S., Sturm, M., Serreze, M. C., McFadden, J. P., Key, J. R., Lloyd, A. H., McGuire, A. D., Rupp, T. S., Lynch, A. H., Schimel, J. P., Beringer, J., Chapman, W. L., Epstein, H. E., Euskirchen, E. S., Hinzman, L. D., Jia, G., Ping, C. L., Tape, K. D., Thompson, C. D. C., Walker, D. A., and Welker, J. M., 2005: Role of land-surface changes in Arctic summer warming. *Science,* 310: 657-660.

Dredge, L. A., 2004: Surficial geology, Ekalugad Fiord (West half), Baffin Island, Nunavut. Geological Survey of Canada, Map 2073A, scale 1:250 000.

Dredge, L. A., 2004: Surficial geology, Lake Gillian, Baffin Island, Nunavut. Geological Survey of Canada, Map 2076A, scale 1:250 000.

Dredge, L. A., 2004: Surficial geology, McBeth Fiord (West half), Baffin Island, Nunavut. Geological Survey of Canada, Map 2074A, scale 1:250 000.

Dyke, A. S., 1978: Indications of Neoglacierization on Somerset Island, District of Franklin. *Scientific and Technical Notes,,* Current Research, Part B; Geologica Survey of Canada: 215-217.

Dyke, A. S., 2000: Surficial geology, Phillips Creek, Baffin Island. Geological Survey of Canada, Map 1961A, scale 1:250 000.

Dyke, A. S., 2000: Surficial geology, Milne Inlet, Baffin Island. Geological Survey of Canada, Map 1962A, scale 1:250 000.

Dyke, A. S., 2000: Surficial geology, Moffet Inlet and Fitzgerald Bay, Baffin Island. Geological Survey of Canada, Map 1963A, scale 1:250 000.

Dyke, A. S., 2000: Surficial geology, Arctic Bay, Baffin Island. Geological Survey of Canada, Map 1964A, scale 1:250 000.

Dyke, A. S., 2000: Surficial geology, Navy Board Inlet, Baffin Island. Geological Survey of Canada, Map 1965A, scale 1:250 000.

Dyke, A. S. and Hooper, J., 2000: Surficial geology, Berlinguet Inlet and Bourassa Bay, Baffin Island. Geological Survey of Canada, Map 1960A, scale 1:250 000.

Dyke, A. S., 2001: Surficial geology, eastern Devon Island. Geological Survey of Canada, Map 1970A, scale 1:250 000.

Dyke, A. S., 2001: Surficial geology, central Devon Island. Geological Survey of Canada, Map 1971A, scale 1:250 000.

Dyke, A. S., 2001: Surficial geology, western Devon Island. Geological Survey of Canada, Map 1972A, scale 1:250 000.

Dyke, A. S., 2001: Surficial geology, Grinnell Peninsula, Devon Island. Geological Survey of Canada, Map 1973A, scale 1:250 000.

Dyke, A. S., 2001: Surficial geology, Cardigan Strait, Devon Island and Ellesmere Island. Geological Survey of Canada, Map 1974A; scale 1:250 000.

Dyke, A. S., 2003: Surficial geology, Erichsen Lake, Baffin Island, Nunavut., *Geological Survey of Canada, Open File 4484. CDROM with digital files (geology, topography, and hydrology) of Open Files 1598-1613 (previously released as paper maps at 1:50 000 scale).*

Dyke, A. S., 2004: Surficial geology, Erichsen Lake, Baffin Island, Nunavut., *Geological Survey of Canada, Map 2066A, scale 1:250 000.*

Dyurgerov, M. B. and Meier, M. F., 2000: Twentieth century climate change: Evidence from small glaciers. *Proceedings of the National Academy of Sciences of the United States of America,* 97: 1406-1411.

Edlund, S. A., 1985: Lichen-free zones as neoglacial indicators on western Melville Island, District of Franklin. *Current Research, Part A, Geological Survey of Canada,* Paper 85-1A: 709-712.

England, J., Kershaw, L., LaFarge-England, C., Bednarski, J., 1981: *Northern Ellesmere Island: A natural resources inventory.* Edmonton: University of Alberta, Department of Geography, 237 pp.

Evans, D. J. A. and England, J., 1992: Geomorphological evidence of Holocene climatic change from northwest Ellesmere Island, Canadian High Arctic. *The Holocene,* 2: 148-158.

Flohn, H., 1974: Background to a geophysical model of the initiation of the next glaciation. *Quaternary Research,* 4: 385-404.

Grove, J. M., 1988: *The Little Ice Age.* London: Methuen, 500 pp.

Hooper, J. and Dyke, A. S., 2000: Surficial geology, Agu Bay and Easter Cape, Baffin Island. Geological Survey of Canada, Map 1959A, scale 1:250 000.

IPCC, 2001: *Climate Change 2001: The Scientific Basis*. Cambridge, New York: Cambridge University Press, 408 pp.

Ives, J. D., 1957: Glaciation of the Torngat Mountains, Northern Labrador. *Arctic,* 10: 67-87.

Ives, J. D., 1962: Indication of recent extensive glacierization in north central Baffin Island, N.W.T. *Journal of Glaciology,* 4: 197-205.

Koerner, R. M., 1980: The problem of lichen-free zones in Arctic Canada. *Arctic and Alpine Research,* 12: 87-94.

Koerner, R. M. and Fisher, D. A., 1990: A record of Holocene summer climate from a Canadian high-Arctic ice core. *Nature,* 343: 630-631.

Krabill, W., Frederick, E., Manizade, S., Martin, C., Sonntag, J., Swift, R., Thomas, R., Wright, W. and Yungel, J., 1999: Rapid thinning of parts of the southern Greenland ice sheet. *Science,* 283: 1522-1524.

Locke, C. W. and Locke, W. W., 1977: Little Ice Age snow-cover extent and paleoglaciation thresholds: North-central Baffin Island, N.W.T., Canada. *Arctic and Alpine Research,* 9: 291-300.

Mann, M. E., Bradley, R. S., and Hughes, M. K., 1998: Global-scale temperature patterns and climate forcing over the past six centuries. *Nature,* 392: 779-787.

Mayewski, P. A., Meeker, L. D., Morrison, M. C., Twickler, M. S., Whitlow, S. I., Ferland, K. K., Meese, D. A., Legrand, M. R., and Steffensen, J. P., 1993: Greenland Ice Core Signal Characteristics - an Expanded View of Climate-Change. *Journal of Geophysical Research-Atmospheres,* 98: 12839-12847.

Meier, M. F., 1984: Contribution of small glaciers to global sea level. *Science,* 226: 1418-1421.

Meier, M. F., Dyurgerov, M. B., 2002: How Alaska affects the world. *Science,* 297: 350-351.

Miller, G. H., Bradley, R. S. and Andrews, J. T., 1975: The glaciation level and lowest equilibrium line altitude in the High Canadian Arctic: maps and climatic interpretation. *Arctic and Alpine Research,* 7: 155-168.

Overpeck, J., K., Hughen, K., Hardy, D., Bradley, R., Case, R., Douglas, M., Finney, B., Gajewski, K., Jacoby, G., Jennings, A., Lamoureux, S., Lasca, A., MacDonald, G., Moore, J., Retelle, M., Smith, S., Wolfe, A., and Zielinski, G., 1997: Arctic environmental change of the last four centruries. *Science,* 278: 1251-1256.

Stroeven, A. P., Fabel, D., and Marshall, S., 2002: Inceptions: mechanisms, patterns and timing of ice sheet inception. *Quaternary International,* 95-6: 1-4.

Taylor, A. E., Wang, K. L., Smith, S. L., Burgess, M. M., and Judge, A. S., 2006: Canadian Arctic Permafrost Observatories: Detecting contemporary climate change through inversion of subsurface temperature time series. *Journal of Geophysical Research-Solid Earth,* 111, doi:10.1029/2004JB003208.

Van de Wal, R. S. W., Wild, M., 2001: Modelling the response of glaciers to climate change by applying volume-area scaling in combination with high resolution GCM. *Climate Dynamics,* 18: 359-366.

Wolken, G. J., England, J.H. and Dyke, A. S., 2005: Re-evaluating the Relevance of Vegetation Trimlines in the Canadian Arctic as an Indicator of Little Ice Age Paleoenvironments. *Arctic,* 58: 341-353.